UNIVERSITÀ DEGLI STUDI DI PADOVA
DIPARTIMENTO DI INGEGNERIA CIVILE, EDILE E AMBIENTALE
Department Of Civil, Environmental and Architectural Engineering

Corso di Laurea Magistrale in Environmental Engineering

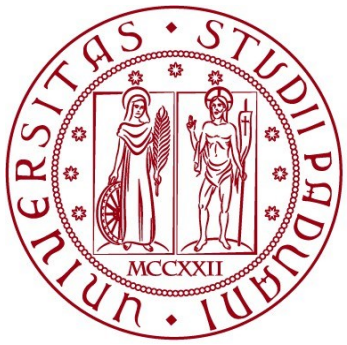

TESI DI LAUREA

PILOT PLANT INVESTIGATION OF A SPIRAL WOUND MEMBRANE MODULE PERFORMANCE FOR OSMOTICALLY ASSISTED REVERSE OSMOSIS (OARO) PROCESS: ANALYSIS AND SIMULATION OF AN INDUSTRIALLY-RELEVANT CASE STUDY

Relatrice:
Chiar.ma PROF.SSA ELENA BARBERA

Laureanda: SERENA TARTARELLI
2092293

ANNO ACCADEMICO 2023-2024

Abstract

Osmotically assisted reverse osmosis (OARO) is a novel membrane-based process which can be implemented as a Zero Liquid Discharge (ZLD) technology for wastewater treatment. This study analyzes OARO process and evaluates its effectiveness for treating highly concentrated solutions. Pilot-scale tests were conducted on a prototype membrane in different ranges of feed and sweep concentrations of NaCl. Positive water fluxes were achieved, even for highly concentrated feed solutions, ranging from 1.00-4.60 LMH at feed pressures from 20 to 28 bar for feed concentrations from 1 M to 4 M of NaCl. Results revealed challenges such as concentration polarization, membrane telescoping under high pressures and dilution of the sweep solution, all of which impact water flux and process efficiency. Then, OARO simulation using experimental data was conducted to explore the process performance in a textile sector application, highlighting energy efficiency advantages of hybrid membrane-assisted ZLD systems over traditional thermal treatment. Three treatment configurations were analyzed: (1) system based on multi-effect evaporation, (2) hybrid system integrating OARO before multi-effect evaporation, (3) hybrid system integrating Ultra-high Pressure Reverse Osmosis (UHPRO) before multi-effect evaporation. Results indicated that the configuration using only thermal treatment presented the highest specific energy consumption (SEC). Both membrane-based processes allowed a significant reduction of energy duties. UHPRO-based configuration demonstrated slightly lower SEC compared to OARO in a base-case scenario. However, opportunities for OARO optimization were identified, which could significantly improve the energetic performance by integrating pressure recovery devices. Moreover, OARO operation at lower pressures offers economic benefits through the use of cost-effective standard components, reducing associated costs. These advantages highlight OARO potential as an energy-efficient and cost-effective solution for industrial wastewater treatment.

Contents

Introduction

Population growth, urbanization, and industrialization have significantly increased the demand for reliable water resources, creating a growing imbalance between clean water supply and demand. This challenge is exacerbated by water pollution and inefficient water management practices, which intensify the issue of water scarcity. Consequently, the development of innovative strategies for water production, management, and conservation has become a critical priority. Wastewater treatment has emerged as a promising solution, enabling the recovery of clean water while reducing the volume of wastewater that requires disposal. This dual-purpose approach alleviates the strain on freshwater resources and ecosystems, transforming wastewater from a harmful byproduct into a valuable resource that supports water sustainability. The Zero Liquid Discharge (ZLD) approach is one of the most ambitious solutions in wastewater management: this strategy seeks to eliminate liquid waste discharge by recovering nearly all water for reuse within a system. ZLD systems not only maximize water recovery but also minimize reliance on freshwater sources, thereby contributing to the preservation of aquatic ecosystems. Early ZLD implementations relied on stand-alone thermal technologies, such as multi-stage flash distillation (MSF), multi-effect distillation (MED), membrane distillation (MD) and mechanical vapor compression (MVC). However, despite their effectiveness, these methods are characterized by high capital and operational costs, as well as significant energy consumption. Therefore, modern ZLD systems incorporate both evaporative and non-evaporative technologies, such as membrane-based processes. In particular, reverse osmosis (RO) is a membrane-based technology that has been integrated into ZLD systems. RO offers the advantage of avoiding phase changes, making it more energy-efficient and cost-effective. However, RO is typically limited to brine concentrations of approximately 75 g/L due to membrane burst pressure constraints, which usually cap operational pressures at 70-80 bar. For higher salinity brines (>75 g/L), evaporative methods are still required. For this reason, ongoing research aims to overcome RO limitations by developing membrane-based processes that achieve high water recovery and brine concentration while maintaining low energy consumption and operating pressures. Osmotically Assisted Reverse Osmosis (OARO) process has emerged as a promising solution to this aim. In OARO, a sweep stream mitigates the

osmotic pressure of the feed solution, reducing the osmotic pressure difference ($\Delta\pi$) across the membrane. This enables water recovery from saline feedwater at pressures lower than its osmotic pressure, overcoming the limitations of conventional RO. The OARO process offers several advantages, such as high water recovery and brine concentration capabilities, lower energy consumption compared to thermal methods, reduced risk of membrane damage due to lower applied pressures and the elimination of the need for high-pressure-resistant materials, reducing equipment costs.

Despite its potential, OARO remains a relatively recent development, with research primarily focused on laboratory-scale experiments and theoretical modeling. Pilot-scale studies are necessary to validate the process under real industrial conditions and to optimize its performance.

This study seeks to deepen the understanding of OARO process operation and potential by conducting experimental tests on a prototype membrane under OARO conditions. The research aims to evaluate the performance of OARO in treating highly concentrated solutions and to compare OARO-based systems with alternative treatment configurations, including thermal-only and hybrid approaches.

After the experimental campaign, data from OARO tests were used to simulate its performance in an industrial context. The effluent treated originates from the textile sector, with energy requirements estimated for three different ZLD configurations. The results provide valuable insights into the energy efficiency and economic implications of each approach, highlighting the advantages of integrating membrane-based technologies like OARO into ZLD systems.

The thesis is structured into four main chapters and follows a logical progression, moving from theoretical foundations to experimental analysis and practical implementation. The first chapter introduces the fundamental concepts of membrane-based processes, explaining specifically RO operating principles and limitations. In this section the OARO process is introduced and an overview of its theoretical principles, advantages and constraints is provided.

The second chapter delves deeper into the theoretical aspects of the OARO process and outlines the methodology used to conduct the experimental campaign on the prototype membrane. It describes the pilot-plant designed to perform the investigation, the operating conditions of the tests and data processing criteria.

The third chapter focuses on presenting and analyzing the results of the experimental tests conducted on the prototype membrane under operational conditions representative of the OARO process. The collected data are evaluated to assess the process performance and to gain more information about OARO functioning.

The final chapter focuses on simulating the OARO process in a real industrial context, using experimental data to model the water flux. A case study involving industrial wastewater treatment is analyzed and an OARO-based system is proposed for its treatment. Then, the energy requirements of the OARO-based treatment system are estimated and compared to two alternative configurations. The first alternative involves a system relying solely on thermal treatment, while the second combines an ultra high-pressure reverse osmosis (UHPRO) stage with a thermal evaporator. This final section aims to understand whether OARO process can be a cost-effective and energy-efficient option to be included in a ZLD system at industrial-scale, when compared to other possible ZLD systems.

I would like to express my sincere gratitude to Eng. Filippo Briani for his valuable support in the development of my Thesis project. Thanks to the internship at his company, I had the opportunity to acquire practical skills and deepen my understanding of important topics for my studies.

1. State of the art

This section provides a general overview of membrane filtration processes, detailing their operating principles and the main membrane configurations. Next, the reverse osmosis process is analyzed, with a comprehensive description of the fundamental parameters governing its operation and its main limitations. The focus then shifts to the innovative Osmotically Assisted Reverse Osmosis (OARO) process, highlighting its technological advantages and presenting a summary of the experimental results reported in scientific literature. Finally, the Zero Liquid Discharge (ZLD) and Minimum Liquid Discharge (MLD) approaches are explained and the aim of the thesis with the motivation behind its development is clarified.

1.1 Membrane processes fundamentals

The non-evaporative process needed to perform freshwater recovery or brine concentration is the filtration, defined as physical process used to remove particulate or dissolved constituents from water by passing water through a filter medium, which retains the target undesirable constituents (Fig. 1.1).

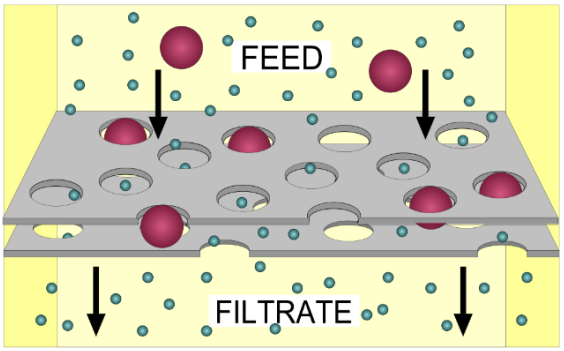

Figure 1.1: *Diagram of a filtration process. Oversize particles are trapped within the filter and fluid and small particles pass through freely. (Wikipedia)*

Filtration processes include surface filtration, characterized by the deposition of particles on the filter surface, and depth filtration, in which the separation is carried out by means of a filter bed of granular material and the deposition occurs within the filter pores (Gushing C Lawler, 1998; Zobel C Gries, 2010). Surface filtration can be performed using membranes, which are semipermeable barriers that allow some molecules or ions to cross them while hindering the passage of others. In membrane separation, a portion

of fluid known as permeate passes through the membrane, while other constituents are rejected by the membrane and retained in the retentate (or concentrate) stream. (Abd El-Ghaffar et al., 2017)

Membrane filtration processes can be classified according to two main aspects: the size of the particles to be retained (Fritzmann et al., 2007) and the driving force of the filtration, which is the energy source that pushes the fluid through the membrane.

According to the particle size (Fig. 1.2):

- Microfiltration retains suspended particles and microorganisms between 0,1 and 10 micrometers in size;
- Ultrafiltration removes solutes between 1 and 100 nanometers in size, including macromolecules such as proteins and polysaccharides;
- Nanofiltration removes multivalent ions and small solutes between 1 and 10 nanometers in size;
- Reverse osmosis removes most dissolved solutes, including salts and organic molecules, with sizes smaller than 1 nanometer.

Figure 1.3 shows the industrial applications expected using membrane processes according to the particle size ranges contained in the treatment water. (Wang, 2013)

The driving force of the filtration process can be (Abd El-Ghaffar et al., 2017):

- Pressure, which pushes the solution through the membrane, with applied pressure increasing from microfiltration to reverse osmosis;
- Electromotive force, which is used to separate charged ionic species my means of an ion selective membrane. An example of this type of process is electrodialysis, used for water desalination and for ions removal from aqueous solutions;
- Concentration gradient, which is the natural driving force for the osmosis process.

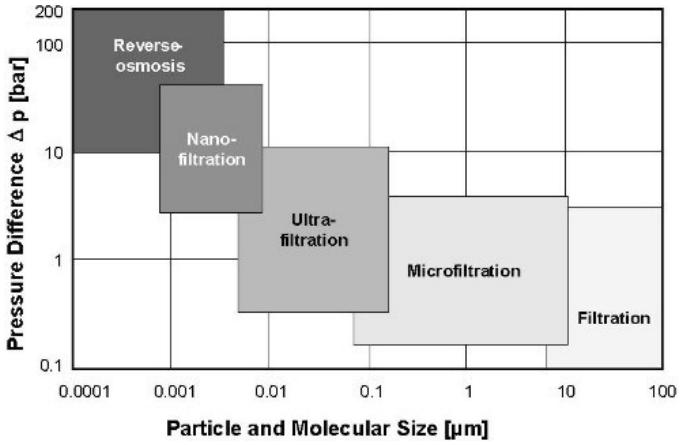

Figure 1.2: *Operative range of membrane processes related to particle size to retain. (Fritzmann et al., 2007)*

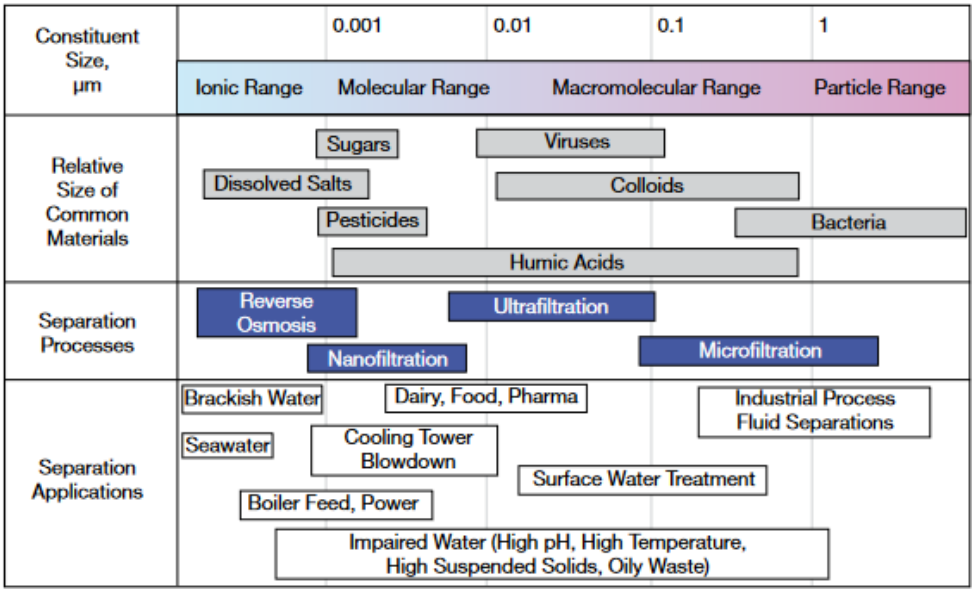

Figure 1.3*: Overview of the pressure-driven membrane separation processes as a function of solute particle size and corresponding industrial applications. (Wang, 2013)*

Membrane filtration can be performed in two main modes: dead-end flow and tangential flow (Wang, 2013). In the dead-end mode, the flow of the feed solution moves perpendicular to the surface of the membrane, crossing it to become permeate (Fig. 1.4a). Particles and aggregates that are repelled by the membrane accumulate on its surface, forming a layer, commonly called a cake, which reduces the filtrate flux over time. Instead, in tangential-flow (or cross-flow) filtration, the flow of the feed solution flows parallel to the membrane surface. Part of the flow crosses the membrane becoming permeate, while the rest remains as retentate and is destined for further processing or

recirculation in the feed stream (Fig. 1.4b). The tangential movement of the flow prevents the accumulation of particles and aggregates on the membrane surface, allowing to maintain a constant permeate flow and low transmembrane pressure. Moreover, avoiding the cake formation as much as possible leads to an improved lifespan of the membrane. For this reason, most large-scale industrial filtration processes employ the tangential flow filtration mode.

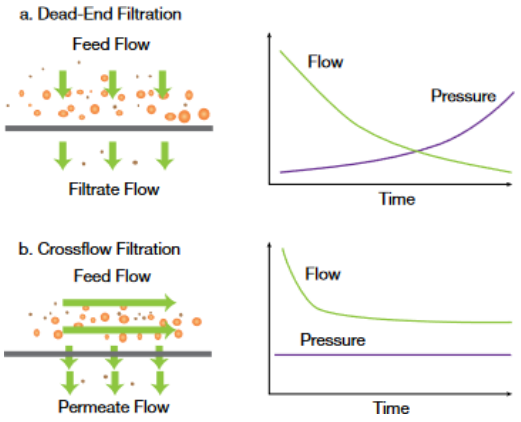

Figure 1.4: *Graphic representation of (a) dead-end filtration and (b) crossflow filtration with the corresponding pressure and flow trends over time. (Wang, 2013)*

1.2 Membrane modules structure, materials and configurations

1.2.1 Membrane internal structure

In general, membrane internal structures are mainly distinguished into symmetrical and asymmetrical (Fig. 1.5), and the choice depends on the resulting properties in terms of filtration efficiency and specific applications. (Pinnau & Freeman, 1999)

Symmetrical membranes have a uniform structure along their entire thickness. This means that the pores in the membrane are evenly distributed and have the same size. Therefore, the flow through the membrane depends only on the size of the pores and the thickness of the material. This type of membrane presents low filtration efficiency for complex applications: since the whole membrane has the same flow resistance, it may be less efficient than asymmetric membranes in situations requiring high selectivity and high

flux. Symmetrical membranes can be made from polymeric or ceramic materials: expanded polytetrafluoroethylene (ePTFE), polyethylene (PE) and polypropylene (PP) are some examples. (Wang, 2013)

On the other hand, asymmetric membranes have a layered structure, with different pore sizes throughout their thickness. Typically, they have a very thin active non-porous layer (top layer) responsible for separation and a porous substrate underneath, which provides mechanical stability and facilitates permeate flow. The support layer protects the membrane from ripping or breaking, while the active layer is responsible for the resistance to mass transport and the selectivity of the membrane (Salama et al., 2021). Membranes of this type have higher filtration efficiency, since the asymmetric pore distribution allows high selectivity while providing good flow through the membrane. Moreover, the lower porous layer reduces hydraulic resistance, improving overall effectiveness. Asymmetric membranes (Fig. 1.5b) are widely used in nanofiltration process, reverse osmosis and other advanced separation applications where high separation efficiency and mechanical strength are needed.

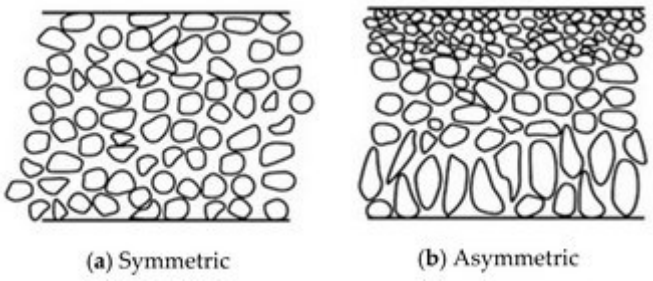

Figure 1.5: *Symmetric (a) and asymmetric (b) porous membranes. (Salama et al., 2021)*

Membranes can also have an asymmetric composite internal structure (Fig. 1.6). Composite membranes are made of a skin layer from polyamide and a microporous support layer of different material, which offers an additional degree of freedom to design a suitable membrane for each application type (Li et al., 2008). Composite membranes are chemically and physically more stable in a wider range of feed pH (3-11), display a strong resistance to bacterial degradation, do not hydrolyze and are less influenced by membrane compaction. However, composite membranes are less hydrophilic and therefore have a stronger tendency for fouling than other types, such as cellulose acetate membranes. (Fritzmann et al., 2007)

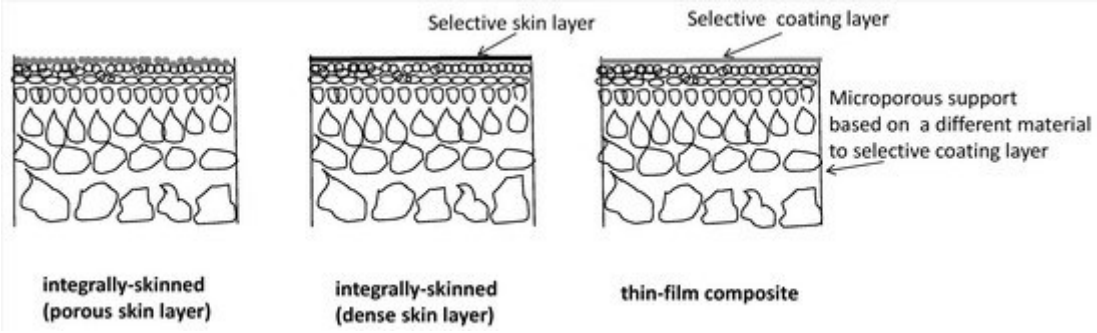

Figure 1.6: *Schematic representation of asymmetric membrane structures. (Buonomenna, 2020)*

1.2.2 Membrane modules configurations

Membrane filtration employs several different membrane configurations: flat, tubular, hollow fiber and spiral wound, together with a wide variety of module designs, such as cassette and cartridge (Abd El-Ghaffar & Tieama, 2017). Membrane format and module design are closely related, since each module design has specific hydrodynamics and is suitable for certain commercial applications based on factors such as process flux, rejection, specific surface area and operating costs (Wang, 2013). Figure 1.7 gives a general comparison of the different module designs.

In general, the desirable characteristics of a membrane configuration are (Mazumder et al., 2023):

- Compactness, so the ability to pack as much membrane surface as possible into a module of limited volume;
- Low resistance to tangential flow, which leads to less friction, less energy expenditure, less pressure drops along the membrane;
- Uniform velocity distribution;
- High degree of turbulence at the retentate side, to minimize fouling and promote mass transfer;
- Easy cleaning and maintenance;
- Low cost per unit membrane area.

	Flat-Sheet Cassette	Hollow-Fiber Cartridge	Spiral-Wound Module
Flow Channel	Narrow (0.03–0.5 cm)	Narrow (0.02–0.25 cm)	Narrow (0.03–0.1 cm)
Crossflow Velocity	2–3 m/s	0.5–2.5 m/s	0.5–1.5 m/s
Reynolds Number	>10,000	500–3,000	500–1,000
Packing Density	Low (300 m^2/m^3)	High (1,200 m^2/m^3)	High (600 m^2/m^3)
Energy Cost	Moderate	Low	Low
Ease of Cleaning	Good	Fair	Poor to Fair
Holdup Volume	Moderate	Low	Low
Particulate Plugging	Moderate	Fair	Very High

Figure 1.7: *Comparison of the principal characteristics of flat sheet cassette, hollow fiber cartridge and spiral wound module designs. (Wang, 2013)*

Membrane cassettes have a complex plate-and-frame assembly of flat sheets of membranes, gaskets, spacers and flow manifolds (Fig. 1.8). This type of configuration is used to perform MF and UF, since it cannot withstand very high pressures. The gaskets provide a tight seal to separate the feed, permeate and retentate streams; the presence of the spacers introduces turbulence in the feed stream, promoting local mixing and effective mass transport, which disrupts concentration polarization and improves process flux (Qasim et al., 2019). However, membrane cassettes with spacers are prone to particulate plugging and are difficult to clean.

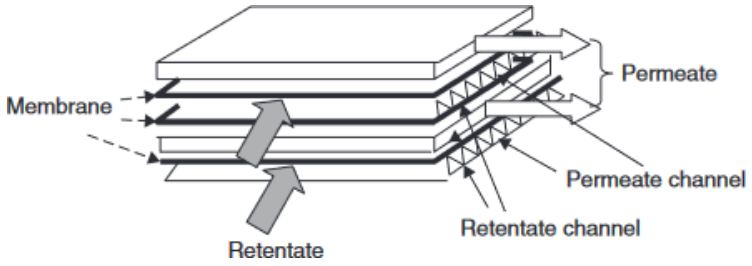

Figure 1.8: *Flat-and-frame cassette configuration. (Berk, 2009)*

In the tubular configuration, the membrane is cast on the inner wall of rigid porous tubes, made of polymer or ceramic. The tubes are connected to end-plates and installed as parallel bundles inside a shell (Fig. 1.9) and may have diameters in the range of 10 to 25 mm (Wang, 2013). Flow direction is usually inside-out, so the retentate flows inside the tubes and the permeate is collected at the shell-side. It is often possible to reverse the flow (outside-in) for cleaning and unclogging of the membrane. Tubular configurations provide the possibility of maintaining high tangential velocity in the feed stream and are therefore particularly suitable for applications where the feed contains a high proportion

of suspended solids or must be strongly concentrated. Because of their relatively large diameter, tubular membranes are easy to clean and inspect. (Xue et al., 2021)

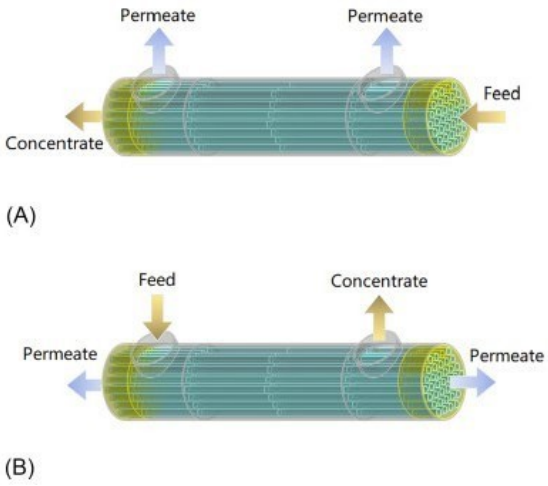

Figure 1.9: *A schematic illustration of tubular membrane modules: (A) internal type module and (B) external type module. (Xue, et al. 2021)*

A hollow fiber module is composed of numerous small diameter (hair-like) fibers contained within a pressure vessel (Touati et al., 2017). On one side, the module consists of an epoxy tube sheet where the fibers ends are potted in epoxy while keeping them open for permeate flow. On the other side, the fiber ends are sealed in epoxy to form an epoxy nub which prevents bypassing of the feed to the concentrate outlet. The module also contains a porous feed distributor (core tube) that runs along the entire length of the module. In outside-in flow, as pressurized feed water enters the module through the core tube, water molecules permeate radially into the fibers and exit through the open fiber ends in the epoxy tube sheet while the concentrate leaves the module at the same end as the feed inlet. In inside-out flow, feed water is added inside the hollow fibers and the water permeates outside, leaving the retentate inside the fibers (Tchobanoglous et al., 2003), (Fig. 1.10).

Hollow fiber modules are economical and exhibit high packing density and recovery. However, they are difficult to clean and highly susceptible to fouling due to small fiber spacing.

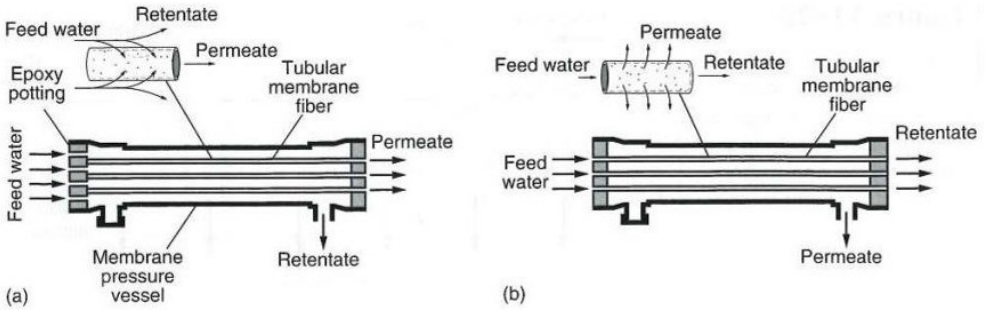

Figure 1.10: *Structure of a hollow fiber module for (a) outside-in flow and (b) inside-out flow. (Tchobanoglous et al., 2003)*

In a spiral wound module (Fig. 1.11), two membrane sheets are placed together with a permeate spacer (made of nylon or dacron) in between to form a leaf. The membrane sheets are glued from three sides with the fourth side left open and connected to a central perforated permeate collector tube. The leaves are then placed together with a feed/concentrate mesh spacer to induce turbulence. The combination of leaves and feed/concentrate spacers is wrapped around the permeate collector tube to create a spiral configuration and is finally placed inside a pressure vessel (Shenvi et al., 2015). Feed water is introduced from one end of the module and travels axially along the length of the module. Water molecules are forced through the membrane and are collected as permeate through the perforated permeate collector tube. The concentrate leaves the module at the opposite end to the feed.

Spiral wound modules are cost effective, possess high packing density and allow for high mass transfer rates due to the presence of feed spacers. However, they are difficult to clean and are susceptible to fouling if pre-treatment is inadequate.

Besides providing a flow path for the feed along the membrane leaf, feed spacers also create eddies, which reduces fouling and thus increases mass flow through the membrane. However, feed spacers inevitably increase feed channel pressure drop and for feed channels below 0.6 mm, excessive loss of productivity has been found due to a strong decrease in transmembrane pressure difference. (Fritzmann et al., 2007)

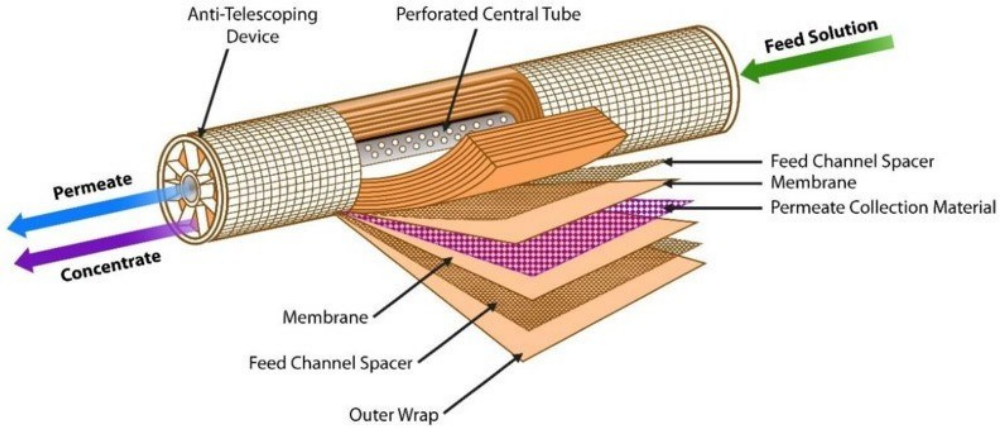

Figure 1.11: *Spiral wound module scheme. (Fonseca-Teodoro et al., 2022)*

1.3 Osmosis process

Among the available membrane processes, membrane-based osmosis is used for freshwater recovery or brine concentration, since semipermeable membranes allow water molecules to diffuse while rejecting the salts.

Osmosis is a natural process in which water molecules spontaneously move from a solution of low solute concentration to a solution of high solute concentration across a semipermeable membrane (Medved & Černý, 2013). The membrane rejects the solutes and only allows water molecules to pass through and the process continues until a state of osmotic equilibrium is reached, where the chemical potentials of water across the membrane become equal. (Fig. 1.12)

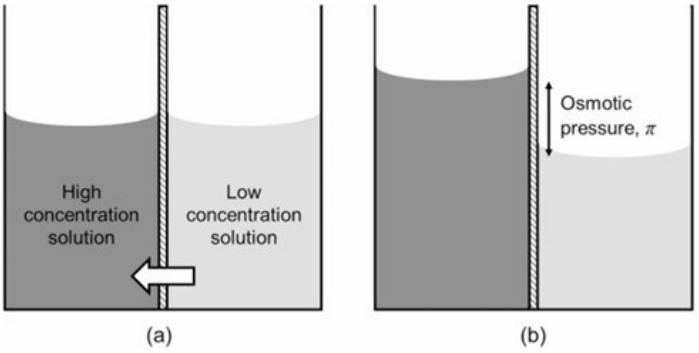

Figure 1.12: *Scheme of (a) osmosis and (b) osmotic equilibrium. (Qasim et al., 2019)*

Solute concentration is strictly related to the osmotic pressure of the solution. Osmotic pressure is defined as the hydrostatic pressure required to prevent the displacement of a pure solvent in a solution across a semipermeable membrane: therefore, it is the pressure needed to counteract osmosis. Osmotic pressure (atm or Pa) is defined as (Fritzmann et al., 2007):

$$\pi = \frac{RT}{V_w} ln \frac{1}{a_w} \qquad (1.\ 1)$$

where V_w is the water molar volume, equal to $18 * 10^{-6}\ m^3/mol$; $a_w = x_w \gamma_w$ is water activity in solution, with x_w being the water molar fraction and γ_w the activity coefficient; $T\ (K)$ is the solution temperature; R is the universal gas constant, equal to $0.0821\ L \cdot atm/(mol \cdot K)$.

For ideal and dilute solution, the equation can be simplified to Van't Hoff equation:

$$\pi = RTC_s \qquad (1.\ 2)$$

where $C_s\ (mol/l)$ is the solute molar concentration.

The natural osmotic flow of water molecules across a semipermeable membrane can be halted or reversed by applying external pressure to the solution with the higher solute concentration. Positive water flux generally refers to the movement of water against the osmotic pressure gradient, flowing from the higher concentration solution to the lower concentration solution across the membrane (Bartholomew et al., 2017). Both hydraulic pressure and osmotic pressure differences across the membrane are critical factors in the osmosis process. Defining P_L and P_H as the hydraulic pressures of low-salinity and high-salinity solutions, π_L and π_H as osmotic pressure of low-salinity and high-salinity

solutions, many osmotic processes can be distinguished based on the possible combinations of hydraulic pressure and osmotic pressure differences between the low-salinity and high-salinity sides. As shown in Figure 1.13:

1. In pressure-assisted forward osmosis (PAFO), a higher hydraulic pressure is applied on the low-concentration side to increase the water transport from the low-salinity side to the high-concentration side. According to the convention, water flux is considered negative.
2. In forward osmosis (FO), hydraulic pressure difference is negligible ($\Delta P \approx 0$) and water flux is then driven from the low-concentration side to the high-concentration side.
3. In pressure retarded osmosis (PRO), higher hydraulic pressure is applied to the high-salinity solution, retarding water transport from the low-salinity to the high-salinity side. The objective is mainly to store energy in the high-concentration side, converting the osmotic pressure from salinity gradients into mechanical or electrical energy via turbines. (She et al., 2017)
4. In reverse osmosis (RO) and osmotically assisted reverse osmosis (OARO), hydraulic pressure is applied to the high-salinity side, to make the hydraulic pressure difference ($\Delta P = P_H - P_L$) higher than the osmotic pressure difference ($\Delta\pi = \pi_H - \pi_L$). Therefore, water transport is driven from the high-concentration to the low-concentration side, so it is considered positive. The difference between RO and OARO is that the osmotic pressure difference is much higher in RO compared to OARO.

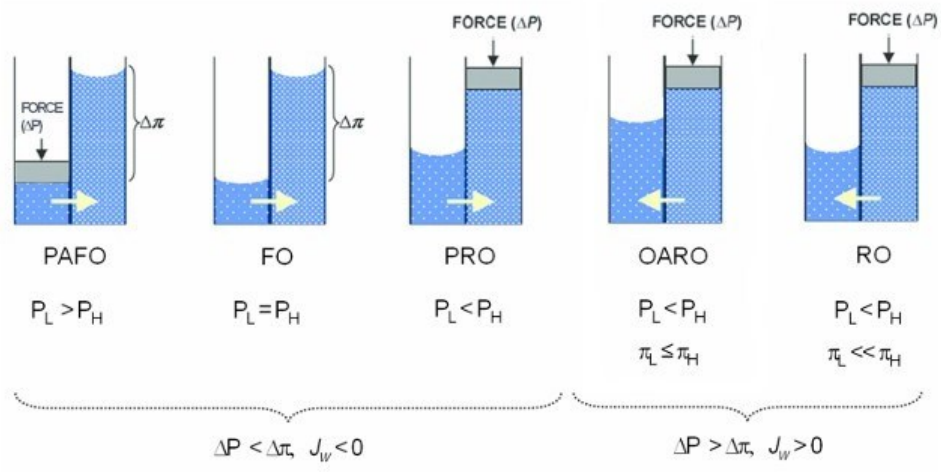

Figure 1.13: *Comparison of flux directions and driving forces in various osmotic membrane processes, including pressure-assisted forward osmosis (PAFO), forward osmosis (FO), pressure-retarded osmosis (PRO), osmotically assisted RO (OARO), and reverse osmosis. (Ju et al., 2023)*

1.4 Reverse osmosis (RO)

Reverse osmosis (RO) is considered the leading and the most optimized membrane-based brine dewatering process that is currently dominating the market. In addition, RO is the most reliable state-of-the-art technique for sea water and brackish water desalination and has been used as an alternative source for producing clean water in order to minimize the desalination associated costs. Currently, around 50% of the desalinated water available globally is produced by using RO. (Zubair et al., 2023)

Based on the quality of the input processed, RO plants can be grouped into (Qasim et al., 2019):

- Seawater RO plants (SWRO) where the salinity is around 30,000mg/L.
- Brackish water RO plants (BWRO) where the salinity is in the range of 500mg/L to 10,000mg/L. BWRO is further sub-grouped into low salinity BWRO that process feed water with salinity between 500 and 2,500mg/L and high salinity BWRO plants that process water with salinity between 2,500 and 10,000mg/L.

1.4.1 Reverse osmosis process analysis

In reverse osmosis (RO), an external hydraulic pressure is applied on the more concentrated side of the membrane, such that the hydraulic pressure difference is greater than the osmotic pressure difference across the membrane, so water molecules are forced to flow in a direction opposite to that of the natural osmosis phenomenon (Fig. 1.14).

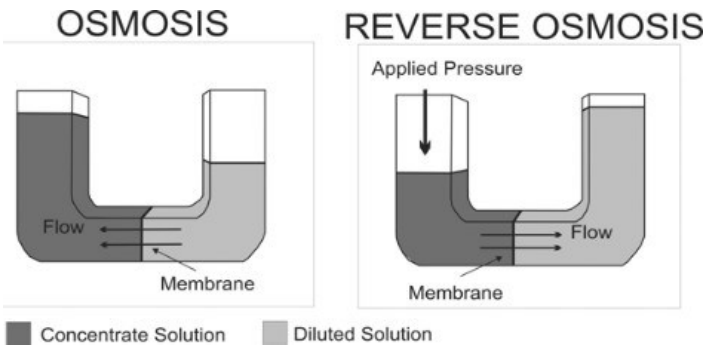

Figure 1.14: *Reverse osmosis principle. Left: osmosis; right: reverse osmosis. (Fritzmann et al., 2007)*

It is a thermodynamically non-spontaneous process, where a transmembrane pressure (TMP) is essential to provide the driving force for mass transport across the membrane (Qasim et al., 2019).

A scheme of a continuous RO process is shown in Figure 1.15. The feed water stream splits into two streams. The first consists of water molecules that have permeated through the membrane. This stream of low solute concentration is called permeate or product water. The second stream consists of a decreased amount of water molecules and the rejected solutes. This stream of higher solute concentration is termed as concentrate or reject.

In conventional RO with almost perfect salt rejection, $\Delta\pi$ is equal to the osmotic pressure of the brine (π_{feed}) because the osmotic pressure of the product water is negligible. According to Van't Hoff equation, π_{feed} increases with the brine concentration c_{feed}. During RO operation, the feed becomes more concentrated, leading to an increased π_{feed}. Once π_{feed} reaches the applied ΔP, permeate is no longer produced and the feed cannot be further concentrated. In other words, the maximum brine concentration ($c_{feed,max}$) of conventional RO is achieved as $\pi_{feed} = \Delta P$. So, for a given ΔP, $c_{feed,max}$ is fixed. In addition, with a fixed $c_{feed,max}$, the maximum water recovery decreases with increasing the initial feed concentration. To avoid damage of high hydraulic pressure on membranes, ΔP is usually less than 80 bar, resulting in a $c_{feed,max}$ of about 94,000 mg/L TDS, which leads to maximum water recovery of about 93, 63 and 26% for feed solutions of 10,000, 35,000

and 70,000 mg/L TDS, respectively (Wang et al., 2021). Therefore, to further enhance water recovery in conventional RO, the allowable ΔP must be increased.

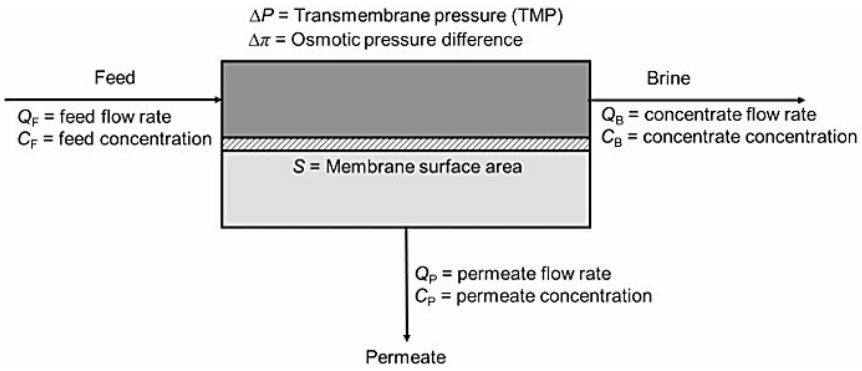

Figure 1.15: *Scheme of a continuous reverse osmosis system. (Qasim, et al. 2019)*

Several parameters describe the RO process, such as transmembrane pressure, water recovery and solute rejection.

Transmembrane pressure represents the pressure difference between the feed side and the permeate side of the process.

The TMP formula for the crossflow configuration is (Water Environment Federation 2005):

$$TMP = \left(\frac{P_F + P_R}{2}\right) - P_P\,[kPa] \qquad (1.\ 3)$$

The TMP formula for the dead-end configuration is:

$$TMP = P_F - P_P\,[kPa] \qquad (1.\ 4)$$

where:

- P_F = feed water pressure (kPa)
- P_R = retentate pressure (kPa)
- P_P = permeate pressure (kPa)

TMP is a crucial factor in determining the rate at which fluid passes through the membrane and the amount of substances retained. On one hand, higher TMP can increase permeate flux and can optimize the particles removal; on the other hand, it can also lead to fouling problems, decreasing the membrane permeability, and to physical damage to

the membrane structure, reducing its lifetime. Thus, TMP should be monitored and carefully chosen to ensure adequate maintenance and protection of the membrane.

Water recovery of an RO process is defined as the volume fraction of feed water that is recovered as permeate or product water. The percentage recovery (r) can be calculated as follows (Qasim et al., 2019):

$$r = \frac{Q_P}{Q_F} * 100\% \qquad (1.\ 5)$$

where:

- Q_P = permeate flowrate (L/h)
- Q_F = feed flowrate (L/h)

In most RO systems, recovery ranges from 50 to 85% and typically depends on the feed characteristics, feed salinity, pretreatment, design configuration and brine disposal choices (Kucera, 2010). Water recovery is an important design parameter that requires careful selection to balance the tradeoff between the concentrate volume generated and the permeate purity. A higher recovery results in a lower amount of concentrate volume that needs to be disposed of. On the other hand, this advantage is gained at the expense of lower permeate purity.

Rejection parameter indicates the effectiveness with which a membrane can retain a particular dissolved or suspended substance present in the feed solution. Rejection is usually expressed as a percentage (%) and is calculated using the following formula (Qasim et al., 2019):

$$R = \frac{(C_F - C_P)}{C_F} \ [\%] \qquad (1.\ 6)$$

where:

- C_F = solute concentration in the feed solution (mg/L)
- C_P = solute concentration in the permeate (mg/L)

A high percentage of rejection means that the membrane is very capable of retaining the solute particles. For instance, a 99% rejection for salt in the RO process means that only 1% of the total solute in the feed solution passes through the membrane, leaving the rest in the retentate flux. Thus, the value of rejection gives information about:

- the efficiency of separation, and this is important in applications where specific solutions need to be purified or concentrated;
- permeate quality, since the permeate must meet specific purity standards and high rejection for contaminants, bacteria or salts is essential to ensure that the permeate is safe;
- filtration system design, since the choice of the membrane and the design of the process depend on the required rejection value.

1.4.2 Module structures and configurations for reverse osmosis process

For efficient reverse osmosis process, membranes should in general display high flux and high rejection. High permeability requires very thin membranes, since the flux is inversely proportional to the membrane thickness.

The first commercially available RO membranes introduced into the market in the early 1970s were cellulose-acetate (CA) membranes (Fig. 1.16). As reported by Buonomenna (2020), these are produced by phase inversion, using the miscibility gap of a polymer, a precipitant and a solvent. A film of dissolved polymer (cellulose acetate and acetone) is immersed into a precipitant (water). Acetone is replaced by water and the polymer rich phase starts to precipitate. After complete solidification the membrane is tempered in hot water to remove existing surface defects. One of the major drawbacks of cellulose acetate membranes is the possibility of membrane deterioration by hydrolysis. This reaction is strongly dependent on pH and is faster under acidic or alkaline conditions. Hence, application of cellulose acetate membranes therefore needs careful pH adjustment and control. In addition, CA membranes under high pressure tend to be strongly affected by compaction and flux as well as overall performance decreases. For this reason, although cellulose acetate membranes are still in use and commercially available, they are more and more replaced by thin-film composite membranes.

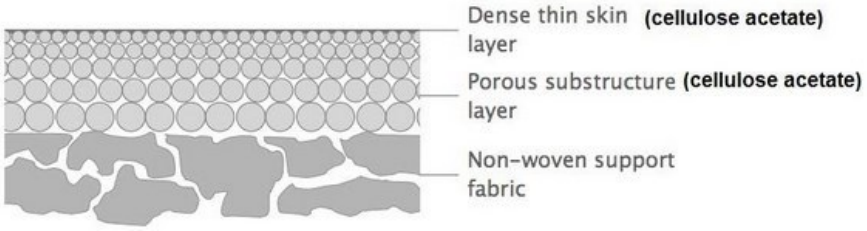

Figure 1.16: *Cellulose acetate (asymmetric) membrane structure. (Buonomenna, 2020)*

For industrial applications, RO membrane modules must feature high packing density. This parameter is essential to allow a large membrane area to fit within a relatively small volume. This characteristic is critical not only to ensure the overall compactness of the process, but also to facilitate membrane installation, simplify cleaning and replacement and reduce the initial capital costs required to implement the system. Initially, RO membranes were based on tubular and plate-and-frame configurations. However, due to their low packing density, these two module configurations were phased out and replaced with hollow fiber and spiral wound modules, whose design is significantly more compact and functional (Wang, 2013). The following Table 1.1 compares the four RO membrane modules in terms of packing density, fouling propensity, ease of cleaning and manufacturing cost.

Table 1.1: *Comparison of RO membrane modules characteristics. (Qasim et al., 2019)*

Module type	Packing density (ft^2/ft^3)	Fouling propensity	Ease of cleaning	Manufacturing cost
Plate and frame	45-150	Moderate	Good	High
Tubular	6-120	Low	Excellent	Very high
Spiral wound	150-380	High	Poor	Moderate
Hollow fiber	150-1500	Very high	Poor	Low

As can be seen, spiral wound and hollow fiber membranes have a considerably higher density compared to tubular and flat configurations, at the expense, however, of the propensity for fouling and the difficulty in adequately cleaning the membrane. Therefore,

to use these configurations, a pre-cleaning and membrane maintenance program must be implemented to ensure that the performance is kept at an optimal level.
Commercial hollow fiber and spiral wound RO membranes are available from manufacturers such as Toyobo (Osaka, Japan), Dupont Water Solutions (Delaware, USA), Toray Membrane (California, USA), Hydranautics (California, USA) and LG Chem (Seul, South Korea).

1.4.3 Reverse osmosis drawbacks and limitations

Reverse osmosis offers a significant advantage over conventional thermal methods, as it does not require phase changes. This aspect means that energy consumption is greatly reduced compared to thermal methods, making RO a particularly appealing technology for large-scale applications where energy savings are crucial. (Skuse et al., 2021)
However, reverse osmosis has some operational limitations. As already pointed out, for water to cross the semipermeable membrane and separate from the solute, the applied hydraulic pressure must be high enough to exceed the osmotic pressure of the concentrated solution. Thus, in the case of solutions with a particularly high osmotic pressure, the hydraulic pressure required to operate the process can become considerably high. This presents a technological challenge, since the membranes used in RO process have a limited capacity to withstand high pressures, so beyond a certain limit of applicable pressure the membrane may suffer structural damage.
This constraint, however, leads to a reduction in the efficiency of the overall process, since limiting the applied pressure compromises the concentrations that can be achieved by reverse osmosis. In other words, when treating solutions with high osmotic pressures, just as there is a limit of applicable pressure (80 bar), so there is a limit of solute concentration that can be achieved. (Togo et al., 2019)
Other major problems include fouling, scaling, concentration polarization and membrane deformation, that adversely affect membrane performance, leading to increased energy consumption and operating costs. High energy consumption is a particularly critical issue, as it accounts for half of the total cost of water production.
Besides that, RO also suffers greatly from a high rate of brine production and current methods of brine disposal are still inadequate to ensure sustainable management. (Goh et al., 2016)

1.4.4 Concentration polarization and fouling phenomena

Despite all the advantages, the widespread application of RO technology is hindered by two limiting problems: fouling and concentration polarization.

Indeed, the direct correlation between fouling and concentration polarization (CP) with energy consumption makes these phenomena the most crucial practical challenges to be addressed to improve RO sustainability. (Bai et al., 2023)

Concentration polarization is a phenomenon present in all membrane filtration processes, as membranes exhibit specific selectivity for different components of a solution. This results in the accumulation of rejected solutes on the membrane surface, forming a concentration boundary layer. The effects of concentration polarization on membrane processes are clearly negative (Qasim et al., 2019). The main negative impact of CP lies in the reduction of permeate flux, caused by the increased concentration of solute in the area immediately close to the membrane, which results in an increase in hydraulic resistance to the water flow through the membrane, consequently reducing permeate flux.

In osmotic processes, concentration polarization can occur on both sides of the membrane: on the feed side, the solute accumulates near the membrane surface, while on the permeate side, the solute is diluted. These are known respectively as concentrative and dilutive external concentration polarization (ECP). (McCutcheon & Elimelech, 2006)

In concentrative ECP, the convective flow of water carries the solute from the bulk solution toward the surface of the active layer of the membrane. The water permeates through the active layer, thus increasing the concentration of the solute on the surface. In contrast, in dilutive ECP, the convective flow moves the dissolved solute away from the membrane surface on the permeate side, reducing the effectiveness of the driving force of the draw solution. (Qasim et al., 2019)

When an asymmetric membrane is used, one of these boundary layers is formed within the porous support layer of the membrane. This phenomenon is called internal concentration polarization (ICP), which can be either concentrative or dilutive.

In the case where the feed is placed against the support layer of an asymmetric membrane (AL-DS) orientation, water flows through the porous layer and diffuses into the active

layer, passing into the permeate. The salt in the feed easily enters the porous layer carried by the convective flow of water, but it cannot penetrate the active layer as easily, thus increasing its concentration in the support layer. This phenomenon is known as concentrative ICP. (Rahman et al., 2023)

When, on the other hand, the feed solution is in contact with the active layer and the draw solution is against the support layer (AL-FS orientation), internal polarization occurs on the permeate side. In this case, the phenomenon is called dilutive ICP, as the permeate water dilutes the draw solution within the porous layer of the membrane.

A graphic explanation of the different concentration polarization profiles is shown in Figure 1.17.

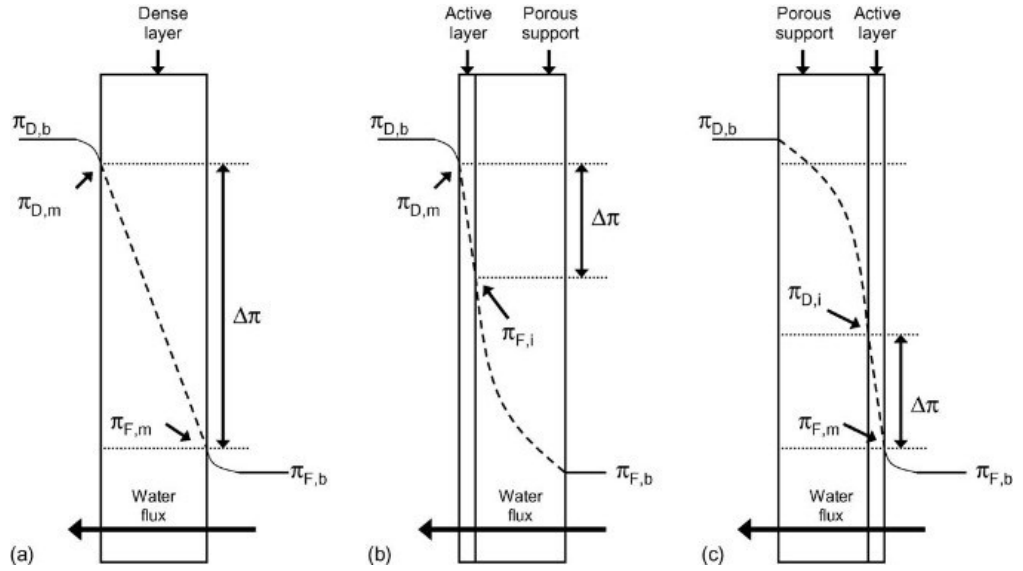

Figure 1.17: *Illustration of osmotic driving force profiles for osmosis through several membrane types and orientations, incorporating both internal and external concentration polarization. (a) A symmetric dense membrane; the profile illustrates concentrative and dilutive ECP. (b) An asymmetric membrane with the dense active layer against the draw solution (PRO mode); the profile illustrates concentrative ICP and dilutive ECP. (c) An asymmetric membrane with the porous support layer against the draw solution (FO mode); the profile illustrates dilutive ICP and concentrative ECP.*
Key: $\pi_{D,b}$ is the bulk draw osmotic pressure, $\pi_{D,m}$ is the membrane surface osmotic pressure on the permeate side, $\pi_{F,b}$ is the bulk feed osmotic pressure, $\pi_{F,m}$ is the membrane surface osmotic pressure on the feed side, $\pi_{F,i}$ is the effective osmotic pressure of the feed in PRO mode, $\pi_{D,i}$ is the effective osmotic pressure of the draw solution in FO mode, and $\Delta\pi$ is the effective osmotic driving force.
Note that it is assumed that no ECP occurs along the porous support layer since NaCl is not reflected by the layer; in these cases, bulk osmotic pressure is equivalent to membrane surface osmotic pressure. (McCutcheon & Elimelech, 2006)

ICP is different from the external concentration polarization since ECP occurs at the membrane surface and can be alleviated by increasing the cross-flow velocity across the surface. On the contrary, ICP can only be marginally reduced as it occurs within the

membrane support layer (Cath et al., 2006). Hence, ICP is more closely related to the membrane characteristics, which can be described by the structural parameter S (m):

$$S = \frac{\tau \cdot l}{\varepsilon} \qquad (1.\ 7)$$

Where τ $(-)$ is the pores structure tortuosity, l (m) is the membrane thickness and ε $(-)$ is the membrane porosity. This relation describes the behavior of the membrane in terms of resistance, considering its structural characteristics. For instance, a thin and porous substrate with interconnected pores (less tortuous) generally results in less severe ICP. (Wang et al., 2018)

Focusing on RO process, a convective flow of solutes from the bulk feed towards the membrane develops. This maximizes the solute concentration on the membrane surface and creates a boundary layer within which the solute concentration is higher than the bulk solute concentration. Higher solute concentration within the boundary layer also causes diffusional back-transport of the solutes away from the membrane, but the dominance of convection over diffusion builds up the solutes in the boundary layer and on the membrane surface. A typical concentration profile is shown in Figure 1.18.

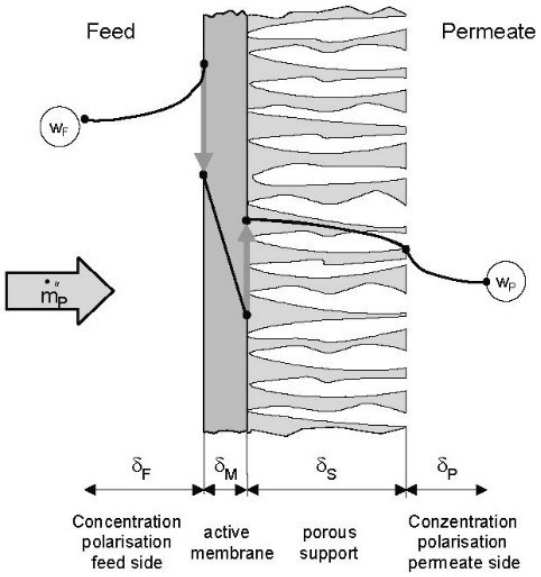

Figure 1.18: *Concentration polarization profile for RO process: w_F is the solute concentration of the feed side; w_P is the solute concentration on the permeate side; m_P is the mass flow on the permeate side. (Fritzmann et al., 2007)*

Another important aspect related to CP is the increase in solute flux across the membrane. In fact, the increase in solute concentration at the membrane surface leads to a reduction in the rejection rate of the membrane, from as shown in Equation (1.5). The direct consequence of this condition is the increase of solute concentration in the permeate. Also, CP exacerbates the probability of precipitation (scaling) of divalent ions and sparingly soluble salts by enhancing their concentrations on the membrane surface over the solubility limits, influencing negatively the mass transfer. (Fritzmann et al., 2007)

The most direct approach to reducing or eliminating CP is to impose external energy to increase mixing within the feed channel, which can potentially disrupt the boundary layer. The external energy can be applied in the form of vibration, ultrasound, chemicals, electricity, magnetic field and light irradiation. (Bai et al., 2023)

Membrane fouling is a phenomenon that occurs when colloidal materials in the water accumulate on the surface or inside the membrane itself, forming a layer of accumulated colloidal material termed as “cake”. It can cause significant decline in the water permeation rates by decreasing the active membrane area and increasing the resistance across the membrane (Qasim et al., 2019). In addition, it also increases pressure loss along the membrane, while rejection is decreased. (Fritzmann et al., 2007)

To minimize this problem, water pretreatment methods are used, including upstream filtration, addition of scale inhibiting agents and periodic cleaning of the membrane

through chemical or mechanical flushing. Moreover, CP and fouling phenomena can occur together, enhancing the entity of the boundary layer of rejected material on membrane surface. (Bai et al., 2023)

A more detailed and deeper analysis of CP phenomenon during filtration processes is a key element in stimulating the development of next-generation membranes, as the ability to control or mitigate CP can lead to an overall improvement in the performance of separation systems.

1.4.5 Scaling

Scaling (inorganic fouling) on the membrane occurs because of supersaturation of poorly soluble inorganic compounds that tend to concentrate on the feed side of the membrane. In fact, when salt in the feed water reaches a concentration above the solubility limit, the ion cluster coalesces to form a crystal and once it grows above a critical size it can precipitate and settle on the membrane surface (Matin et al., 2019). This process leads to the formation of a thin layer of material that acts as a physical barrier to mass transfer, reducing permeate flux (Warsinger et al., 2015). Therefore, it is common practice not to exceed solubility limits. This phenomenon is due to the continuous transport of crystals to the surface of the membrane itself. Once the cake layer is formed, it can facilitate the formation of further fouling, exacerbating the problem. This process contributes to increased resistance to water flow through the membrane, as the formation of fouling on the surface progressively reduces permeability. (Peters et al., 2022)

Some of the most important scaling substances are $CaCO_3$, $CaSO_4$, $BaSO_4$ and silica. Hydroxides of Al, Fe and Mn are normally precipitated before reaching membrane surface. Mineral salts such as $CaCO_3$, $CaSO_4$ and $BaSO_4$ are almost always present near their saturation levels in brackish water feeds, thus, even at moderate levels of product water recovery, there is a good probability of inorganic fouling taking place. (Matin et al., 2019)

To overcome this problem, pre-treatment strategies for water fed to membrane plants are commonly adopted, such as pH adjustment and antiscalants dosage (Prihasto et al., 2009).

Antiscalants are chemical additives which act by interfering with the crystal growth process. Some examples of antiscalants are polyphosphates, polyacrylic acids and organophosphorus derivatives. (Jafar Mazumder, 2020)

1.5 Osmotically assisted reverse osmosis (OARO)

Osmotically assisted reverse osmosis (OARO) is an advanced and innovative technology for water recovery and concentration of high salinity brines, based on the use of semipermeable membranes (Chong et al., 2024). It is a non-evaporative process that is distinguished by its ability to provide high water recovery while minimizing energy consumption compared to other desalination and concentration technologies. (Nakagawa et al., 2020)

Indeed, RO water recovery is limited for high salinity brines (> 50 g/L) because the hydraulic pressure cannot exceed the membrane burst pressure, which typically about 70-80 bar. For this reason, ongoing research is focused on decreasing the operating pressure, while obtaining high water recovery, high brine concentration and low energy consumption. (Bartholomew et al., 2017)

OARO process is based on reverse osmosis principle of employing hydraulic pressure to force water through a membrane but differs by using unpressurized sweep saline solutions in the permeate side, which reduce the osmotic pressure difference across the membrane, leading to higher water flux and thus higher water recovery than conventional RO (Fig. 1.19).

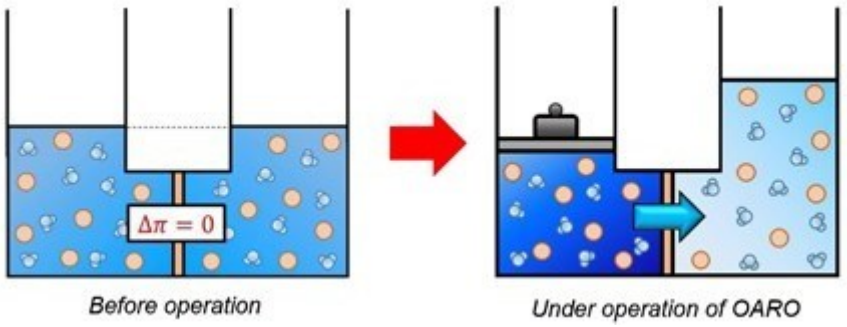

Figure 1.19: *Graphic representation of OARO process. In this case the difference of osmotic pressure between the two sides of the membrane is zero because the same concentration is used on the feed and permeate side. (Nakagawa et al., 2020)*

In the traditional RO process, the osmotic pressure difference between the feed and the permeate becomes limiting when the dissolved solids concentration (TDS) in the feed

solution is relevant. This phenomenon occurs because the permeate in RO has a TDS close to zero, which intensifies the osmotic pressure gradient, making water transport difficult when the salinity of the feed solution is very high, so when the feed solution is highly concentrated. In contrast, in the OARO, the saline sweep solution in the permeate side of the membrane reduces this gradient, allowing water transport to be maintained even when the osmotic pressure of the feed solution exceeds the limits that the membrane could normally withstand (Chae et al., 2024). In fact, the osmotic pressure of the sweep reduces $\Delta\pi$ across the membrane from π_{feed} to $\pi_{feed} - \pi_{sweep}$. Therefore, since the working principle of RO implies that ΔP applied must be higher than the osmotic pressure of the feed solution, π_{feed} in OARO can exceed ΔP, thereby achieving a higher water recovery than conventional RO with the same applied ΔP (Wang et al., 2021). For this reason, OARO can be operated at lower applied hydraulic pressures and this allows dewatering of more saline feed streams without exceeding the maximum allowable hydraulic pressure of the membrane module (Peters C Hankins, 2019). Therefore, OARO expands the maximum TDS from which water can be recovered from a pressure driven membrane process. Additionally, the lower operating pressures make OARO more energy efficient than conventional RO.

Multiple OARO stages can be linked in series, enabling the recovery of more freshwater from high salinity brines. The sweep concentration is reduced in successive stages until the diluted sweep can be effectively treated using a traditional RO process.
A schematic description of this process is shown in Figure 1.20, from Bartholomew et al. (2017), the first published paper about OARO which develops a model to identify feasible operating conditions and to estimate water recovery and energy consumption across a range of feed concentrations. A high-salinity feed solution is introduced into the OARO module under high hydraulic pressure. On the permeate side, a low-pressure sweep solution, characterized by lower salinity, flows in the opposite direction from the feed. This countercurrent flow creates a hydraulic pressure difference greater than the osmotic pressure difference across the membrane, allowing water transport. The resulting water flow further concentrates the feed, while simultaneously diluting the sweep solution. The

concentrated feed represents the effluent of the OARO process that can be subsequently treated through appropriate methods, such as thermal technologies.

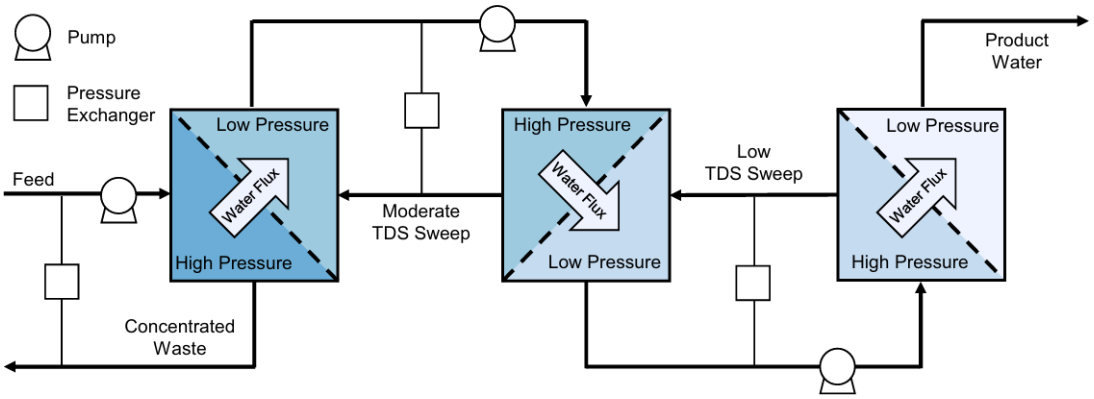

Figure 1.20: *Process diagram of the OARO process. The first two stages are OARO, the final stage is RO. (Bartholomew et al., 2017)*

If the concentration of the diluted sweep is relatively high and the target recovery cannot be achieved by reverse osmosis, the diluted sweep can be pressurized and introduced into a second OARO module. Since the concentration of the diluted sweep is lower than that of the original feed, an equivalent volume of permeate can be obtained with a reduced sweep concentration. This second OARO module re-concentrates the first diluted sweep and dilutes the second sweep. The first sweep, once re-concentrated, can be reused as the input sweep in the first OARO module, while the second diluted sweep may require an additional OARO stage. In this way, sweep concentrations are progressively reduced through a series of OARO stages until they reach a level low enough for the application of conventional reverse osmosis.

1.5.1 OARO design considerations

The OARO process has several key design considerations, such as freshwater recovery, inlet feed and sweep concentration, hydraulic pressure of the feed, number of stages and membrane area. (Bartholomew et al., 2017)

First, the first sweep concentration is strictly correlated to water recovery, number of modules and energy consumption. For instance, in a multistage OARO process, if a high sweep concentration is chosen for the first stage, freshwater recovery increases since a higher sweep concentration decreases the osmotic pressure difference across the membrane, thus increasing water flux. However, the number of modules increases

because a higher first sweep concentration directly magnifies the concentration of the first diluted sweep and so additional stages are required to lower the concentration to the target imposed or to the point at which an RO module can be used. Consequently, a higher number of modules increases the energy demand needed to operate the pressure pumps and to compensate for the mechanical energy loss from the pressure drop along the additional module. Moreover, in situations where the number of modules stays constant and a final RO stage is added, a higher first sweep concentration will result in a higher diluted sweep concentration into the RO module, that will require increased RO operating pressures and thus more energy consumption to recover the same freshwater. As Bartholomew et al. (2017) reported, while the first sweep TDS ranges from 100 to 225 g/L, the recovery increased from 17 to 42%, but the number of modules went from 3 to 7 and the energy consumption from 5.7 to 14 kWh per m^3 of produced water. These considerations lead to the conclusion that while higher freshwater recovery using higher sweep concentration will be beneficial, increasing the number of modules and energy consumption will also increase the capital and operating costs of the OARO system.

Another important design element is the membrane area for each module. Indeed, increasing membrane area will benefit freshwater recovery, but it also widens pressure drop, salt permeate and capital and operating costs of the OARO module. If membrane area increases, the water flux can be lower to obtain the same desired recovery, thereby allowing a lower first sweep concentration. This results in a fewer number of modules or a lower concentration of the diluted sweep into the final RO module. Therefore, fewer number of modules or a lower operating pressure requirement on the RO unit decreases energy consumption.

In cases where a small increase in membrane area per module decreases the number of modules, the total membrane area of the OARO process is reduced. For example, Bartholomew et al. (2017) reported that for an increase in area per module from 9 to 10 m^2 for a 35% recovery, the total membrane area decreased from 45 m^2 (5 modules at 9 m^2 each) to 40 m^2 (4 modules at 10 m^2 each). In these cases, not only does increasing the membrane area per module decrease the energy consumption but it also reduces the total

amount of membrane area and likely the associated membrane costs. In addition, while multiple modules suggest a high total membrane area, it is expected that most of the capital costs will derive from the physical modules, pumps and pressure exchangers, so for a given recovery it is better to have fewer large OARO modules rather than more numerous small ones. This realization suggests that a cost optimal OARO process will likely have a small number of stages, such as 2 to 3 large modules. However, larger membrane areas also demand capital and operating costs, so the trade-off between the performance improvement with increased cost will be a critical design consideration. Generally, the fewest number of modules that can achieve the desired treatment specifications is found to be the cost-optimal number of OARO stages. (Bartholomew et al., 2018)

The hydraulic pressure applied to the feed solution is another design factor, since it increases the driving force for water flux, thus allowing a lower first sweep concentration to obtain the target recovery. The lower first sweep concentration results in lower energy consumption, since fewer modules are needed or a lower pressure demand in the final RO module is required, but at the expense of the energy demand of the pressure pump. In addition, further increases in feed pressure are physically limited by the burst pressure.

In addition to the process layout and membrane dimensions, also the configuration and the characterization of the module will influence the OARO process. Indeed, it was found that an ideal OARO module configuration should have counter-current feed and sweep flow, relatively high turbulence and low hydraulic pressure drop. Counter-current feed and sweep flow is preferred since it minimizes the osmotic pressure difference across the membrane and it allows a more uniformly distributed water flux along the module. Finally, as in RO, a relatively high turbulence is needed to reduce concentration polarization effects and a low hydraulic pressure drop across the module will increase water flux and pressure recovery.

The OARO process is also dependent upon membrane properties. An ideal OARO membrane should have (Peters & Hankins, 2019):

- High water permeability coefficient;
- High water selectivity, thus low solute permeability coefficient;
- High membrane burst pressure;

- Low structural parameter S, which is related to the structural properties of the membrane's support layer.

Regarding ICP, the membrane with less affected ICP (corresponding to low S parameter) would be suitable for the achievement of high concentration by OARO process. In fact, RO membranes are usually not designed for low structural parameter of the membrane support layer, since RO does not experience permeate-side concentration polarization. In contrast, FO membranes have low structural parameters but are not typically designed for high membrane burst pressures (Tiraferri et al., 2011). Ultimately, OARO membrane requirements are a combination of those expected for FO and RO, such as high membrane burst pressure and low structural parameter, which are in common with pressure retarded osmosis (PRO) (Coday et al., 2013). However, there are currently few commercially available PRO membranes and therefore FO membranes are generally employed instead. In particular, cellulose triacetate (CTA)-based hollow fiber (HF) membrane is one of the commercially successful semipermeable membranes that has a long historical development due to its reliable excellent performances especially for drinking water production from seawater (Nakao et al., 2021). For this reason, CTA-based HFs have caught attention for the usage of different methods, such as FO, RO, PRO, PAFO and can be considered also for OARO experiments. The OARO process can be analyzed by considering an asymmetric hollow fiber configuration of the module.

Currently, the leading hollow fiber membranes suitable for the OARO process are produced by Toyobo (Japan), whose cellulose triacetate (CTA) hollow fibers have been used extensively in many desalination industries. Toyobo’s pressure retarded osmosis and reverse osmosis hollow fiber membranes can withstand the maximum pressures of up 29 bar and 69 bar under the out-to-in mode (from the shell side to the lumen), respectively. However, the modules pressure drops are considerably high (about 30-60 % of the operative pressure) due to the hollow fibers’ outer selectivity property (the selective layer is on the shell side) and their small dimensions (inner diameter/outer diameter ≅ 80/180 μm). (Liang et al., 2021)

1.5.2 OARO associated costs

All the presented key design considerations need to be elaborated to choose the best OARO configuration in terms of performance and economic feasibility. To understand which might be the proper solution from an economic perspective, it is necessary to investigate the capital and operative costs associated with the OARO process.

Energy consumption is a crucial metric for assessing the adequate performance and the economic feasibility of the process. Thus, it can be useful to give a framework of the energy demand observed for other brine treatment processes. Generally, RO energy consumption ranges from 1 to 2 kWh per m^3 of produced water for brackish water (5 g/L TDS) and seawater (35 g/L TDS) at a 50% recovery (Fritzmann et al., 2007); mechanical vapor compression (MVC) energy consumption ranges from 11 to 25 kWh per m^3 of produced water for seawater (35 g/L TDS) to high salinity brines (150 g/L TDS) at recoveries of 35 to 50% (Shaffer et al., 2013). Instead, in Batholomew et al. (2017) OARO energy consumption is estimated as 2.9 to 3.7 kWh per m^3 of produced water for feed TDS of 60 g/L at 35% and 50% recovery, respectively. At a higher feed TDS of 140 g/L, these values increase to 12.4 and 19.3 kWh per m^3 of produced water for recoveries of 35 and 50%. These estimates account for losses associated with pressure drop across the module, losses in the pressure exchangers and the isentropic efficiency of the high-pressure pump, without accounting for some inefficiencies due to membrane fouling and incomplete utilization of membrane area. In general, the membrane-based processes require less energy demand compared to MVC.

In the configuration presented by Batholomew et al. (2017) the primary energy demand of the OARO process is the one required to power the feed pressure pumps. Pressure exchangers can be employed to lower the energy demand by transferring energy from the high-pressure concentrate streams to the low-pressure feed solutions before they are pumped to the designed pressure. The final goal of using multiple pressure exchangers is lowering the overall energy consumption of the process. Then, as already pointed out, the energy consumption depends also on the number of OARO stages because most of the energy loss in the system is associated with the pressure drop along the membrane stage and inefficiencies of the pressure pumps and pressure exchangers.

Batholomew et al. (2018) observed that the OARO process energy consumption ranges from 5 to 20 kWh per m^3 of product water for feed concentrations between 25 and 150

g/L, and this result can be narrowed to 5-12 kWh per m^3 for economically viable conditions, which is less than the MVC energy consumption range.

Regarding OARO capital costs, membrane cost is the largest component, accounting for 41-53% of total costs, while electricity costs account for 13-23%. The contribution of these components to the total cost for OARO process is different from that of a typical RO process, for which the electricity costs account for 30-40% of the total and membrane costs account for only 15-25% (Bartholomew et al., 2018). The contribution of the membrane costs for OARO is larger because there are usually multiple membrane stages and each of them produces water fluxes of about 1-5 LMH, much lower compared to typical RO fluxes of 10-20 LMH. In a N-stage OARO system, capital costs involve not only the expense for N membrane modules but also the expenses for N high-pressure pumps and eventually N energy recovery devices (Wang et al., 2021). Ultimately, OARO membrane unit costs are expected to be significantly higher compared to current commercialized spiral-wound RO modules, due to the OARO module structural requirements.

Bartholomew et al. (2018) used a nonlinear optimization model to investigate the performance and economic viability of OARO processes over a range of feed salinities and water recoveries in three case studies, with the final goal of identifying the cost-optimal OARO process designs and operating parameters. For all three conditions, it was observed that the optimal inlet feed pressure for the OARO and RO stages is the maximum allowable pressure of 65 and 85 bar, respectively. Moreover, the optimal membrane area was found to decrease by 25-45% for each successive OARO stage and the RO stage has at least 85% less area than the first OARO stage. Moreover, cost optimal OARO operating conditions decrease the feed and sweep flow rates with each successive OARO stage: a lower inlet sweep flow rate enables a higher inlet sweep concentration, which increases the average net driving force and water flux in the stage. This also has the effect of decreasing total membrane area in the stage, which is a significant driver of OARO cost. In fact, the membrane area can be reduced in later stages because lower salinities are less impacted by concentration polarization, resulting in higher water flux.

Thus, optimal OARO operating conditions favor higher sweep flow rates in the initial stages of the OARO process, where the membranes are exposed to higher salinities and concentration polarization has a more negative effect on water recovery and process performance.

In conclusion, the investigation found that the cost-optimal OARO process should involve as few stages as possible, no saline makeup streams, purge from the first sweep cycle and successively decreasing stage membrane area and sweep flow rate. In addition, the system should be operated as close as possible to the burst pressure of the membrane. Future research to minimize OARO costs should focus on minimizing the membrane structural parameter, while maximizing the membrane burst pressure and reducing the membrane unit cost.

1.5.3 Overview of OARO experimental studies

OARO is a recent field of research, which has gained great attention in the past few years. There is ample opportunity to research novel applications, designs and models on this topic. In this sense, there have been several innovative scientific publications on this subject, such as experimental studies on OARO that analyze different configurations, membrane types and operating conditions. The following section is an insight of many investigations and the results obtained are reported to acquire an indication of what the appropriate operating conditions might be and what ranges of water flux can generally be expected from OARO, since it is still a process undergoing development and analysis.

For instance, Nakagawa et al. (2020) performed concentration tests on a multistage OARO system that used two types of hollow fiber membrane modules made from cellulose triacetate (CTA) with different numbers of hollow fibers (HFs), one with 90 HFs and the other with 180 HFs. The same feed solution with sodium chloride was supplied to the shell and bore sides and the concentrated solution was returned to the feed tank and recirculated. Feed solutions contained sodium chloride at 1 M and 2 M with applied pressure of 10 and 15 bar to the shell side.

A ten-stage concentration test was performed using the H180 modules connected in series: the concentration was increased from 1.0 M to 1.12 M at an initial feed pressure of 15 bar and water flux between 1.0 and 1.3 LMH, while the concentration was increased from 1.0 M to 1.042 M in single-stage operation under the same conditions, with a water

flux of 1.17 LMH. This clearly demonstrates that the degree of concentration is enhanced as expected by multistage operation. For the single-stage concentration test the water flux in the H90 module was 1.41 LMH, while the flux in the H180 module was 1.17 LMH, because the initial linear velocity on the bore side was higher for the H90 module compared to that of the H180 module due to the different number of HFs. The concentration difference between the bore side and the shell side is consequently lower in the H90 module than in the H180 module. As expected, the water flux increased linearly with the applied pressure for both HF modules: for the multistage test on H180 module, the flux went from 0.6 LMH at 10 bar to 1.3 LMH at 15 bar. Then, the investigation showed that the water flux decreases with increasing initial feed concentration. For instance, for the multistage test on H180 module, the flux resulted in 1.3 LMH at 15 bar with an initial feed concentration of 1 M and was 0.5 LMH for 2 M of initial feed concentration at the same pressure. This is because the ICP increases with the feed concentration, resulting in a decrease in the effective applied pressure driving force, thereby reducing the water flux under the same externally applied pressure. This limits the degree of concentration achievable by OARO processes and the limit depends on the feed concentration and applied pressure.

These findings make it clear that lower initial feed concentration and higher applied pressure result in a higher degree of concentration.

Also Togo et al. (2019) conducted studies of OARO process using a cellulose triacetate (CTA) hollow fiber membrane module, provided by Toyobo (Osaka, Japan). In this case, the initial concentration of the solution with sodium chloride was adjusted to 0.5 M and 1.0 M. The active layer faced the shell side and the concentrated and diluted solutions were recirculated. The pressure difference across the membrane ranged from 8 to 12 bar. The results demonstrate that performing the OARO process with low applied pressure allowed concentration of solutions with high osmotic pressure up to 50 bar (corresponding to 1.0 M). Also in this case, the higher relative degree of concentration (final concentration divided by initial concentration) was achieved in the case of lower initial solution concentration. In addition, the water flux was found to increase by

increasing the shell-side flow rate and the external applied pressure: in the case of initial feed concentration of 0.5 M, it went from 0.5 to 1 LMH for pressures from 8 to 12 bar and shell-side flow rate from 4 to 10 L/min. Ultimately, water flux decreased while increasing the initial feed concentration: it ranged between 0.3 and 0.5 LMH for 1 M in the feed solution.

Bartholomew et al. (2017) defined a base-case scenario to provide a basis from which is possible to compare other operating conditions: 125 g/L sodium chloride brine is treated to achieve more than 30% freshwater recovery, with the sweep inlet flow rate equal to half the feed. The results predict that four modules are required and the average water flux is 1.3 LMH, with a recovery of 34% and energy consumption of 8.6 kWh per m^3 of produced water. The three OARO modules successively decrease the sweep TDS concentration to 37 g/L, which is sufficiently low to be treated by the final RO module. Using saline sweeps increases the recovery for a given feed concentration and recoveries higher than 30% are obtained for feed concentration up to 145 g/L with sweep TDS up to 200 g/L. The study also provides the results for an OARO module with an inlet feed TDS of 125 g/L across a range of feed pressures (from 0 to 120 bar) and sweep inlet concentrations (from 0 to 250 g/L). For this high salinity feed, RO processes (sweep TDS of 0 g/L) are not capable of recovering any freshwater using membranes with a burst pressure of 70 bar. Therefore, it is necessary to use a saline sweep to obtain higher recoveries at feasible operating pressures. Recoveries above 30% at 70 bar occur only for sweep TDS above 150 g/L. In these instances, the inlet sweep TDS is greater than the inlet feed TDS of 125 g/L, but the feed concentration is greater than the sweep concentration along the membrane since the module operates in counter-current flow.

Liang et al. (2021) developed ultra-strong polymeric thin film composite (TFC) hollow fiber membranes with hydraulic burst pressures of up to 110 bar and NaCl rejection of about 98%. These membranes were tested under the OARO conditions, by circulating sodium chloride solutions with the same concentration at both the lumen and shell sides of the membranes under a counter-current flow mode. A first set of tests were performed using NaCl concentrations ranging from 0.3 to 1.2 mol/L, while the final test used a single NaCl concentration to study the OARO performance varying feed pressures between 10 and 30 bar. The results showed that the water flux declined for all the membranes from about 50 to 2 LMH while increasing NaCl concentration. Specifically, membranes with

larger structural parameters exhibited a lower water flux, since it may take a longer time for the water permeated from the lumen side to mix with the sweep solution diffused from the shell side. In other words, the membrane with a larger structural parameter may suffer from a more severe ICP. On the contrary, ECP may have similar impact for all cases because the flow rates at the shell and lumen sides are kept the same; moreover, ECP declines as the permeate water flux decreases. The final test used a NaCl solution of 0.6 mol/L to study the effects of operating pressure: the water flux increased from the lowest value of 4.4 LMH at 10 bar to the highest one of 24.9 LMH at 30 bar. It is important to notice that the water flux can be further increased by increasing the operating pressure, because these TFC hollow fiber membranes can withstand a hydraulic pressure much higher than 30 bar, which is needed for highly concentrated solutions. However, working at higher hydraulic pressure means that the membrane should have the appropriate burst pressure and this implies having higher structural parameter, which is not preferred for OARO applications, as already explained. Therefore, it can be confirmed that in real OARO applications membrane characterized by a decent burst pressure but a relatively low structure parameter should be chosen.

Ju et al. (2023) presented a laboratory-scale investigation of the OARO process, using a plate-and-frame OARO module and varying many operating conditions, such as applied pressure, feed and sweep concentrations. NaCl concentration in the solutions varied from 30 g/L to 130 g/L and the applied pressure was adjusted from 5 to 20 bar. The first test was performed with feed and sweep concentrations of 50 g/L (osmotic pressure of approximately 44.6 bar) and as the pressure increased, the initial flux increased due to a higher driving force. For example, the initial flux at 5 bar was 3.32 LMH, while that at 20 bar was 12.8 LMH. As the experiment continued, the flux decreased with time due to the dilution effect: initially, the osmotic pressure difference between the feed and sweep solutions was negligible, but it increased over time as the feed was concentrated and the sweep was diluted, resulting in lower water flux. The other tests were performed at 20 bar for different combinations of feed and sweep concentrations, maintaining always 20 g/L of difference between the two. For instance, the flux was initially 6.0 LMH and decreased

to 4 LMH for feed and sweep solutions of 50.0 g/L and 30.0 g/L, respectively. On the other hand, the initial and final fluxes were 0.51 LMH and 0.34 LMH, respectively, when the feed concentration was 130 g/L and the sweep concentration was 110 g/L. In fact, the flux may be different even with the same concentration difference between the feed and sweep due to the concentration polarization.

The initial feed and sweep solutions osmotic pressure ranged from 44.6 to 104.3 bar, which cannot be treated by a conventional RO process at 20 bar. Therefore, although the tests were conducted in a laboratory-scale system in a short period of time, it was experimentally confirmed that the feed solution with high osmotic pressure can be further concentrated by OARO at relatively low pressure. This implies that OARO could be used to reduce the volume of highly concentrated brine, at affordable pressures.

1.5.4 OARO limitations

The effectiveness of OARO process is inevitably limited by several factors, such as:

- Internal and external concentration polarization phenomena;
- Membrane fouling;
- Membrane deformation.

This happens since OARO membranes are exposed to high hydraulic pressures, ideally have a thin substrate to minimize internal concentration polarization (ICP) and are used to treat highly concentrated solutions with impurities. (Peters et al., 2022)

The OARO process, like all membrane filtration processes, is affected by the phenomenon of concentration polarization. A typical concentration profile is depicted in Figures 1.21 and 1.22: it is an asymmetric membrane that has a support layer, so the dilutive ICP and the concentrative ECP occur. Both dilutive and concentrative ECP can be mitigated by altering hydrodynamic conditions, such as increasing turbulence.

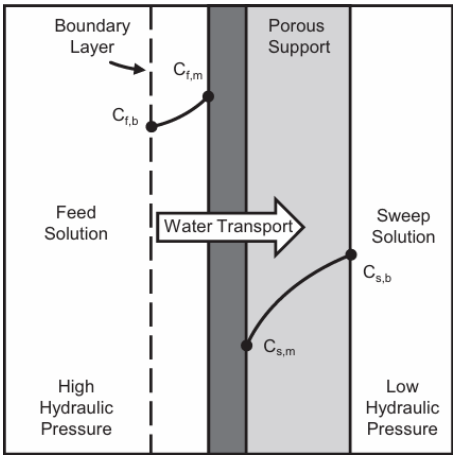

Figure 1.21: *Schematic diagram of an OARO module and the effects of concentration polarization on the solute concentration at the membrane surface (C∗,m) relative to the bulk concentration (C∗,m) of the feed (f) and sweep (s). (Bartholomew et al., 2017)*

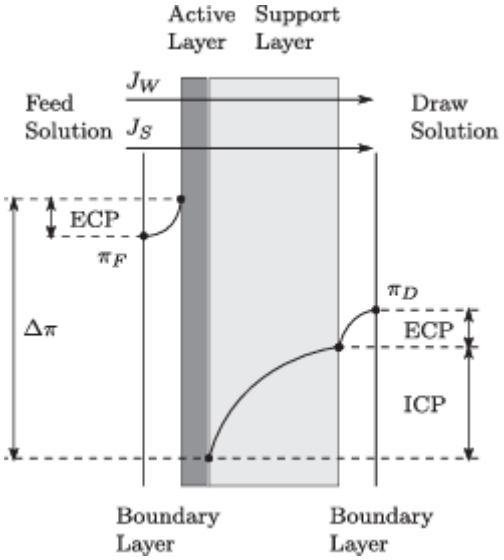

Figure 1.22: *Concentration profile in the OARO process with ICP and ECP. (Peters & Hankins, 2019)*

The OARO system can employ the same feed and sweep solution, which can contain a wide range of contaminant species, both organic and inorganic. These solutions can range from wastewater, seawater to highly concentrated brines. As a result, fouling is very likely to occur on both sides of the OARO membrane. Indeed, in the case of internal membrane fouling (which occurs on the sweep side) there is a risk of pollutants penetrating the porous substrate of the membrane, causing pore clogging.

Under particularly severe fouling conditions, in RO and FO it is possible for the entire membrane surface to become completely covered with contaminants. At this point, the development of fouling becomes independent of the original characteristics of the uncontaminated membrane: after a prolonged period of fouling, water flux tends to stabilize at a pseudo-stable value, termed as “limiting flux”. (She et al., 2017)

Peters et al. (2022) performed a comprehensive study on OARO membrane fouling, testing two commercially available RO membranes considering five different combinations of feed and sweep solutions, setting 50 bar as hydraulic pressure applied. In the first place, the results reported that the water flux for a solution containing only NaCl reduced from 23 LMH to 18 LMH after a 4-h OARO operation. This flux reduction is caused by the increasing transmembrane osmotic pressure difference, as the feed solution was concentrated and the sweep solution was diluted. Then, the study concluded that also for OARO process a limiting flux is observed and it is found to be pressure independent: for a feed solution containing NaCl and other scaling precursors, the initial water flux increased from 10 to 30 LMH when the operating pressure increased from 30 to 60 bar. However, a higher initial water flux is associated with a higher fouling rate and so a steeper flux reduction was observed at higher operating pressures. A limiting flux was observed at approximately 9 LMH for the OARO process, reached for both the 50 and 60 bar experiments.

Regarding scaling, the investigation concluded that in OARO process solute precipitation is mainly expected on the feed side, as the feed solution is continuously concentrated while the sweep is diluted; on the contrary, fouling and scaling are negligible on the sweep side in OARO and cause no significant loss in OARO performance, given that the permeate water flow opposes the accumulation of foulants within the membrane substrate. This finding suggests that membrane fouling is only likely to be a concern on the feed side.

The other important factor limiting OARO process is membrane deformation. In particular, the configuration where the active layer faces the feed solution and the sweep solution comes into direct contact with the porous support layer (AL-FS mode of operation) is necessary to prevent membrane damage by the sweep solution spacer. For this reason, the spacer in the OARO sweep channel must be denser than the feed spacer to prevent membrane deformation under high feed pressures. (Peters C Hankins, 2019)

Generally, to reduce the internal concentration polarization, which hinders the osmotic pressure of the sweep solution, minimizing the structural parameter S can be an option, since dilution of the sweep solution in the support layer is counteracted by the back-diffusion of sweep solute ions towards the active layer. Therefore, membranes with a lower structural parameter S experience less resistance towards ion diffusion and so ICP is less impactful. However, to reduce S, the membrane support layer must be thin, non-tortuous and highly porous, and this results in the reduction of the membrane's structural strength and integrity. Clearly, this is problematic at high hydraulic pressures, because it can lead to severe membrane deformation and eventually to the rupture of the active layer. It can be concluded that the OARO process appears to have some issues for which experimentation and scientific research is deemed useful, to understand what the optimal performance and operating conditions might be, especially towards the implementation of the process on an industrial scale.

1.6 Minimum Liquid Discharge (MLD) and Zero Liquid Discharge (ZLD) approach

The recovery and recycling of wastewater have become increasingly prominent over the last decade, driven by the growing global demand for water (Date et al., 2022). This shift is motivated by the need to minimize the volume of wastewater discharged into the environment and to address the associated ecological risks. By adopting reuse practices, wastewater can be seen as a valuable resource that contributes to the goal of water sustainability. A fundamental approach in this context is the implementation of Zero Liquid Discharge (ZLD) systems. ZLD is a comprehensive wastewater management strategy aimed at eliminating the release of liquid waste beyond the boundaries of industrial facilities or treatment plants (Tong C Elimelech, 2016). It ensures that most of the water is recovered and reused, effectively transforming wastewater into a usable resource. By doing so, ZLD not only prevents the environmental pollution typically associated with wastewater discharge but also optimizes water usage efficiency (Panagopoulos, 2020). In addition, ZLD approach is based on the circular economy

model, which is a modern sustainable development concept promoted by the European Union (Ismail & Matsuura, 2016). The importance of ZLD has become particularly evident in recent years due to the escalating severity of water scarcity and the widespread contamination of aquatic environments. Additionally, several external factors are driving the interest in ZLD technologies. These include stricter environmental regulations, the increasing economic value of freshwater, and the rising costs associated with wastewater disposal (Muhammad Yaqub & Lee, 2019). Together, these factors underscore the potential of ZLD as a critical component of modern industrial wastewater treatment. At its core, the ZLD approach is centered on maintaining a closed water cycle within industrial systems (Tong & Elimelech, 2016). This means that all water within the system is treated and reused wherever possible, ensuring that no water is discharged into the environment. Under the ZLD approach, approximately 100 per cent of the fresh water contained in the effluent is recovered, while the residual salts are converted to a solid form, which can be disposed of in a more environmentally friendly way (Muhammad Yaqub & Lee, 2019). Alongside the ZLD system, the MLD model is gaining increasing attention due to its lower investment costs and energy requirements compared to the ZLD model. In the case of MLD, the goal is to recover up to 95 per cent of the fresh water in the effluent, offering an effective compromise between efficiency and economic sustainability (Panagopoulos & Haralambous, 2020). Both approaches represent significant steps towards a more responsible management of saline wastewater, helping to reduce the environmental impact of industrial activities.

A ZLD system is essentially made up of the following components (Singha et al., 2021):

- Pre-treatment (physicochemical and biological)
- Treatment (membrane processes and thermal processes).

Pre-treatment is performed with processes like chemical precipitation, chemical oxidation and ion exchange. Instead, treatment technologies used in MLD and ZLD systems include numerous brine concentration processes, which can be grouped into two categories: membrane-based and thermal-based (Panagopoulos, 2020). The thermal-based technologies include brine concentrator (BC), brine crystallizer (BCr), multi-stage flash distillation (MSF), multi-effect evaporation (MEE), spray dryer (SD), eutectic freeze crystallization (EFC) and wind-aided intensified evaporation (WAIV) (Panagopoulos &

Haralambous, 2020). Instead, membrane-based technologies include RO, high-pressure reverse osmosis (HPRO), forward osmosis (FO), osmotically-assisted reverse osmosis (OARO), membrane distillation (MD), membrane crystallization (MCr), electrodialysis (ED), electrodialysis reversal (EDR) and electrodialysis metathesis (EDM). Early Zero Liquid Discharge (ZLD) systems were based on thermal processes, in which wastewater was evaporated through a brine concentrator, followed by a crystallizer or evaporation pond (Tong C Elimelech, 2016). The condensed distilled water was recovered for reuse, while the residual solids were disposed of or turned into valuable by-products. However, these systems, which use mechanical vapor compression (MVC) for evaporation, require high investment and energy consumption, making them economically challenging. For this reason, the focus of ZLD technology has been on reducing the volume of concentrated brine entering the brine crystallizers or evaporation ponds. As a result, membrane-based technologies can be used to pre-concentrate the feed solution before undergoing thermal processes, increasing both energy and cost efficiencies of ZLD systems (Muhammad Yaqub & Lee, 2019). For instance, current RO membrane modules cannot operate at very high hydraulic pressure, which typically corresponds to a salinity of ~70 000 mg/L of the RO exit brine. This restriction of RO systems imposes a ceiling on the salinity of water that can be treated by RO in ZLD systems. This salinity limit is much lower than that achieved by brine concentrators (i.e., up to 250 000 mg/L). Thus, a stand-alone RO system is not able to reduce the volume of concentrated brine to the same extent as brine concentrators. Accordingly, in ZLD processes RO can be employed as pre-concentration method, followed by a brine concentrator (Fig. 1.23). (Mickley, 2008)

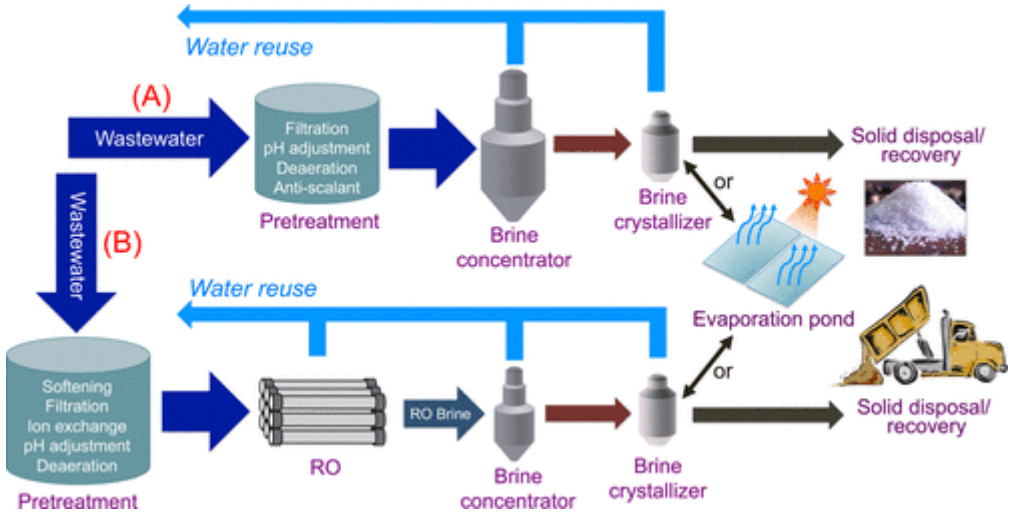

Figure 1.23: *Schematic illustration of (A) thermal and (B) RO-incorporated ZLD systems. Incorporation of RO reduces the volume of wastewater entering the brine concentrator, which consumes much higher energy per volume of treated water than RO. (Tong & Elimelech, 2016)*

Novel membrane-based processes such as membrane distillation (MD), forward osmosis (FO), and electrodialysis (ED) are emerging as alternatives in ZLD systems to achieve further concentration after RO. In these cases, RO brine is further concentrated using these technologies and the produced brine serves as feed to the brine crystallizer or the evaporation pond (Muhammad Yaqub & Lee, 2019). MLD systems are more energy-efficient than ZLD systems, since MLD approach implements only membrane-based technologies (Dupont Water Solutions). In fact, membrane-based technologies use electric energy and have energy consumptions ranging from 1 kWh/m^3 to 19 kWh/m^3 of freshwater produced (Panagopoulos & Haralambous, 2020). Instead, the energy consumption of thermal-based technologies starts at 7.7 kWh/m^3 and can reach up to 72 kWh/m^3 at the crystallization stage (Panagopoulos, 2020), considering also heat losses during evaporation and condensation.

One of the businesses that make the largest use of chemicals and water is the textile industry. Therefore, it has the greatest potential for various intensive chemical recovery and water recycling alternatives. In fact, a large amount of ZLD research has been performed in the field of textile industry wastewater. In general, textile wastewater has high color, high BOD/COD and TDS. Salts are employed in the dyeing process to help in the fixing of colors onto the cloth. Consequently, substantial levels of total dissolved solids (TDS) and chlorides are produced in the effluents, both of which are resistant to

biodegradation (Vishnu et al., 2008). Therefore, conventionally many pre-treatment processes like physical, chemical and biological processes are followed.

Thermal evaporation is often considered an effective method for separating salt and dissolved solids from concentrated solutions and water from dye bath in textile industries (Lin et al., 2023). However, in scientific literature, treatment schemes to treat textile wastewater include a combination of membrane processes, such as MF, UF, RO (Vergili et al., 2012) (Moreira et al., 2022) (Lin et al., 2015). Therefore, ZLD textile treatment plant can use an integrated system of membrane filtration and evaporation to treat the effluent: membrane filtration is used to concentrate the pre-treated waste stream, then the reject is sent to an evaporator and finally the evaporator concentrate is conveyed to a crystallizer or spray dryer (Tamil Nadu Government Portal).

In conclusion, recovery and recycling of wastewater through advanced treatment strategies such as Zero Liquid Discharge (ZLD) and Minimal Liquid Discharge (MLD) represent a transformative step toward achieving sustainable water management. By integrating innovative thermal- and membrane-based technologies, these wastewater management approaches continue to evolve, offering scalable solutions for diverse industrial applications.

1.7 Aim of the Thesis

In the implementation of the ZLD/MLD strategy, innovative membrane processes such as OARO can be employed to maximize freshwater recovery and reduce the brine volumes to be further treated or disposed of. However, OARO process is still a topic under experimentation and analysis, so this technology is not implemented on an industrial scale yet. In fact, the challenge preventing OARO implementation is the lack of experimental data on industrial-scale modules operation. This lack of information significantly limits the in-depth understanding of the process and hinders the possibilities of optimizing it for real industrial applications. In fact, as already presented, currently available studies are mainly based on research conducted at laboratory level or use theoretical models that adopt simplifying assumptions regarding the operating conditions

and performance of the membranes used, thus reducing their ability to accurately represent complex industrial scenarios. Therefore, results obtained at the laboratory level cannot always be directly translated to industrial settings without a significant loss of accuracy. In this context, the lack of empirical data from pilot or industrial plants is a major obstacle to fully implement the OARO process on large-scale. In fact, it is crucial to evaluate the performance of OARO using commercially available membrane modules or dedicated industrially relevant prototypes designed specifically for this process, utilizing a proper mathematical model that can simulate membrane performance, especially in a real industrial configuration.

In this study, a series of experimental tests on a prototype membrane was carried out under the OARO conditions at pilot scale, and the results are collected to gather more information on the process operation and the membrane performance. Then, a simulation of OARO process in a real industrial situation of textile sector is performed, using data obtained from the experimental campaign to properly formulate the mass balances governing the process. Subsequently, the energy requirements of the proposed OARO-based treatment system were estimated and compared to two alternative treatment configurations. The first alternative considered a system relying solely on thermal treatment technology. The second configuration included a hybrid approach, where an ultra-high pressure reverse osmosis (UHPRO) stage was integrated before the thermal evaporator. As previously highlighted, Zero Liquid Discharge (ZLD) strategies can be implemented using exclusively thermal treatment processes or through combined systems that integrate membrane-based filtration with thermal processes. The aim of this study is to analyze and compare the energy efficiency of these different treatment configurations, providing valuable insights into the potential advantages of membrane-assisted ZLD systems over conventional thermal methods.

2 Materials and methods

This chapter sets out in detail the methodological framework that guided the development of the experimental campaign. First, it is essential to develop a comprehensive theoretical discussion of the OARO process, describing the equations regulating the process and the parameters that characterize it. Next, the configuration of the pilot plant specially designed to conduct the experiment is illustrated and described. Finally, the experimental methodology adopted to conduct the tests is described in detail. This includes information on how the experiments were set up and conducted, justifying the choices made, with the aim of providing an overview of the practical stages of the experimental work. So, this discussion provides an understanding of how the methodological choices made contributed to the experimental results and their subsequent interpretation.

2.1 Theoretical framework

Flowrates involved in OARO and the general configuration of the process is depicted in Figure 2.1. (Peters C Hankins, 2019)

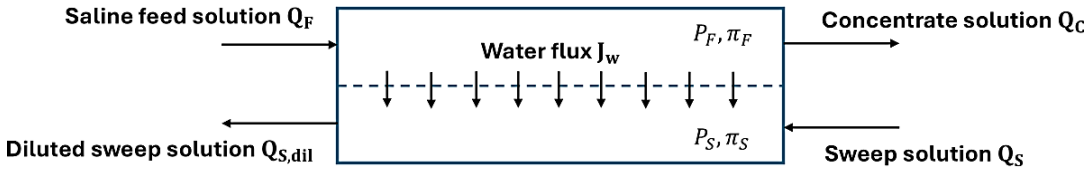

Figure 2.1: *Schematic configuration of OARO process.*

Water flux from the feed solution to the sweep solution in OARO process depends on the hydraulic and osmotic pressure differences across the membrane according to (Beigi et al., 2022):

$$J_w = A \cdot [(P_F - P_S) - (\pi_{F,m} - \pi_{S,m})] \qquad (2.\ 1)$$

where J_w is the water flux ($L/(m^2 \cdot h)$ or LMH); $\pi_{F,m}$ and $\pi_{S,m}$ (bar) represent the osmotic pressure of the feed and the sweep solution on the active layer of the membrane; P_F and P_S (bar) are the hydraulic pressure of the feed solution and the hydraulic pressure

of the sweep solution, respectively; A $(L/(m^2 \cdot h \cdot bar))$ is the pure water permeability coefficient.

Similarly, the salt flux through the membrane J_s $(g_{NaCl}/(m^2 \cdot h)\ or\ gMH)$ is described as (Qasim et al., 2019):

$$J_s = B \cdot (C_{F,m} - C_{S,m}) \qquad (2.\ 2)$$

where $C_{F,m}$ and $C_{S,m}$ (g_{NaCl}/L) are the concentrations of the solute at the active layer of the membrane in the feed and sweep solution side, respectively, and B $(L/(m^2 \cdot h))$ is the salt permeability coefficient.

These equations include the concentration and osmotic pressure of the solute in correspondence of the active layer, which differs from the bulk values because of the significant impact of internal and external concentration polarization in OARO process.

The equations to calculate the concentration at the active layer on both sides of the membrane can be derived from Fick's law and are as follows (Bartholomew et al., 2017):

$$C_{F,m} = C_{F,bulk} \cdot \exp\left(\frac{J_w}{k_f}\right) - \frac{J_s}{J_w} \cdot \left(\exp\left(\frac{J_w}{k_f}\right) - 1\right) \qquad (2.\ 3)$$

$$C_{S,m} = C_{S,bulk} \cdot \exp\left(-J_w\left(\frac{S}{D} + \frac{1}{k_s}\right)\right) + \frac{J_s}{J_w} \cdot \left(-\exp\left(-J_w\left(\frac{S}{D} + \frac{1}{k_s}\right)\right)\right) \qquad (2.\ 4)$$

where S is the structural parameter of the membrane; D $\left(\frac{m^2}{s}\right)$ is the NaCl diffusion coefficient; k_f and k_s $\left(\frac{m}{s}\right)$ are the mass transfer coefficients of the solute in the feed and sweep solution side, respectively.

Considering a spiral wound membrane to perform an OARO process, it is possible to write the global mass balance and the salt mass balance for the two different sides of the membrane, resulting in four equations.

The general formulation of a mass balance is expressed as (Doran, 2013):

$$A = I - O \mp R \quad (2.\ 5)$$

where A in the accumulation term, I and O are the input and output terms, respectively, and R is the chemical reaction contribution, which can be positive for production process and negative for consumption process.

Assuming a steady-state system without accumulation and chemical reaction, the mass balance results in:

$$I - O = 0 \quad (2.\ 6)$$

In the case of OARO, the water and salt fluxes leave the feed side and enter the sweep solution side. Therefore, for the feed side the global mass balance is expressed as (Turetta et al., 2024):

$$Q_F * \rho_F - (J_w * \rho_w + J_s) * Am - Q_C * \rho_C = 0 \quad (2.\ 7)$$

where Q_F and Q_C (L/h) are the volumetric flow rates of the feed and concentrate; ρ_F, ρ_C, ρ_w are the densities (g/L) of the feed, concentrate and pure water respectively; Am is the membrane area (m^2).

The salt mass balance is given as:

$$Q_F * C_F - J_s * Am - Q_C * C_C = 0 \quad (2.\ 8)$$

where C_F and C_C (g/L) are the salt concentrations in the feed and concentrate, respectively.

On the sweep side, the mass balances present opposite signs for the fluxes. The global mass balance is:

$$Q_S * \rho_S + (J_w * \rho_w + J_s) * Am - Q_{S.dil} * \rho_{S.dil} = 0 \quad (2.\ 9)$$

where Q_S (L/h) is the volumetric flow rate of the inlet sweep solution; ρ_S (g/L) is the sweep solution density; $Q_{S.dil}$ is the diluted sweep solution in outlet and $\rho_{S.dil}$ is its density.

The salt mass balance is expressed as:

$$Q_S * C_S + J_s * Am - Q_{S.dil} * C_{S.dil} = 0 \qquad (2.\ 10)$$

where C_S and $C_{S.dil}$ (g/L) represent the salt concentrations in the sweep solution and in the diluted sweep solution, respectively.

2.2 Pilot plant set up

A membrane prototype made by Aquaporin A/S was utilized. The module is a spiral-wound design of standard size 4040, with an area of 4.2 m^2, tested to withstand a maximum pressure of 30 bar. Membrane permeability coefficient is $A = 2.3\ LMHbar$.

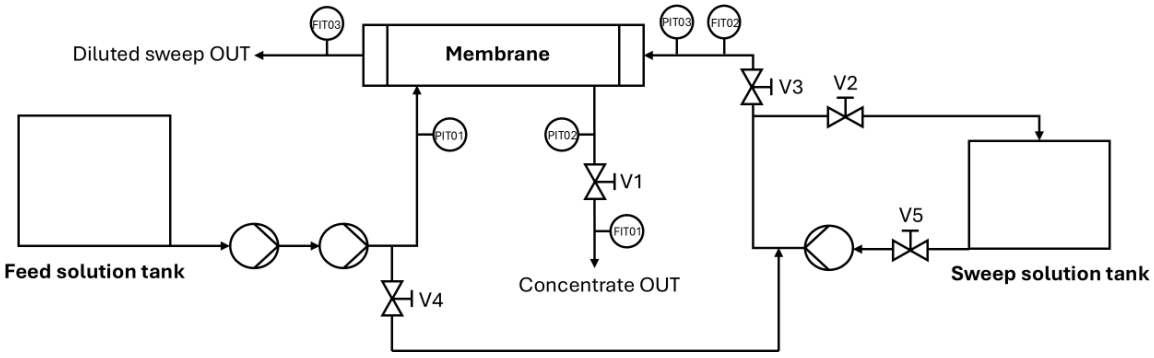

Figure 2.2*: Graphic representation of the pilot plant.*

OARO tests were performed using the pilot plant illustrated in the scheme of Fig. 2.2, designed by Hydrotech Engineering s.r.l. The plant comprises a 1 m^3 tank containing the feed (Q_F), which is delivered to the membrane via two pumps, one at low pressure (up to 5 bar) and one at high pressure (up to 80 bar). The pressure is adjusted by acting on a valve V1 placed in the line of concentrate exiting the membrane, and the concentrate is directed to another 1 m^3 tank.

The inlet and outlet pressure of the membrane on the feed side are measured with pressure gauges PIT01 and PIT02 respectively, while FIT01 (KEYENCE FD-Q) provides the measurement of the concentrate flow rate $Q_C\ (L/h)$.

The sweep solution is contained in a 200 L tank and enters the membrane by means of a pump at the desired flow rate, which can be regulated by acting on the valve V2 in the bypass. The flow rate (Q_S) and pressure of the inlet sweep solution are measured by FIT02

(KEYENCE FD-X) and manometer PIT03, respectively. The pressure displayed by PIT03 is equivalent to the pressure drops that the fluid undergoes as it passes through the membrane on the sweep solution side, since the diluted sweep solution is at atmospheric pressure. Finally, the flow rate of dilute sweep solution ($Q_{S,dil}$) is measured by FIT03 (KEYENCE FD-X) and is collected in another tank for reuse in subsequent tests.

In tests conducted at the same concentration in the feed and sweep solutions ($C_F = C_S$), the inlet pipe of the sweep solution was connected to the 1 m³ feed tank and the process is managed by valves V4 and V5. This arrangement allowed the membrane to be fed using the same tank for both the feed and sweep solutions, thus ensuring uniformity in system operating conditions.

2.3 Experimental methodology

This study investigated the performance of a prototype spiral wound 4040 module for OARO in a pilot plant, using NaCl solutions at various concentrations in the feed and sweep solutions.

An in-depth analysis of a wide range of concentrations and pressures was conducted, with the aim of evaluating performance in contexts of relevance to the application of OARO process. In particular, the experiments focused on exploring concentration ranges above those generally treatable through conventional reverse osmosis (RO) and ultra high-pressure reverse osmosis (UHPRO) systems. This choice was motivated by the desire to expand the limits of conventional technologies in order to gain crucial information about the feasibility of the OARO process under conditions outside the normal treatment limits. This investigation is aimed at determining not only the operational viability but also the effectiveness of OARO in contexts that would traditionally require the use of more complex technologies or larger energy duties. The ultimate goal is to broaden the prospects for the applicability of this innovative technology, opening new scenarios in the field of water treatment at high concentrations.

The process performance was investigated by considering sweep solution concentrations also lower than those of the feed solution: this approach allows a deeper analysis of the limitations associated with external concentration polarization (ECP), thus providing a more comprehensive knowledge on the dynamics of the OARO process.

The experiments were conducted considering:

- Feed concentrations of 58 g/L (1M), 116 g/L (2M), 176 g/L (3M) and 233 g/L (4M);
- Sweep solution concentrations equal to or less than feed solution concentrations;
- Pressures of the feed solution were imposed from 20 up to 28 bar;
- Pressure of the sweep solution was maintained constant at 3 bar, while varying the feed pressure.

Although the concentration of 58 g/L can be treated with conventional RO, exploration of this range is interesting because it allows the two processes to be compared in terms of energy efficiency. Similarly, the concentration of 116 g/L is treated with the ultra high-pressure reverse osmosis (UHPRO) process, but it involves higher costs than conventional RO due to higher energy consumption and the need for more sophisticated equipment to operate at such high pressures (110 bar), consequently it can be relevant to understand whether the OARO process can be a possible option. For solutions in the concentration ranges of 176 g/L and 233 g/L, there are currently no membrane processes developed at industrial scale that are capable of treating them.

The criterion for selecting the concentration of the inlet sweep solution was based on the calculation of the osmotic pressure corresponding to each feed concentration: three different concentrations of the sweep solution were chosen for each feeding condition, considering an osmotic pressure of 20, 15 and 10 bar below that of the feed. In addition, three levels of applied pressure in the feed were examined for each concentration condition: 20, 24 and 28 bar.

Clearly, tests at 20 bar applied pressure were omitted in cases where the osmotic pressure of the sweep solution was 20 bar lower than that of the feed, since it results in no water flux through the membrane. Ultimately, in the cases of feed concentrations equal to 176 g/L and 233 g/L, tests were also conducted using sweep solution at the same concentration of the feed ($C_F = C_S$). Therefore, the experiments were 24 in total.

At the beginning of each trial, the feed and sweep solution tanks are loaded with the amount of salt required to achieve the desired concentration. Once the solutions have been appropriately mixed, the pilot plant is started and the outgoing feed and sweep solutions

are recirculated to the associated inlet tanks to allow the solutions to adjust and equalize. After that, the feed and sweep concentrations of NaCl are measured using a Thermobalance KEN DAB. The procedure involves placing a sample of approximately 10 ml of solution in the balance to completely evaporate the solution by removing all moisture. The residual salt is weighed and the balance calculates the concentration as a mass fraction. Subsequently, the mass fraction is used to calculate the concentration (g/L), the density of the solution, the osmotic pressure and the diffusion coefficient of NaCl, thanks to empirical correlations obtained from fitting experimental data taken from Batholomew et al. (2017).

A resume of the details and operating conditions of the conducted experiments is presented in the following Table 2.1.

Table 2.1: *Feed and sweep solutions characteristics and operating conditions of the OARO experiments.*

C feed in (g/L) (target)	C sweep in (g/L) (target)	P feed in (bar)
58	35	24
		28
	40	20
		24
		28
	46	20
		24
		28
116	94	28
	102	20
		24
		28
	106	20
		24
		28
176	163	20
		24
		28
		20

C feed in (g/L) (target)	C sweep in (g/L) (target)	P feed in (bar)
	176	24
		28
233	233	20
		24
		28

The water flux is calculated from the material balance applied to the side of the sweep solution (Eq. *2.9*). The salt rejection of the membrane used in the experiments is very high, so it can be assumed that $J_s \ll (J_w * \rho_w)$, so the balance becomes:

$$Q_S * \rho_S + J_w * \rho_w * Am - Q_{S.dil} * \rho_{S.dil} = 0 \qquad (2.\ 11)$$

Where the product of J_w and Am represents the net permeate flow rate through the membrane (Q_P), which can thus be calculated as:

$$Q_P = \frac{Q_S * \rho_S - Q_{S.dil} * \rho_{S.dil}}{\rho_w} \qquad (2.\ 12)$$

Therefore, the water flux is calculated as:

$$Jw = \frac{Q_P}{Am} \qquad (2.\ 13)$$

The feed flow rate is then obtained by:

$$Q_F = Q_C + Q_P \qquad (2.\ 14)$$

Considering the same density for the solutions.

In the described configuration of the pilot plant, the sweep solutions in and out of the system were registered during the operation: in this way, it was possible to calculate the permeate flowrate and, therefore, the water flux.

3 Experimental results

The prototype membrane, inserted in the described pilot plant, was tested by performing OARO experiments under the operating conditions shown in Table 3.1. Data from the experiments conducted are exposed and discussed to fully analyze the performance of the membrane and the OARO process.

3.1 Set of experiments with saline solutions: results and discussion

Data resulting from experiments with saline solutions are presented. Each test had a variable duration, necessary to reach the steady-state condition. The experimental operating conditions and results are presented in the Table 3.1. The values reported for each test represent an average of the last recorded point results over time, in correspondence of which the net permeate resulted a constant value. Standard deviations are also included. Finally, Figures 3.1, 3.2, 3.3 and 3.4 show water flux results depending on the feed pressures for each feed and sweep condition.

Table 3.1: *Results of the OARO experiments.*

C_F target (g/L)	C_F measured (g/L)	C_S measured (g/L)	$P_{F,avg}$ (bar)	J_w (LMH)	Q_S (L/h)	$Q_{S,dil}$ (L/h)	$Q_{P,net}$ (L/h)	Q_F (L/h)	Q_C (L/h)	Dilution (%)
58	58,62	34,81	24	1.84	127.88	135.22	7.34	934.83	927.49	5
				± 0.375	± 0.756	± 0.744	± 0.138	± 0.415	± 0.525	
			28	2.75	112.63	123.63	11	923.72	912.72	9
				± 0.299	± 0.540	± 0.655	± 0.148	± 1.877	± 2.025	
		38,06	20	1.90	129.91	137.51	7.60	949.78	942.17	6
				± 0.086	± 0.147	± 0.197	± 0.285	± 0.983	± 1.063	
			24	2.67	120.48	131.18	10.70	938.07	927.37	8
				± 0.284	± 0.478	± 0.657	± 0.251	± 0.515	± 0.430	
			28	3.81	112.54	127.77	15.24	927.04	911.80	12

C_F target (g/L)	C_F measured (g/L)	C_S measured (g/L)	$P_{F,avg}$ (bar)	J_w (LMH)	Q_S (L/h)	$Q_{S,dil}$ (L/h)	$Q_{P,net}$ (L/h)	Q_F (L/h)	Q_C (L/h)	Dilution (%)
				± 0.363	± 0.690	± 0.762	± 0.100	± 0.821	± 0.808	
		46,72	20	3.52	146.94	161.02	14.08	948.23	934.15	9
				± 0.139	± 0.323	± 0.232	± 0.229	± 0.812	± 0.907	
			24	4.43	132.11	149.81	17.70	936.09	918.39	12
				± 0.428	± 0.721	± 0.990	± 0.269	± 0.311	± 0.042	
			28	4.59	95.52	113.87	18.36	923.91	905.55	16
				± 0.288	± 0.536	± 0.615	± 0.122	± 1.326	± 1.263	
116	116,57	93,94	28	1.21	91.60	96.43	4.83	892.07	887.24	5
				± 0.095	± 0.375	± 0.007	± 0.382	± 0.354	± 0.735	
	118,31	101,87	20	0.93	133.23	136.96	3.73	920.85	917.12	3
				± 0.300	± 0.653	± 0.545	± 0.110	± 0.830	± 0.910	
			24	1.36	118.11	123.55	5.44	905.20	899.76	4
				± 0.031	± 0.096	± 0.029	± 0.125	± 0.950	± 0.997	
			28	1.69	100.25	107.01	6.76	891.66	884.90	6
				± 0.246	± 0.441	± 0.542	± 0.122	± 0.573	± 0.694	
	116,57	106,04	20	1.50	113.78	119.78	6.00	918.91	912.91	5
				± 0.162	± 0.419	± 0.229	± 0.318	± 1,577	± 1,627	
			24	1.54	108.86	115.02	6.16	904.16	898.00	5
				± 0.149	± 0.271	± 0.326	± 0.151	± 0.900	± 1.046	
			28	1.91	96.46	104.10	7.64	891.52	883.89	7
				± 0.102	± 0.199	± 0.210	± 0.091	± 0.934	± 0.853	
176	176,58	163,11	20	1.00	98.76	102.76	4.00	897.06	893.05	4

C_F target (g/L)	C_F measured (g/L)	C_S measured (g/L)	$P_{F,avg}$ (bar)	J_w (LMH)	Q_S (L/h)	$Q_{S,dil}$ (L/h)	$Q_{P,net}$ (L/h)	Q_F (L/h)	Q_C (L/h)	Dilution (%)
				± 0.269	± 0.597	± 0.478	± 0.160	± 0.510	± 0.359	
			24	1.15	87.48	92.09	4.61	882.13	877.52	5
				± 0.155	± 0.256	± 0.366	± 0.110	± 0.182	± 0.263	
			28	1.38	75.80	81.33	5.54	867.79	862.25	7
				± 0.066	± 0.138	± 0.126	± 0.225	± 1.678	± 1.492	
		176,58	20	1.48	105.15	111.08	5.93	891.58	885.65	5
				± 0.053	± 0.159	± 0.054	± 0.167	± 0.843	± 0.995	
			24	1.75	92.20	99.19	6.98	879.19	872.20	7
				± 0.117	± 0.232	± 0.238	± 0.055	± 1.590	± 1.571	
			28	2.05	78.25	86.45	8.20	869.54	861.34	9
				± 0.096	± 0.123	± 0.261	± 0.191	± 0.504	± 0.436	
233	230,73	230,73	20	1.07	89.16	93.44	4.28	874.01	869.73	5
				± 0.098	± 0.172	± 0.221	± 0.070	± 0.379	± 0.318	
			24	1.14	80.81	85.36	4.55	860.17	855.62	5
				± 0.118	± 0.278	± 0.194	± 0.265	± 1.280	± 1.253	
			28	0.95	72.67	76.47	3.81	846.43	842.62	5
				± 0.375	± 0.707	± 0.295	± 0.742	± 0.526	± 0.015	

Figure 3.1 presents the flow results with concentration in the feed equal to 58 g/L (1 M). In general, the fluxes have an increasing trend as applied pressure and sweep concentration rise. Consequently, the maximum flux recorded is equivalent to 4.59 LMH for sweep concentration of 46 g/L and applied pressure of 28 bar; on the other hand, the

minimum flux is 1.84 LMH for sweep concentration of 35 g/L and applied pressure of 24 bar.

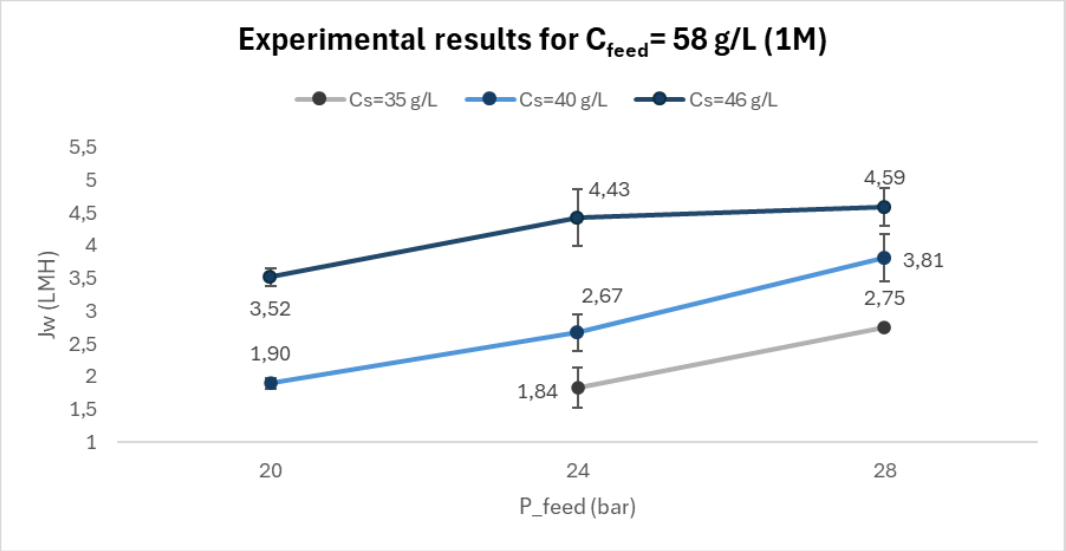

Figure 3.1: *Experimental results of OARO process on prototype membrane for* $C_{feed} = 58\ g/L\ (1\ M)$.

As shown in Figure 3.2, in the case of feed concentration of 116 g/L (2 M) the fluxes are overall lower compared to the 1 M feed condition. In addition, the results from one sweep condition to the next have closer values than in the previous case where the fluxes vary over a wider range. In this case, the largest flux is 1.90 LMH and is clearly recorded for higher sweep concentration and applied pressure, corresponding to 106 g/L and 28 bar.

Again, tests at 94 g/L and pressures of 20 and 24 bar were excluded because they resulted in no or negligible flux.

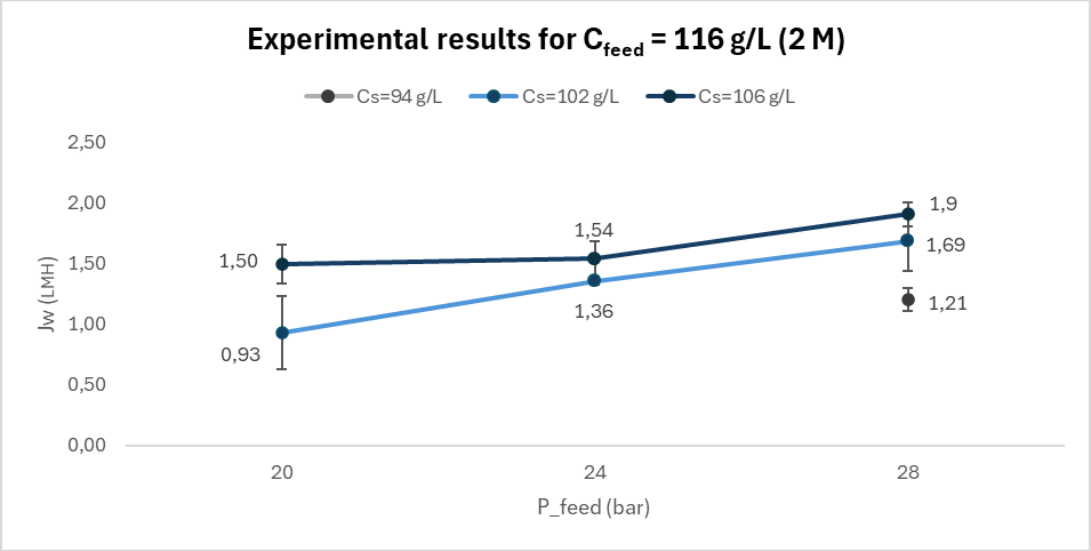

Figure 3.2: *Experimental results of OARO process on prototype membrane for* $C_{feed} = 116\ g/L\ (2\ M)$.

In the case of feed concentration of 176 g/L (3 M), the fluxes are quite comparable to those of 2 M case in the feed (Fig. 3.3). The maximum flux obtained is 2.05 LMH, which is higher than that of the previous condition. Only two sweep solutions were used: $C_S = 163\ g/L$ which is equivalent to 15 bar osmotic pressure difference with the feed; $C_S = 174\ g/L$ with which no $\Delta\pi$ is associated because it is the same concentration as the feed.

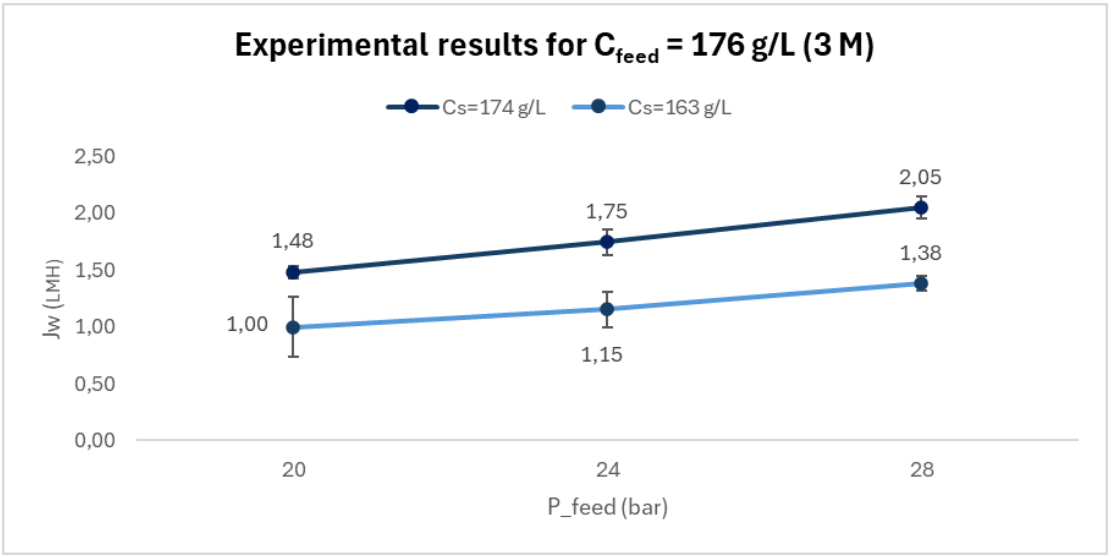

Figure 3.3: *Experimental results of OARO process on prototype membrane for* $C_{feed} = 176\ g/L\ (3\ M)$.

In Figure 3.4 the results obtained for feed concentration of 233 g/L (4 M) are presented. The water flux is around 1 LMH for all the feed pressures. At 28 bar, the flux is 0.95 LMH, which is less than the flux at the other pressures applied. However, the results obtained are generally affected by error since they are average values over time. So, since there is some relevant fluctuation in the flow result at 28 bar, it can be considered that the flux trend from 20 to 28 bar remains upward or stable at 1 LMH.

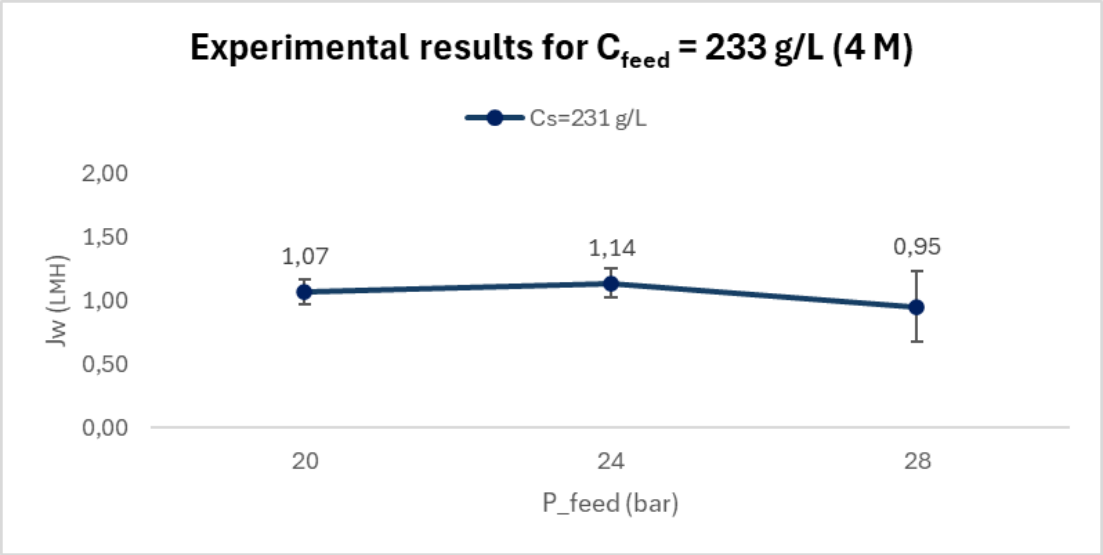

Figure 3.4: *Experimental results of OARO process on prototype membrane for* $C_{feed} = 233\ g/L\ (4\ M)$.

First, it must be pointed out that during the execution of the experiments it was not possible to fully reach a steady-state regime. This limitation arose because the pilot plant was designed without recirculation in the system, restricting the duration of each test to a maximum of 20 minutes per condition. In the configuration with recirculated flows, the system temperature increases because the operating pumps transfer heat to the flowing fluids and the osmotic pressure is affected by the temperature change. In addition, with recirculating solutions the concentration values in the streams fluctuate. In contrast, with the configuration adopted the temperature remains stable and the concentrations do not vary, allowing more accurate results to be obtained. Thus, the limitation of the system without recirculation is the reduced duration of the experiments. As a result, although it was not possible to reach a complete steady-state, a trend towards steady-state behavior

was observed, consisting in a very slow and gradual decrease in the permeate flow rate and quite stable water flux.

For this reason, the experimental results presented are derived as average values from the final set of data points, where the system had stabilized and exhibited a clear tendency to approach a steady-state condition. Therefore, it is important to note that a further gradual variation in the permeate flow rate is expected if the system had been allowed to operate for a longer period, since the trend observed suggests that this would occur over time.

Going into more detail about the results obtained, under every feed concentration condition positive flow ranging globally from 1 to 4 LMH was observed: for feed concentrations of 1 M and 2 M the flux varies from about 2 to 4 LMH, with a maximum flux of 4.59 LMH for feed at 1 M and sweep concentration of 46 g/L at 28 bar; for feed at 3 M and 4 M the fluxes were comprised between 1 and 2 LMH. The results obtained are particularly encouraging and provide a clear indication of the potential offered using OARO membrane technology for highly concentrated solutions.

Overall, increasing the pressure applied to the feed significantly increases the transmembrane water flux, as expected from a pressure-driven membrane filtration process. An increasing tendency of water flow is obtained under all conditions, which suggests that to achieve high water fluxes and narrow membrane areas, the most reasonable option is to operate at feed pressures of 28 bar, considering that the higher costs are represented by the membrane manufacturing. However, it is important to notice that in the feed concentration condition of 233 g/L (4 M), the water flow remains fairly stable at 1 LMH, despite the pressure increasing from 20 to 28 bar. This suggests that for high concentrations, water transport across the membrane is limited despite higher applied pressures by other factors, such as concentration polarization that has a major impact.

Moreover, at constant feed concentration, higher sweep concentration further boosts the water flux, as expected from equation *(2.1)*: higher concentrations in the sweep side of the membrane decrease the osmotic pressure difference between the two solutions, making water transport easier.

It can be noticed from the results that maintaining a consistent osmotic pressure difference between feed and sweep solutions, the cases with higher feed concentration reported a lower water flux. For instance, in the case where the feed is at 116 g/L and the sweep is

at 102 g/L the osmotic pressure difference turns out to be 15 bar and the corresponding water flow is 1.36 LMH for a pressure applied to the feed of 24 bar; in the case where the feed concentration is 176 g/L, considering the same osmotic pressure difference and feed pressure, the water flow decreases to 1.15 LMH. Or again, for a feed at 58 g/L and a sweep at 35 g/L (resulting in an osmotic pressure difference of 20 bar) at 28 bar the water flux is 2,75 LMH, which is reduced to 1,21 for the same osmotic pressure difference but the feed at 116 g/L. This behaviour is attributable to the concentration polarization phenomenon, which becomes more pronounced as the concentration in the feed solution increases. The results suggest that although the difference in osmotic pressure between the two sides of the membrane remains the same, the water flux decreases at higher concentrations due to a more impactful increase in effective osmotic pressure near the membrane surface.

The sweep flow rate depends on the pressure applied to the feed side and to the sweep side, which was consistently maintained at 3 bar throughout all experiments. The results from Table 3.1 clearly show that the sweep flow rates decrease as the pressure applied to the feed side increases, even though the sweep pressure remains constant. This behavior could be attributed to the progressive compression of the membrane module, which reduces the available space for the passage of the sweep solution, leading to a decrease in the sweep flow rate. This phenomenon suggests that the compression of the membrane module under higher feed pressures directly impacts the global system performance.

In general, the phenomenon that affects spiral wound membranes is telescoping, which occurs when the different layers of the wound membrane move or compress irregularly along the longitudinal axis of the module due to hydraulic pressure and fluid flow.

Indeed, the membrane and its supports are wrapped around the central permeable tube, forming a compact and uniform structure. However, if the pressure applied to the system is excessive or poorly distributed, progressive displacement or elongation of the different layers of the membrane may occur, causing a telescopic stretch of the structure. This can damage the module, lead to inefficiencies in the process, increase propensity for fouling and reduce membrane life. Thus, telescoping depends on the membrane structural feature

that can adversely affect the efficiency of the membrane filtration process and may require preventive measures, such as proper control of operating pressure and proper installation of the module. Halfway through the experimental research, the membrane was removed from the vessel for a structure inspection and the first hint of telescoping was found. Thus, despite the promising results of membrane performance, the physical limitations of the operation must be considered because they may prove to be a critical factor in the process. Another issue that can be crucial for the OARO process is the sweep solution excessive dilution. Experimental results report that sweep flow rates are between 70 L/h and 120 L/h, compared to feed flow rates which are between 850 L/h and 950 L/h. Having low flow rates of the sweep solution compared with those of the feed stream results in early and gradual dilution of the sweep solution along the membrane. Such dilution reduces the effectiveness of the OARO process, since the gradual increase in transmembrane osmotic pressure difference reduces the passage of water. Consequently, as the sweep solution dilutes, the ability to maintain an adequate osmotic pressure difference is compromised, resulting in reduced water flux.

In conclusion, the experimental results demonstrate the potential of OARO technology for treating highly concentrated solutions, offering promising water fluxes under various operating conditions. However, the study also highlights critical factors that need to be overcome to optimize the process. These include the impact of concentration polarization, telescoping of the membrane structure under high pressures and dilution of the sweep solution, all of which can adversely affect system performance. Future work should focus on addressing these challenges to maximize the efficiency and reliability of the OARO process in industrial-scale applications.

3.2 Comparison between two membrane prototypes under OARO conditions at pilot-scale

Turetta et al. (2024) presents an experimental study which investigates the performance of a prototype spiral wound membrane similar to the current one but with different characteristics, such as permeability of 4.4 LMHbar and module area of 3.5 m^2. Instead, the operating conditions are the same and the structure of the pilot plant is very similar. The results of Turetta et al. (2024) are obtained in steady-state condition and indicate that the water fluxes are comparable to those of the present study: they vary globally from 1

to 3 LMH, with maximum fluxes of 3.36 and 3.91 LMH under the conditions of feed concentration of 1 M and sweep concentration of 40 and 46 g/L, respectively, at pressure 28 bar.

For instance, in the case of 2 M in the feed and 106 g/L in the sweep solution at 28 bar, the flux obtained from the previous membrane is 1.89 LMH, comparable to the flux obtained with this prototype of 1.90 LMH. For sweep concentration of 102 g/L, the flux obtained with this prototype is 1.69 LMH, while in Turetta et al. (2024) it is 1.88 LMH. Similarly, in the case of 3 M in the feed, at a pressure of 28 bar and sweeps of 163 and 176 g/L, fluxes of 1.49 and 1.95 LMH are obtained, respectively, comparable to 1.38 and 2.05 LMH in the present case. Finally, in the case of 4 M in the feed, the flux at 28 bar was found to be 1.31 LMH, whereas in this case it is about 1 LMH.

It is important to notice that the sweep flow rates obtained in Turetta et al. (2024) range from 30 to 50 L/h, while in this case they range from 90 to 140 L/h, about three times higher. This represents an advantageous result of the membrane performance, which allows the transport of higher sweep flow rates. Figures 3.5(A), 3.5(C) and 3.5(E) show the diluted sweep flow rates comparison between the membrane prototype used in Turetta et al. (2024) (denominated "Prototype 1") and the module used in the current investigation (referred to as "Prototype 2") in three operative conditions: $C_F = 58\ g/L$ and $C_S = 46\ g/L$, $C_F = 116\ g/L$ and $C_S = 106\ g/L$, $C_F = C_S = 176\ g/L$. Clearly, flow rates decrease while increasing the operative pressure and for Prototype 2 the reduction is greater. Moreover, diluted sweep flow rates decrease with more concentrated feed solutions.

Having higher sweep flow rates is advantageous because it reduces the sweep dilution effect. In fact, the same permeate flow rates dilutes more a reduced sweep solution rather that a higher one, leading to the aggravation of filtration performance. On the contrary, if the dilution effect is reduced by means of higher sweep flow rate, the osmotic pressure difference between the two membrane sides remains uniform for a larger area, resulting in higher permeate flow rate and better OARO performance.

The impact of water fluxes on sweep solution dilution is very different between the two membrane prototypes. In general, in the case of the Turetta et al. (2024) prototype, dilution rates vary globally in the range of 10 to 40 percent, whereas for Prototype 2 they are between 3 and 10 percent. The dilution effect on sweep solutions is properly shown in Figures 3.5(B), 3.5(D) and 3.5(F), which represent the comparison between the dilution rates of the two membrane prototypes under $C_F = 58\ g/L$ and $C_S = 46\ g/L$, $C_F = 116\ g/L$ and $C_S = 106\ g/L$, $C_F = C_S = 176\ g/L$. For both prototypes, the greater dilution is registered for $C_F = 58\ g/L$ and $C_S = 46\ g/L$, ranging from 19 to 38 % for Prototype 1 and from 9 to 16 % for Prototype 2. The lower dilution rates are obtained for $C_F = 116\ g/L$ and $C_S = 106\ g/L$, ranging from 12 to 23 % for Prototype 1 and from 5 to 7 % for Prototype 2, and these results are very similar to those of the last operative condition ($C_F = C_S = 176\ g/L$). Thus, the reduction in the efficiency of the OARO process due to dilution is less significant for Prototype 2.

It is important to note that Prototype 2 has a permeability that is half that of Prototype 1. This means that the membrane performance is limited by its structural characteristics, although the results are promising. In fact, in the conditions of $C_F = 58\ g/L$ and $C_S = 46\ g/L$, the improvement of the dilution effect can be said to be significant between Prototype 1 and 2 (from 38 % to 16 % at 28 bar) and this consequently led to a beneficial improvement in water flux (from 3.90 LMH to 4.60 LMH at 28 bar), despite the membrane permeability of Prototype 2 being half. This indicates that Prototype 2 design can compensate for structural limitations under those operating conditions. In contrast, in the other cases, the differences in dilution rates between the prototypes did not translate into significant variations in water fluxes, suggesting that other factors, such as membrane structural characteristics, may limit performance under these scenarios.

In conclusion, these findings highlight the importance of balancing membrane design parameters with operational conditions to optimize OARO performance. The results for Prototype 2, despite its lower permeability, demonstrate promising potential for further development and refinement.

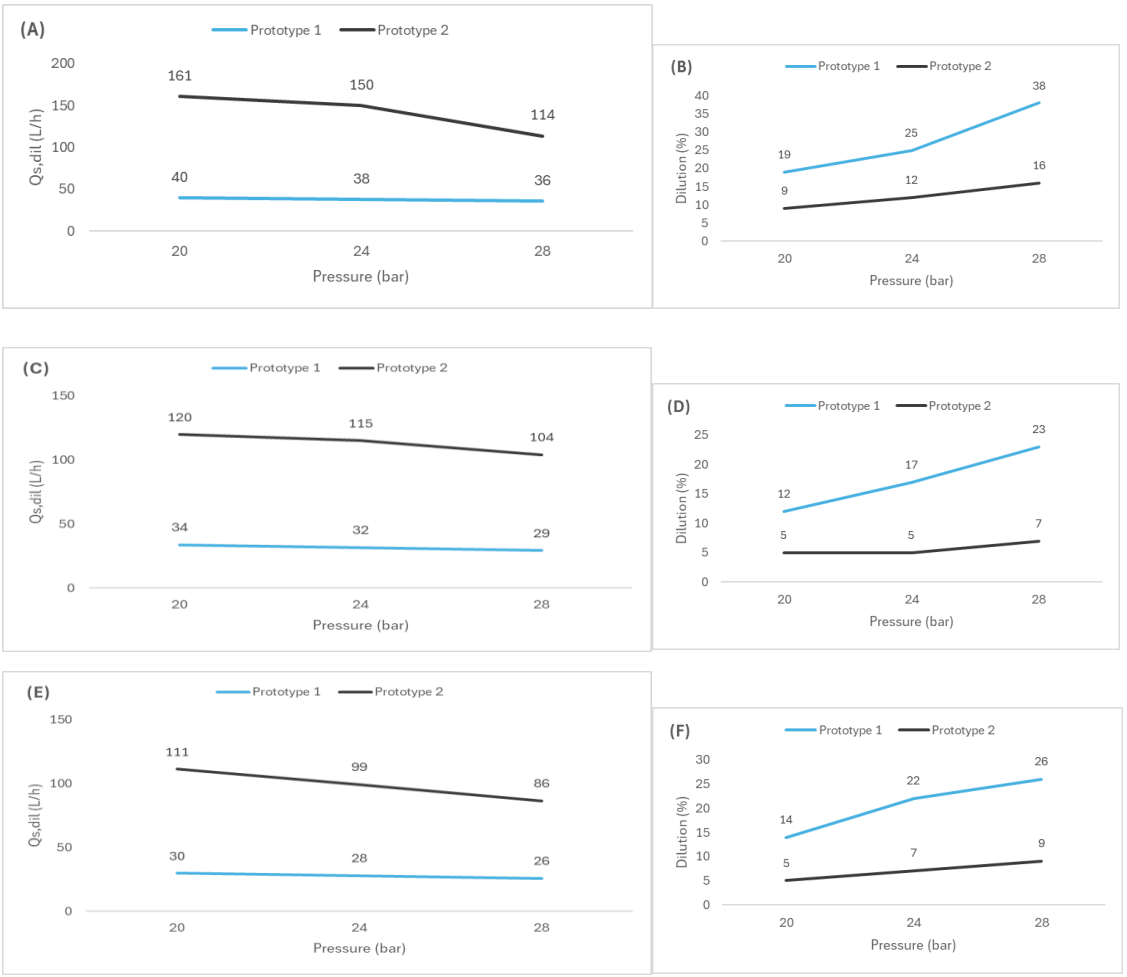

Figure 3.5: *(A) Comparison of diluted sweep profiles for $C_F = 58\ g/L$ and $C_S = 46\ g/L$. (B) Comparison of dilution rates for $C_F = 58\ g/L$ and $C_S = 46\ g/L$. (C) Comparison of diluted sweep profiles for $C_F = 116\ g/L$ and $C_S = 106\ g/L$. (D) Comparison of dilution rates for $C_F = 116\ g/L$ and $C_S = 106\ g/L$. (E) Comparison of diluted sweep profiles for $C_F = 176\ g/L$ and $C_S = 176\ g/L$. (F) Comparison of dilution rates for $C_F = 176\ g/L$ and $C_S = 176\ g/L$.*
Prototype 1 is the membrane module used in Turetta et al. (2024) and Prototype 2 is the membrane module used in the current investigation.

Sweep solution dilution is also influenced by membrane compression under high pressures, which affected both the modules. With the use of a membrane that is less prone to deformation, even higher sweep solution flow rates could therefore be achieved, overall improving the efficiency of the process. Therefore, from the experimental analysis of the performance of both membrane modules, it can be concluded that the key prerogative is to develop a membrane structure such that it provides greater resistance to deformation,

allows the transport of greater sweep flow rates to reduce the dilution problem, and has a good permeability to achieve higher water flux and, consequently, a better performance.

4 OARO process simulation on an industrially relevant case study

The OARO process analyzed through the experiments conducted on the pilot plant is now simulated for the treatment of a real industrial effluent from the textile sector. For this purpose, a configuration of the OARO process specifically adapted to the objectives imposed by the real case study is proposed. The simulation is based on the results obtained during the experimental tests and the initial characteristics of the effluent to be treated. The OARO analysis is performed using a series of mass balances and constraints equations to describe the system. The main objective of the simulation is to identify the design specifications that will achieve the performance target imposed by the industrial scenario under consideration. Then, the energy requirement of the proposed treatment system is estimated and is compared with other two system configurations, one including only the thermal treatment and the other including an ultra-high pressure reverse osmosis (UHPRO) stage before the evaporation step. Indeed, traditional thermal methods for concentrating brines involve intensive energy consumption, so it is useful to analyze a system in which less energy-consuming processes such as OARO or UHPRO are integrated. Ultimately, comparing OARO and UHPRO processes is necessary to understand which of them is more energy efficient.

4.1 Comparison between OARO and UHPRO processes for water desalination

The maximum operating pressure for a standard seawater RO membrane is typically around 80 bar to achieve a concentrated brine with osmotic pressure of about 60 bar (corresponding to ~70,000 mg/L) (Fritzmann et al., 2007). This pressure limitation prevents RO from achieving economically viable product water recovery for feed waters with higher salinity than seawater. Therefore, hypersaline brines (≥70,000 mg/L) can usually be treated via thermal processes. Thermal technologies are used to concentrate brine streams to approximately 250 000 mg/L ($\pi \cong 290$ bar) (Chen et al., 2019). To reach these targets, these technologies typically imply high capital costs (CAPEX) and

especially high operating costs (OPEX), due to the large energy required to perform the process. (Muhammad Yaqub & Lee, 2019)

As already explained, with recent developments in RO process research, OARO is one of the innovative processes designed to treat high salinity brines. Another option is the ultra-high pressure reverse osmosis (UHPRO), performed with specific spiral wound membranes capable of withstanding 120 bar of hydraulic pressure. In fact, UHPRO process is increasingly being used in industrial effluents treatment processes for Zero Liquid Discharge (ZLD) and Minimal Liquid Discharge (MLD) applications. (Davenport et al., 2021)

While OARO generally concentrates brines up to 200,000 mg/L of TDS, the UHPRO process enables the concentration of highly concentrated solutions up to 130,000 mg/L of TDS for NaCl, which means a 50% decrease in brine volume produced compared to the conventional RO process (Lenntech Water Treatment). Typical brine concentration limits and volume reduction ratios are summarized in the following Figure 4.1.

Technology	TDS brine limit (mg/L)	Brine Volume Reduction relative to SWRO
SWRO (1,200 psi)	80,000	1.0x
UHPRO	130,000	1.6x
Evaporator (thermal/MVR)	220,000	2.8x

Figure 4.1: *TDS concentration limits and concentrate volume reduction ratios of seawater RO, ultra-high pressure RO and thermal treatment. (Lenntech Water Treatment)*

This results in more freshwater being produced and so less brine to be further treated with thermal technologies. In addition, the capital cost of UHPRO systems is higher than the cost of brackish or seawater RO systems but is much lower compared to the cost of thermal evaporators. Davenport et al. (2018) observed that due to the inherent efficiency of membrane-based processes, UHPRO is expected to consume from 2 to 3 times less energy for brine treatment than state-of-the-art thermal technologies (Fig. 4.2). Therefore, UHPRO or OARO can be applied upstream of evaporators to reduce the latter's size, thereby lowering the CAPEX and OPEX of the thermal process. The advantage is that far

less thermal brine concentration is needed to achieve the same ZLD and MLD treatment objectives. (Panagopoulos C Haralambous, 2020)

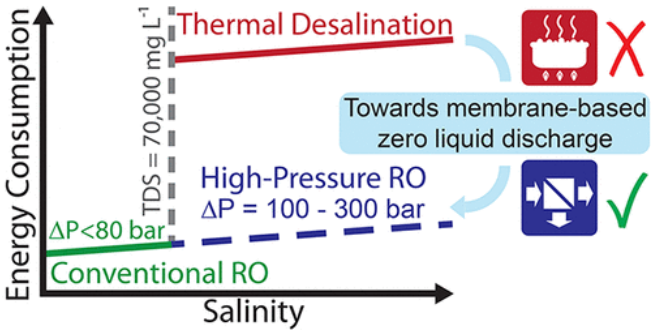

Figure 4.2: *Energy consumption profile in function of solution salinity for conventional RO, UHPRO and thermal treatment. (Davenport et al., 2018)*

In the scientific literature, there are not many studies testing UHPRO process, since membranes structured to withstand such high hydraulic pressures are required. It appears that seawater RO water fluxes (10-20 LMH) should theoretically be attainable for UHPRO, despite the increased concentration polarization due to the high feed osmotic pressure. Moreover, one of the crucial unknown aspects of UHPRO is the effect of membrane compaction on process performance at high pressure. At present, only a few studies have assessed RO above 100 bar, and decreased water permeability was observed at high pressure and it was attributed to compaction. (Davenport et al., 2020)

Both OARO and UHPRO technologies enable membrane-based treatment of more concentrated brines and provide brine volume reduction, reducing the capacity required for downstream thermal treatment. Therefore, even if evaporators can generally achieve higher brine concentrations and produce relatively low volumes, for larger flow rates a combination of these technologies can be the most economically feasible solution.

4.2 Case study: wastewater treatment plant description

The case study focuses on the treatment of a wastewater originating from one of the largest textile manufacturers in India. The process, shown in Figure 4.3, is developed by Hydrotech Engineering srl. Treatment begins with an equalization phase, where the incoming flow is homogenized to stabilize its characteristics and reduce fluctuations that could negatively impact the efficiency of the subsequent stages. The flow

is then directed to a biological treatment unit, where microorganisms degrade the organic matter present in the wastewater. After the biological treatment, the outgoing flow is subjected to microfiltration followed by ultrafiltration, to remove suspended particles and larger impurities. The flow then passes through the softening unit, where the concentration of hard ions, such as calcium and magnesium, is reduced to prevent scaling and ensure the efficiency of the downstream processes. At this point, the flow is divided into two streams. One portion, which contains a high TDS concentration but a low amount of colorants, is directed to the regeneration step to recover and reuse resources from the wastewater, followed by the evaporation and drying unit; the other portion continues to the reverse osmosis unit, where it undergoes further purification by separating dissolved substances from the flow. The concentrate produced in the reverse osmosis unit is finally sent to the evaporation and drying unit. In this final stage, the remaining water is removed, leaving a concentrated product that can either be disposed of in a controlled manner or potentially recovered, depending on operational needs and regulatory requirements.

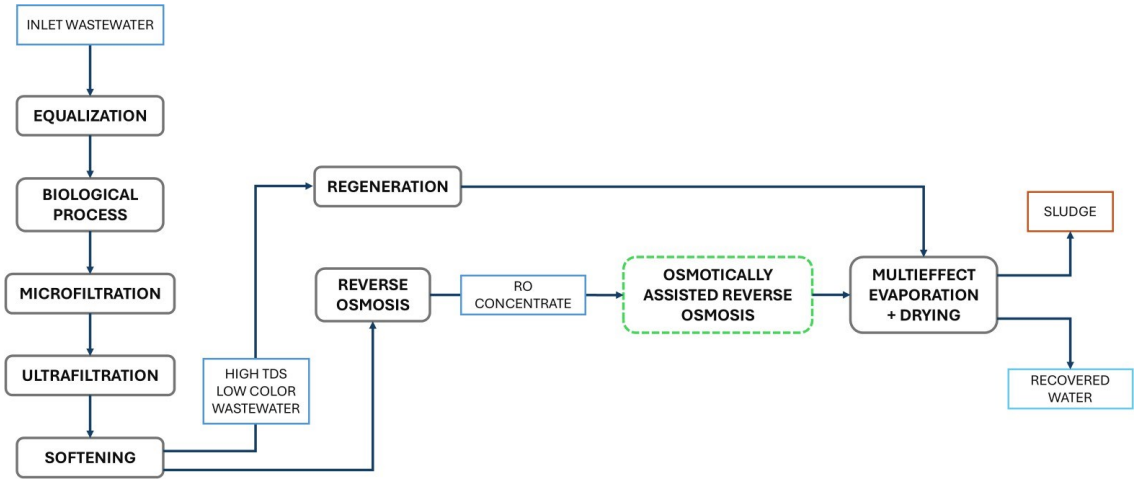

Figure 4.3: *Block diagram of the wastewater treatment plant. The green dotted line indicates the possibility of adding the OARO unit to the process.*

The idea is to modify the treatment process by inserting the OARO unit immediately after RO in order to further increase the concentration of the rejected stream coming out of the RO step as much as possible. This technological choice can optimize the handling of the

concentrate considering the less energy demand for the subsequent evaporation process and the reduced volume to be treated.

4.2.1 Focus on reverse osmosis (RO) step

To create a suitable process configuration, it is necessary to know the composition of the effluent to be treated. The effluent is the concentrate coming out of the RO unit (Fig. 4.3) and its characterization is shown in Table 4.1.

Table 4.1: *Characterization of the concentrate flow produced by reverse osmosis process.*

Parameters	Unit	RO Concentrate
Design flow	L/h	11,292
TDS	**ppm**	**55,357**
Color	HU	26,000
Iron	ppm	0.7
Silica	ppm	400
Sodium	ppm	14,930
Calcium	ppm	13.3
Magnesium	ppm	4
Alkalinity tot.	ppm ($CaCO_3$)	12,400
Sulphate	ppm	8,840
Chloride	ppm	16,050

The component of interest is the total amount of dissolved solids, which consists mainly of sodium and chloride in the form of sodium chloride (NaCl); the other predominant species are sulphates and alkaline compounds (expressed in ppm of calcium carbonate $CaCO_3$).

Based on the TDS concentration value, the experimental results obtained in Chapter 3 can be used to set an average water flux expected from an OARO stage based on the osmotic pressure of the feed solution. Indeed, it is clear from the experimental results how much the average flux is for a certain salt concentration in the feed solution and in the sweep. However, since the experiments were conducted with solutions containing only NaCl, it is necessary to find the NaCl concentration that corresponds to the osmotic pressure of the real solution. This step provides a reliable reference for predicting the performance of the process under practical conditions. In other words, by knowing the osmotic pressure

of the feed solution, it is possible to estimate how the OARO process will perform. This allows us to choose a realistic value for the average water flow, tailoring it to the specific solution to be treated. The solution to be treated in the case study has an osmotic pressure of around 34.3 bar for 53.36 g/L TDS and the corresponding NaCl concentration is 43.43 g/L.
On the other hand, the stream feeding the RO process has a TDS concentration of 4.15 g/L, which corresponds to an osmotic pressure of 2.6 bar. At the same osmotic pressure, this TDS concentration corresponds to a NaCl concentration of 3.39 g/L.

The other RO variables of the case study are the inlet flowrate of 150,583 L/h and the concentrate flowrate of 11,292 L/h.
Data about RO inlet and outlet streams and composition are used to perform the OARO process simulation for the case study.

4.3 OARO simulation for the case study

The simulation represents a theoretical analysis that includes the development of mass balance equations and constraints relations governing a system consisting of a single-stage RO and a three-stage OARO. In this section, the process proposal is first presented and described. Then, mass balances and constraints equations are formulated, and the known variables to be set and the unknowns to be found as a solution are defined. The known variables are either given by the case study or are reasonably chosen based on the results obtained from the experimental analysis. The aim is to find the right process configuration to concentrate the incoming solution as much as possible. The idea is to assume a process where the water flux is set as an average value and the equations to be used to solve the system are the mass balances for each treatment unit and process node. By setting the average water flux and the other fixed variables, the system of equations finds the results of the area required for each OARO stage, the values of flow rates and concentrations of all the streams involved in the proposed process and, ultimately, the power demand to perform the process.

4.3.1 Theoretical OARO stages requirement

The final concentration target was set around 110 g/L NaCl equivalent by Hydrotech Engineering, because otherwise there could be problems with precipitation of the salts formed in the solution. To determine how many theoretical stages are needed to increase the initial concentration of 43.43 g/L NaCl to the target concentration, considerations are made based on the experimental results.

The focus is on experiments conducted at 1 M and 2 M concentrations in the feed, since these values are representative of the case study conditions analyzed. It is observed that a feed solution of 58 g/L can be concentrated using a sweep solution of 35 g/L, thus with an initial $\Delta\pi$ applied of 20 bar. This implies that, in a stage operating in counter-current split-feed mode (same concentration in both feed and sweep sides), it is possible to obtain a concentrate with an osmotic pressure 20 bar higher than the feed and a diluted sweep with an osmotic pressure 20 bar lower than the feed. Therefore, based on the starting conditions, a graph can be constructed to see how many theoretical stages of OARO are needed in the counter-current configuration to obtain the final concentration target.

Figure 4.4 shows the profile of inlet and outlet concentrations that would be obtained in each OARO stage to reach the imposed target concentration of 110 g/L.

It is important to note that the change in osmotic pressure $\Delta\pi$ does not translate into a linear change in concentration. For example, in the first stage at an initial concentration of 43.43 g/L, a $\Delta\pi$ of 20 bar corresponds to a concentration change of 24 g/L, resulting in a concentrate at 68 g/L and a dilute sweep at 19 g/L. In the second stage, starting with 68 g/L, a $\Delta\pi$ of 20 bar results in a change in concentration of 23 g/L, bringing the concentrate to 91 g/L and the dilute sweep to 44 g/L. Finally, in the third stage, with an initial concentration of 91 g/L, a $\Delta\pi$ of 20 bar results in a concentration difference of 22 g/L, bringing the concentrate to 113 g/L and the diluted sweep to 69 g/L.

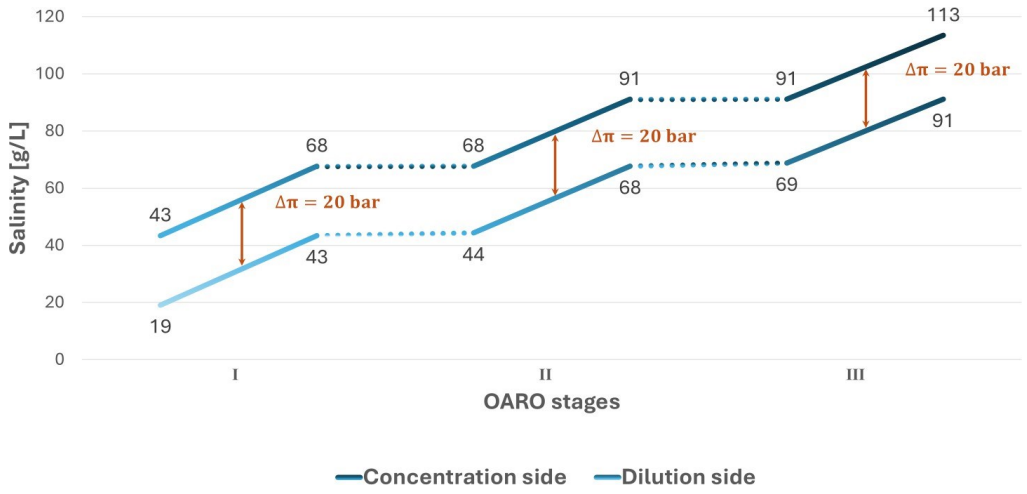

Figure 4.4: *Theoretical profile of inlet and outlet concentrations from each OARO stage of the case study.*

Considering the initial concentrations corresponding to each theoretical stage (Fig. 4.4), water flux values for each OARO stage were selected based on experimental results, observing what range of water fluxes were obtained for a given NaCl concentration in the feed. Then, an average flux is set for each OARO stage consistent with the feed concentration as follows:

- First OARO stage: the initial concentration is 43.44 g/L, which is slightly lower than 58 g/L (equivalent to 1 M). Under these conditions, experimental flux values at 28 bar applied pressure ranged between 2 and 4 LMH (Fig. 3.1). Therefore, an average flux of $J_{w1} = 2.5\ LMH$ was chosen for this stage.
- Second OARO stage: the initial concentration is 68 g/L, which is closest to the 1 M feed case but still higher than 58 g/L. Given this condition, an average flux of $J_{w2} = 2\ LMH$ was selected, aligning with experimental results at 28 bar.
- Third OARO stage: the initial theoretical concentration for this stage is 91 g/L, which is closer to 2 M. Experimental results for a 2 M feed (Fig. 3.2) at 28 bar indicate flux values in the range of 1-2 LMH. Consequently, the imposed average flux for this stage is $J_{w3} = 1.5\ LMH$.

4.3.2 Multistage OARO process proposal

The configuration that is proposed involves a multi-stage OARO system to concentrate the effluent under investigation, characterized by 43.4 g/L NaCl. The schematic diagram of the entire process is described in Figure 4.5. Each OARO stage operates in split-feed mode (SF-OARO): the incoming solution is divided into two streams, one is pressurized and represents the feed and the other remains at low pressure becoming the sweep entering OARO module in counterflow (Mo et al., 2022). In this way, no specifically prepared solution is used to perform the process and the osmotic pressure difference between the two sides of the membrane is zero, with the advantage of maximizing water flux. However, potential drawbacks of the split-feed configuration include the high capital costs due to the many stages that may be necessary for a high recovery operation and complicated control systems to maintain system stability and performance (Bouma C Lienhard, 2018). This process configuration was developed from Al-Amoudi et al. (2023), who proposed a concentration system for a membrane concentrate coming from a desalination plant.

The first unit provided is reverse osmosis, which is already present in the real treatment plant. Then, the concentrate coming out of the RO process is treated by three stages of SF-OARO. The diluted sweep stream coming out of each stage is recycled to the head of the previous treatment unit: the diluted sweep solution coming out of the first stage is recycled to the head of the RO process, the second diluted sweep is recycled to the head of the first OARO stage, and so on for the third diluted sweep, which is sent back to the supply of the second OARO stage. Thus, in general, the supply streams are mixed with the corresponding diluted sweeps of the next OARO stage. The initial flow (Initial Feed) is mixed in node 1 with the diluted sweep of the first stage OARO (Diluted Sweep 1) to become the RO process feed (RO Feed). RO produces the output stream of permeate (RO Permeate) and concentrate (RO Concentrate), which is mixed in node 2 with the diluted sweep of the second OARO stage (Diluted Sweep 2), generating the first intermediate feed (Intermediate Feed 1), which is then split in node 3 into Feed 1 and Sweep 1 to proceed with the first OARO stage. The procedure is the same for the second OARO stage: the concentrate coming out of the first stage (Concentrate 1) is mixed in node 4 to the diluted sweep of the third stage (Diluted Sweep 3) and the resulting stream (Intermediate Feed 2) is in turn divided in node 5 into Feed 2 and Sweep 2. Finally, the

concentrate exiting the second stage OARO (Concentrate 2) is not mixed with any stream, it is only partitioned at node 6 into the feed and sweep solutions of the third stage (Feed 3 and Sweep 3). The final stream is the concentrate exiting the third stage OARO (Concentrate 3), which must have the imposed target concentration and will be further treated by thermal process.

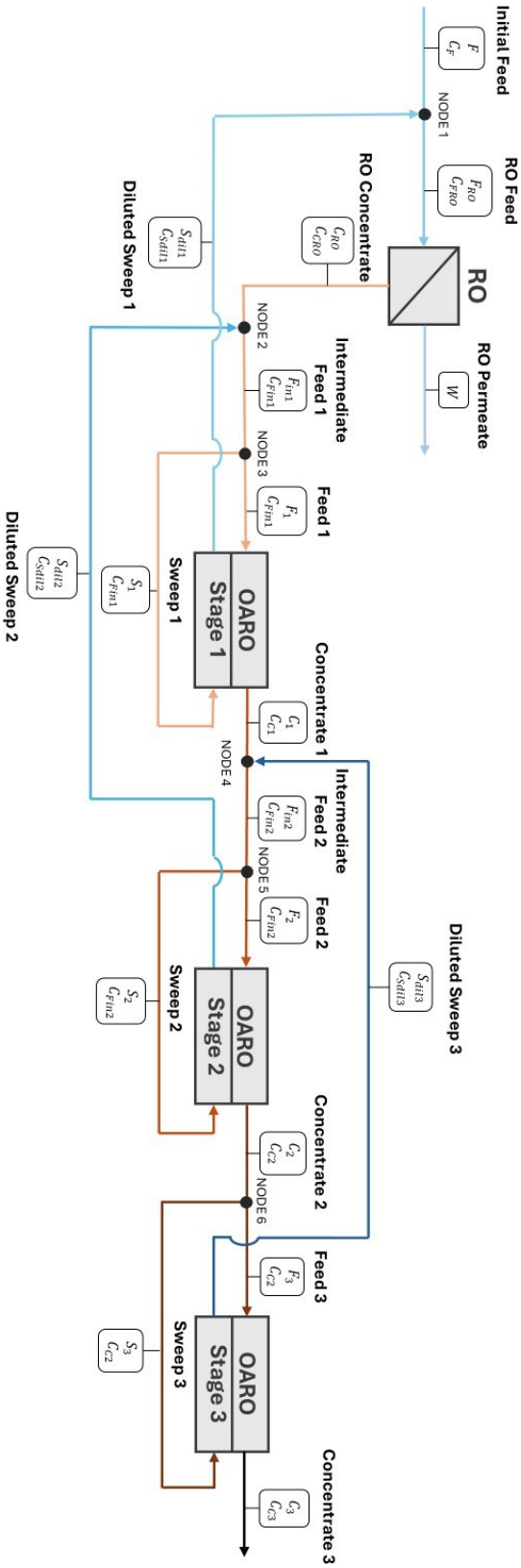

Figure 4.5: *Treatment process proposed to treat the effluent under consideration. The system is composed of a single RO stage and a three-stage OARO process.*

Table 4.2 follows with a list of the streams included in the process and the associated terminology for the flow rates and concentrations used in Figure 4.5. Note that, in the nodes into which the flows are divided (Node 3, Node 5 and Node 6), the composition of the incoming and outgoing streams is the same, only the flow rates change.

Table 4.2: *List of the flows involved in the process proposal, with their associated acronyms for flowrates and concentrations.*

Stream	Flowrate	Concentration
Initial Feed	F	C_F
RO Feed	F_{RO}	C_{FRO}
RO Permeate	W	≈ 0
RO Concentrate	C_{RO}	C_{CRO}
Intermediate Feed 1	F_{in1}	C_{Fin1}
Feed 1	F_1	C_{Fin1}
Sweep 1	S_1	C_{Fin1}
Concentrate 1	C_1	C_{C1}
Diluted Sweep 1	S_{dil1}	C_{Sdil1}
Intermediate Feed 2	F_{in2}	C_{Fin2}
Feed 2	F_2	C_{Fin2}
Sweep 2	S_2	C_{Fin2}
Concentrate 2	C_2	C_{C2}
Diluted Sweep 2	S_{dil2}	C_{Sdil2}
Feed 3	F_3	C_{C2}
Sweep 3	S_3	C_{C2}
Concentrate 3	C_3	C_{C3}
Diluted Sweep 3	S_{dil3}	C_{Sdil3}

4.3.3 Mass balances formulation

To simulate the performance of the proposed treatment process, mass balances governing each stage of the process are formulated. In addition to the fundamental mass balances, a series of constraint relationships that complete the system of equations are also integrated, to impose $\Delta\pi$ of 20 bar for each OARO stage, as presented in Paragraph 4.3.1. The defined system of equations is solved using the software MATLAB®, whose script is provided in the Appendix. This approach makes it possible to simulate the behavior of the process, providing useful indications for the design and optimization of the proposed treatment. Table 4.3 below provides a summary of the system known variables.

Table 4.3: *Known variables of the system for OARO simulation.*

$\boldsymbol{F}$	150,583 L/h
$\boldsymbol{C_F}$	3.39 g/L
$\boldsymbol{C_{CRO}}$	43.43 g/L
$\boldsymbol{J_{w1}}$	2.5 LMH
$\boldsymbol{J_{w2}}$	2 LMH
$\boldsymbol{J_{w3}}$	1.5 LMH

Once these values are fixed, the solutions that the system finds are all other values of fluxes and concentrations included in the process. The membrane areas required for each OARO stage are also unknown:

- A_{m1} (m^2) is the membrane area required for the first OARO stage
- A_{m2} (m^2) is the membrane area required for the second OARO stage
- A_{m3} (m^2) is the membrane area required for the third OARO stage

Thus, the mass balances for each node and each unit in the process are formulated and the constraint relationships are added to make the system determined. Mass balances are formulated considering constant fluid density. Table 4.4 below presents all the equations of the system.

Table 4.4: *Mass balances and constraint relationships of the mathematical model used to simulate the proposed treatment process.*

NODE 1	$F + S_{dil1} - F_{RO} = 0$	*(4. 1)*
	$F \cdot C_F + S_{dil1} \cdot C_{Sdil1} - F_{RO} \cdot C_{FRO} = 0$	*(4. 2)*
RO	$F_{RO} - W - C_{RO} = 0$	*(4. 3)*
	$F_{RO} \cdot C_{FRO} - C_{RO} \cdot C_{CRO} = 0$	*(4. 4)*
NODE 2	$C_{RO} + S_{dil2} - F_{in1} = 0$	*(4. 5)*
	$C_{RO} \cdot C_{CRO} + S_{dil2} \cdot C_{Sdil2} - F_{in1} \cdot C_{Fin1} = 0$	*(4. 6)*
NODE 3	$F_{in1} - F_1 - S_1 = 0$	*(4. 7)*
OARO STAGE 1	$F_1 - J_{w1} \cdot Am_1 - C_1 = 0$	*(4. 8)*
	$F_1 \cdot C_{Fin1} - C_1 \cdot C_{C1} = 0$	*(4. 9)*
	$S_1 + J_{w1} \cdot Am_1 - S_{dil1} = 0$	*(4. 10)*
	$S_1 \cdot C_{Fin1} - S_{dil1} \cdot C_{Sdil1} = 0$	*(4. 11)*
NODE 4	$C_1 + S_{dil3} - F_{in2} = 0$	*(4. 12)*
	$C_1 \cdot C_{C1} + S_{dil3} \cdot C_{Sdil3} - F_{in2} \cdot C_{Fin2} = 0$	*(4. 13)*
NODE 5	$F_{in2} - F_2 - S_2 = 0$	*(4. 14)*
OARO STAGE 2	$F_2 - J_{w2} \cdot Am_2 - C_2 = 0$	*(4. 15)*
	$F_2 \cdot C_{Fin2} - C_2 \cdot C_{C2} = 0$	*(4. 16)*
	$S_2 + J_{w2} \cdot Am_2 - S_{dil2} = 0$	*(4. 17)*
	$S_2 \cdot C_{Fin2} - S_{dil2} \cdot C_{Sdil2} = 0$	*(4. 18)*
NODE 6	$C_2 - F_3 - S_3 = 0$	*(4. 19)*
OARO STAGE 3	$F_3 - J_{w3} \cdot Am_3 - C_3 = 0$	*(4. 20)*
	$F_3 \cdot C_{C2} - C_3 \cdot C_{C3} = 0$	*(4. 21)*
	$S_3 + J_{w3} \cdot Am_3 - S_{dil3} = 0$	*(4. 22)*
	$S_3 \cdot C_{C2} - S_{dil3} \cdot C_{Sdil3} = 0$	*(4. 23)*
CONSTRAINTS	$C_{C1} = C_{Fin1} + 24$	*(4. 24)*
	$C_{C2} = C_{Fin2} + 23$	*(4. 25)*
	$C_{C3} = C_{C2} + 22$	*(4. 26)*
	$C_{Fin1} = C_{Sdil1} + 24$	*(4. 27)*

$$C_{Fin2} = C_{Sdil2} + 23 \quad (4.\ 28)$$

$$C_{C2} = C_{Sdil3} + 22 \quad (4.\ 29)$$

Thus, twenty-nine equations for twenty-nine unknowns are obtained. Constraints equations were set to meet the Δπ of 20 bar for each OARO stage. From the first to the third stage, with Δπ of 20 bar the concentration jumps are 24 g/L, 23 g/L and 22 g/L, respectively, both for feed and sweep sides, as already explained in Paragraph 4.3.1. These starting values were initially set and were subsequently updated until the solutions converged.

4.3.4 OARO simulation results

This section details the results obtained through the resolution of the equations previously formulated. After defining the input parameters of the system and implementing the equations simulating the behavior of the treatment process under consideration, it was possible to calculate the flow rates and concentrations of each stream involved in the process. In addition, the values of the membrane areas required for each OARO step were reported. Table 4.5 below shows the results on the composition of the flows.

Table 4.5: *Results obtained through the mathematical model of flow rates and concentrations of each stream of the proposed system.*

Initial Feed	F	$150{,}583\ L/h$
	C_F	$3.39\ g/L$
RO Feed	F_{RO}	$163{,}130\ L/h$
	C_{FRO}	$4.54\ g/L$
RO Permeate	W	$146{,}080\ L/h$
RO Concentrate	C_{RO}	$17{,}047\ L/h$
	C_{CRO}	$43.44\ g/L$
Intermediate Feed 1	F_{in1}	$25{,}500\ L/h$
	C_{Fin1}	$43.44\ g/L$
Feed 1	F_1	$20{,}205\ L/h$

	C_{Fin1}	43.44 g/L
Sweep 1	S_1	5,295.0 L/h
	C_{Fin1}	43.44 g/L
Concentrate 1	C_1	12,956.0 L/h
	C_{C1}	67.74 g/L
Diluted sweep 1	S_{dil1}	12,543.0 L/h
	C_{Sdil1}	18.34 g/L
Intermediate Feed 2	F_{in2}	17,229 L/h
	C_{Fin2}	67.74 g/L
Feed 2	F_2	11,809 L/h
	C_{Fin2}	67.74 g/L
Sweep 2	S_2	5,420.0 L/h
	C_{Fin2}	67.74 g/L
Concentrate 2	C_2	8,777.2 L/h
	C_{C2}	91.14 g/L
Diluted Sweep 2	S_{dil2}	8,452.1 L/h
	C_{Sdil2}	43.44 g/L
Feed 3	F_3	5,601.3 L/h
	C_{C2}	91.14 g/L
Sweep 3	S_3	3,176.0 L/h
	C_{C2}	91.14 g/L
Concentrate 3	C_3	4,504.1 L/h

	C_{C3}	$\mathbf{113.34\ g/L}$
Diluted Sweep 3	S_{dil3}	$4{,}273.1\ L/h$
	C_{Sdil3}	$67.74\ g/L$

The initial stream is first mixed with the diluted sweep of the first OARO stage and becomes the RO feed stream at a concentration of 4.54 g/L. RO process produces a permeate of 146,080 L/h, which accounts for 90% of the feed; the remaining 10% becomes the concentrate from RO at the fixed concentration of 43.43 g/L. At node 2 the concentrate mixes with the diluted sweep of the second OARO stage, which is at 43.43 g/L too, and becomes the feed concentration of the first OARO stage. The feed and sweep streams of the first OARO stage are divided at node 3 and at the outlet the first OARO concentrate is obtained at 67.74 g/L, while the diluted sweep is at 18.34 g/L. Concentrate 1 stream is in turn mixed in node 4 with the diluted sweep of the third OARO stage at the same concentration of 67.74 g/L. At node 5 the inflow rate of the second OARO stage (Intermediate Feed 2) is again divided and 8,777 L/h of concentrate stream at a concentration of 91.14 g/L is produced. The concentrate is no longer mixed with other streams after the second stage, so the flow rate is divided at node 6 into feed and sweep of the third stage. What is finally obtained at the outlet is 4,504 L/h of final concentrate at 113.34 g/L NaCl, with the dilute sweep exiting at 67.74 g/L.

Table 4.6 summarizes the obtained values of area required to perform each stage of OARO, coupled with each imposed water flow for the stages. In fact, the area depends on the imposed flow, because the inlet and outlet concentrations are fixed, so the value of permeate to be produced is determined. Thus, if the permeate is fixed, the change in flow leads to the change in area required to treat the effluent with that specific flux value. Indeed, according to the relationship (2.14), flux and area are inversely proportional: if the flux through the membrane is increased, the area required to reach the target concentration is less, and vice versa if the water flux is relatively low, more area will be required to reach the target concentration.

The results show that the area required decreases for each successive stage. Specifically, the area of the first stage is 2,899 m^2 and decreases by 50% to 1,516 m^2 from the first to the second stage and again by 50% to 731 m^2 from the second to the third stage.

Table 4.6: *Membrane area values obtained through the mathematical model for each OARO stage, with the associated water flux imposed.*

J_{w1}	2.5 LMH
A_{m1}	2,899 m^2
J_{w2}	2 LMH
A_{m2}	1,516 m^2
J_{w3}	1.5 LMH
A_{m3}	731 m^2

The final concentration of the solution obtained by the simulation is $C_{C3} = 113.34\ g/L$ NaCl, which reflects the initial target. This result represents a significant value, as it demonstrates the ability of the OARO process to efficiently concentrate a solution initially at a high salt concentration, bringing it to levels compatible with the requirements of specific industrial processes. The flow rate results obtained are valuable since they will subsequently be used to estimate effectively the energy required by the proposed OARO system.

4.4 Energy consumption comparison between MEE, OARO and UHPRO processes

The energy demand is a key aspect in assessing the efficiency and sustainability of different treatment technologies applicable to the wastewater under consideration. Indeed, the choice of the most suitable technology depends not only on the ability to achieve the desired result in terms of concentration and freshwater recovery, but also on the energy impact and associated operating costs. In this perspective, a detailed comparison of three different treatment configurations was developed, analyzing their respective energy consumption:

(1) The RO concentrate effluent undergoes a purely thermal treatment, in which it is concentrated through a multi-effect evaporator (MEE).
(2) The effluent is treated using a combined system composed of two main phases: a first one based on three-stages OARO process to pre-concentrate the effluent and a second phase in which the final concentrate is further treated with a multi-effect evaporator. The use of OARO in the initial phase should allow for a significant reduction in the thermal load on the evaporation stage. This approach aims to combine the advantages of the two technologies, optimizing the overall energy balance.
(3) The effluent is treated with another combined system, which uses a single stage of UHPRO to pre-concentrate the effluent, again followed by thermal treatment of the residual concentrate. Also in this configuration, the aim is to reduce the energy requirements of the evaporation stage.

Thus, the energy analysis of the different alternatives focuses on the part of the process that starts with the RO concentrate. This approach is justified by the fact that all previous steps of the case study are considered common to all the analyzed configurations and are therefore not included in the energy quantification.
The analysis of energy consumption for each configuration allows an assessment of which approach offers the best energy efficiency. In particular, the comparison aims to highlight how the introduction of innovative membrane technologies, such as OARO and UHPRO, can represent a more sustainable solution than traditional pure heat treatment, especially in industrial settings where the reduction of energy consumption and emissions is a strategic priority. Lastly, the most relevant final discussion focuses on the direct comparison between the two membrane processes: the OARO system and the UHPRO system. This discussion is of particular interest because both technologies aim to reduce the energy load of thermal treatment by exploiting innovative and high-performance approaches for the concentration of wastewater. However, differences in the operating modes, such as operating pressure, process complexity and energy requirements of the two processes can significantly affect the overall efficiency of the combined system. Therefore, the objective of the comparison is to identify which of the two membrane-based processes represents the optimal solution to further reduce energy consumption and improve treatment sustainability, while ensuring high performance in the treatment of

concentrated wastewater in an industrial context. It is important to notice that OARO can achieve NaCl brine concentrations much higher than UHPRO, but this increase in brine concentration capability comes at the expense of added process complexity compared to traditional reverse osmosis processes. In fact, the key difference between UHPRO and OARO is that UHPRO produces fresh water directly, while OARO produces a less saline stream that needs to be recirculated back to the system, adding complexity to the global process (Al-Amoudi et al., 2023). For this reason, given that both the UHPRO and OARO processes facilitate the treatment system when combined with conventional thermal evaporation, it may be useful to understand which of the two processes is more energy efficient and convenient.

The specific energy consumption (SEC) becomes a critical performance metric for the comparison between the different technologies in MLD/ZLD applications. Generally, SEC is defined as the total energy consumption normalized by the volume of the recovered or produced freshwater (Wang et al., 2021). In this analysis, the specific energy consumption is normalized by the feed water flow rate. Thus, in an OARO or UHPRO process with N-pumps, specific energy consumption (SEC) is defined as the total energy consumption given by the operation of the pumps to pressurize the flows within the system, normalized to the volume of feed entering the system:

$$SEC = \frac{\sum_{i=1}^{N} \frac{Q_i \cdot \Delta P_i}{\eta_i}}{Q_F} \qquad (4.\ 30)$$

where Q_F is the flow rate of the feed water, Q_i is the flow rate to be pressurized, ΔP_i is the operating pressure and η_i is the efficiency of the pump (taken as xx%).

In this study, the flow rate used to normalize the energy consumption is the concentrate stream exiting the RO process of the case study, which is $11{,}292\ L/h$ (Table 4.1).

So, energy consumption in OARO and UHPRO processes is mainly determined by the pressurization of flows by pumps. To estimate the energy required, it is essential to know

the flow to be handled, the pressure at the pump inlet and the pressure required at the outlet. The pressures known from the actual case study are:

- Pressure of the feed RO flow rate, that is $P_{FRO} = 55\ bar$
- Pressure of the concentrate exiting the RO process, which is $P_{CRO} = 45\ bar$

To make a consistent comparison of the energy required in the cases (2) and (3), the final target concentration achieved by OARO and UHPRO must be the same: this value is therefore set at $113.34\ g/L$, result found by simulating the OARO process for (C_{C3}).

4.4.1 Energy consumption results

CASE (1)

Case (1) represents the current case, which includes only thermal treatment of the concentrate leaving RO (Fig. 4.3). From the actual data on the case study, it is known that the evaporator specific energy consumption is $13\ kWh/m^3$ of feed flow rate. The inlet flow rate is the concentrate stream exiting RO, that is $11{,}292\ L/h$ (Table 4.1). Therefore, the energy consumption results in 147 kW (Table 4.7). The specific energy consumption of $13\ kWh/m^3$ is considered also for the other two configurations.

Table 4.7: *Resume of thermal energy consumption data of the evaporator in case (1).*

EVAPORATOR		
Flowrate	m^3/h	11.292
SEC	$\boldsymbol{kWh/m^3}$	**13**
E_t	kW	147

CASE (2)

The overall system consists of a first phase of membrane treatment, consisting of three OARO stages, followed by a second phase of thermal treatment of the concentrate produced by the OARO process.

In the OARO process, the operating pressure is 30 bar. Consequently, if the flow has a pressure above 30 bar, a lamination valve must be inserted to generate pressure drops and

reduce the pressure. In contrast, for flows with pressures below 30 bar, pumps are used to restore the flow to the desired pressure. The configuration of pumps and lamination valves adopted for the OARO system proposed is shown in Figure 4.6.

The concentrate exiting the RO process has a pressure of 45 bar, so a lamination valve is installed to reduce it to 30 bar. In addition, the inlet sweeps to each OARO stage must be at 3 bar, which is why lamination valves are added to lower the pressure from 30 bar to 3 bar for each sweep inlet flow rate.

Within each OARO stage, the flow enters at 30 bar but suffers pressure losses through the modules. Therefore, to restore the pressure to 30 bar booster pumps are used on the concentrate exiting each stage. From the data sheets of the commercially available RO membranes, it appears that the pressure drops are about 1 bar per element, with typical configurations of 6 elements in series within each vessel, resulting in overall losses of about 5 bar per OARO stage.

Finally, additional pumps are installed on the diluted sweep outlet of each stage. In this case, the flow exits at atmospheric pressure and must be recirculated within the system to dilute the flow at 30 bar. For this reason, it is necessary to pressurize the diluted sweep streams from 0 bar of relative pressure to 30 bar.

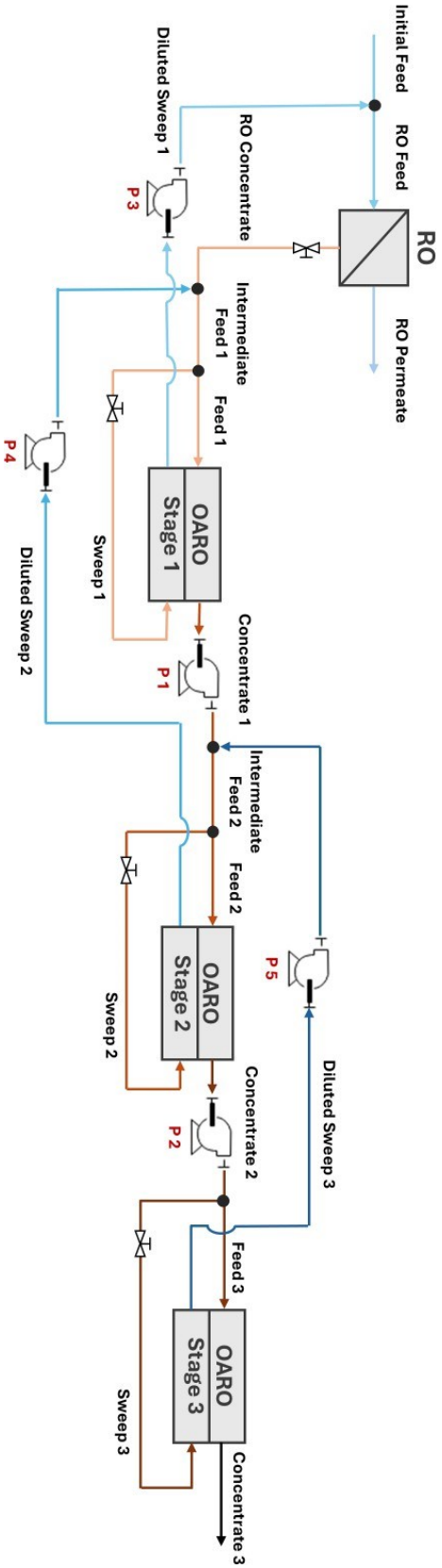

Figure 4.6: *Pumps and lamination valves configuration for OARO system proposal for the case study.*

Table 4.8 summarizes the operating conditions of the system and the final energy required for the described OARO process. The electrical power demand for each pump is calculated as:

$$E_i = \frac{Q_i \cdot \Delta P_i}{\eta} \qquad (4.\ 31)$$

where the pump efficiency η is set to 0.75 for all the pumps.

Table 4.8: *Operative conditions and energy consumption data for the three-stage OARO system.*

OARO						
		PUMP 1	**PUMP 2**	**PUMP 3**	**PUMP 4**	**PUMP 5**
Flowrate	m^3/h	12.956	8.777	12.543	8.452	4.273
Pressure IN	bar	25	25	0	0	0
Pressure OUT	bar	30	30	55	30	30
E	kW	2.40	1.63	25.55	9.39	4.75
Total E	kW	43.71				
SEC	$\boldsymbol{kWh/m^3}$	**3.87**				

Pumps 1 and 2 are the booster pumps that transport the concentrate flows exiting the second and third stages of OARO, respectively. The inlet pressure is 25 bar because there is a 5 bar pressure drop in the modules for each stage. Therefore, $\Delta P_1 = \Delta P_2 = 5\ bar$ is a relatively low pressure drop, which is why the estimated energy consumption is lower than that of the other pumps: $2.40\ kW$ and $1.63\ kW$, respectively. The most impactful contribution of energy consumption is provided by pump 3, which is installed to recirculate and pressurize the diluted sweep stream of the first stage OARO from 0 bar of relative pressure to the RO inflow pressure of 55 bar. The pressure drop $\Delta P_3 = 55\ bar$ is the largest expected from the process and, in fact, the energy consumption is $25.55\ kW$, which represents about 60% of the total consumption of $43.71\ kW$. The specific energy consumption calculated on the incoming flow equals $3.87\ kWh/m^3$, which will be compared to the UHPRO result.

In the second thermal treatment step, the concentrate flow rate leaving OARO $C_3 = 4\ 504\ L/h$ enters the multi-effect evaporator to further increase the concentration. The results of consumed thermal energy are summarized in Table 4.9 below.

Table 4.9: *Resume of thermal energy consumption data of the evaporator in case (2).*

EVAPORATOR		
Flowrate	m^3/h	4.504
E_t	kW	59
SEC	$\boldsymbol{kWh/m^3}$	**5.19**

In this case, the volumetric flowrate entering the evaporator needs $59\ kW$ of thermal energy to be treated, corresponding to $5.19\ kWh/m^3$of specific energy consumption.
In conclusion, the total specific energy consumption for the case (2) is:

$$SEC_{tot} = 3.87\ kWh/m^3 + 5.19\ kWh/m^3 = 9.06\ kWh/m^3 \qquad (4.\ 32)$$

CASE (3)

The overall system consists of a first phase of UHPRO and a second phase of thermal treatment of the concentrate exiting the membrane process. The UHPRO operates with a single stage at 120 bar. The initial pressure of the flow is 45 bar and the pump must therefore pressurize it to 120 bar. The pump efficiency is set at 0.75 also in this case. Table 4.10 below shows the expected energy consumption results for the UHPRO process.

Table 4.10*: Operative conditions and energy consumption data for the single stage UHPRO process.*

UHPRO		
Flowrate	m^3/h	11.292
Pressure IN	bar	45
Pressure OUT	bar	120
E	kW	31.37

SEC	$\boldsymbol{kWh/m^3}$	**2.78**

With applied $\Delta P = 75\ bar$, the energy consumption is $31.37\ kW$. The corresponding SEC is calculated based on the incoming flowrate for UHPRO, resulting in $2.78\ kWh/m^3$.

To obtain the heat consumption data of the evaporator, the inlet flow rate must be calculated. This corresponds to the concentrate flow rate exiting the UHPRO process, which will have a target concentration of $113.34\ g/L$. Considering a zero concentration in the permeate leaving UHPRO, the concentrate flow rate of UHPRO can be easily calculated from the available data as:

$$C_{UHPRO}\ (L/h) = \frac{C_{RO}\ (L/h) \cdot C_{CRO}\ (g/L)}{C_{CUHPRO}\ (g/L)} = \frac{11{,}292\ L/h \cdot 43.44\ g/L}{113.34\ g/L} \qquad (4.\ 33)$$
$$= 4\,327.9\ L/h$$

where $C_{UHPRO}\ (L/h)$ is the concentrate flow rate exiting the UHPRO process and $C_{CUHPRO}\ (g/L)$ is the corresponding concentration target.

Table 4.11 presents the thermal energy consumption data for the evaporation of the inlet flow rate.

Table 4.11: *Resume of thermal energy consumption data of the evaporator in case (3).*

EVAPORATOR		
Flowrate	m^3/h	4.328
E_t	kW	56
SEC	$\boldsymbol{kWh/m^3}$	4.98

In this condition, $56\ kW$ of thermal energy consumption are required to treat the inlet flowrate. The total specific energy consumption is:

$$SEC_{tot} = 2.78\ kWh/m^3 + 4.98\ kWh/m^3 = 7.76\ kWh/m^3 \qquad (4.34)$$

4.4.2 Energy consumption comparison

Table 4.12 summarizes the results for absolute and specific energy consumption per unit of inlet flow rate obtained for the analyzed configurations and Figure 4.7 shows the results of specific energy consumption graphically. The data clearly show that, predictably, a Zero Liquid Discharge (ZLD) treatment system that relies exclusively on thermal processes results in much higher energy consumption than a combined system that integrates membrane technologies for effluent pre-treatment.

Table 4.12: *Specific energy consumption results for the three treatment configurations analyzed.*

	CASE (1)	**CASE (2)**	**CASE (3)**
Total E (kW)	147	102.71	87.37
SEC (kWh/m^3)	13	9.06	7.76

In particular, the results show that in configurations (2) and (3), which include pre-treatment using membrane technologies, the energy consumption is approximately 64% of that required by configuration (1), which uses only thermal treatment. This highlights the energy advantage of combined systems, where membranes reduce the volumetric flow rate to be sent to the final evaporator, thus decreasing the overall energy requirement.

In configuration (2), the volumetric flow rate sent to the evaporator is less than half that of configuration (1). This results in a significant reduction in thermal consumption from 147 kW (13 kWh/m³) to 59 kW (5.19 kWh/m³), a reduction of 60%. A similar trend is also observed in configuration (3), where the flow rate sent to the evaporator is comparable to that of configuration (2), with a slightly lower heat consumption of 56 kW (4.98 kWh/m³). This slight improvement is attributable to the fact that the inlet flow rate is slightly lower in this case.

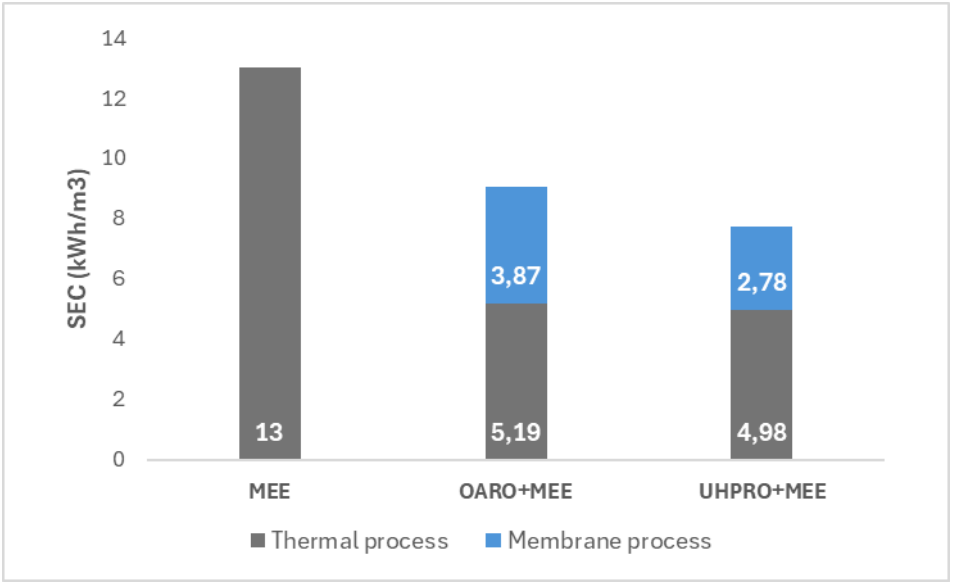

Figure 4.7: *Specific energy consumption (SEC) results for the process configurations (1) MEE, (2) OARO+MEE and (3) UHPRO+MEE.*

A distinctive element between configurations (2) and (3) lies in the specific energy consumption associated with the pre-concentration process: in configuration (3) using the UHPRO technology, the energy consumption is 31.37 kW, while in configuration (2) based on the OARO process, this value rises to 43.71 kW. Consequently, the overall specific consumption (SEC) is lower for configuration (3) than for configuration (2): 7.76 kWh/m³ versus 9.06 kWh/m³.

A more detailed comparison of the specific consumption shows that the OARO process in configuration (2) consumes more energy than the UHPRO process, with values of 3.87 kWh/m³ and 2.78 kWh/m³, respectively. However, to best interpret these results, some observations must be made on the energy analysis conducted. Firstly, the analyzed OARO configuration does not include the use of energy recovery devices, such as pressure exchangers. These devices, if installed, could significantly reduce the work of the pumps and, consequently, the overall energy consumption. For instance, in the current OARO system, the most energy-intensive component is Pump 3, which is responsible for pressurizing the diluted sweep solution exiting the first OARO stage from atmospheric pressure to 55 bar. Additionally, a lamination valve is used to reduce the pressure of the

concentrated RO stream from 45 bar to 30 bar, dissipating valuable energy in the process. By integrating a pressure exchanger, the excess pressure from the concentrate stream could be recovered to partially pressurize the diluted sweep solution. This would significantly reduce the energy demand on Pump 3 and improve the overall efficiency of the system. Therefore, incorporating such a recovery mechanism represents a practical and impactful strategy for optimizing energy consumption in the OARO process. This suggests that an optimization of the OARO process, with the integration of energy recovery technologies, could lead to further energy efficiency benefits.

Secondly, in the case of the UHPRO process, the pressure losses occurring in membrane modules were not considered. However, as the process operates at very high pressures, these losses can be significant and affect the overall energy requirement. Furthermore, in the UHPRO configuration, a multi-stage system was not planned, which could further increase pressure losses. In contrast, in the OARO process, a multi-stage system was simulated and pressure losses were included in the calculations, making the results more realistic.

A further aspect to consider is the economic impact of operating pressures. The UHPRO process, operating at extremely high pressures, requires specific, resilient equipment, increasing implementation and maintenance costs. In contrast, the OARO process operates at much lower pressures, allowing the use of more readily available and less expensive standard components. This makes the OARO process more cost-effective, even if the process configuration can be more complex and the energy consumption more impactful.

In conclusion, the results obtained clearly show that configurations (2) and (3), which incorporate membrane technologies, are an energy-efficient option compared to configuration (1), which is based solely on heat treatment. In particular, the OARO process used in configuration (2) involves higher specific consumption compared to UHPRO. However, while the UHPRO process demonstrates lower specific energy consumption in its current configuration compared to the OARO process, several factors suggest that the OARO process has potential for optimization. The inclusion of energy recovery devices, such as pressure exchangers, could reduce the energy demand of key components in the OARO system, making it more competitive. Furthermore, the current UHPRO simulation may underestimate the actual energy requirements due to

unaccounted pressure losses and the lack of a multi-stage system, which could increase operational complexity and energy consumption in practice. Moreover, as already pointed out in Paragraph 4.1, membranes specifically designed for withstanding such high hydraulic pressures for UHPRO process are still being developed. In fact, due to excessive compaction, the UHPRO process does not consistently operate at 120 bar but often at lower pressures. As a result, it is necessary to test the membranes under these conditions to determine whether UHPRO can actually achieve a permeate with a concentrate stream of 110 g/L.

Finally, the lower operating pressures of the OARO process offer a clear advantage, enabling the use of standard, cost-effective equipment and reducing overall implementation and maintenance costs. Ultimately, while both processes present relevant benefits, the OARO process stands out as a promising option for further development.

Conclusions

The aim of this study was to assess the effectiveness of OARO in treating highly concentrated solutions and exploring its potential applications in a real industrial scenario within the textile sector. In fact, while the OARO process shows significant promise for enhancing freshwater recovery and reducing brine volumes in ZLD/MLD strategies, its industrial implementation remains limited due to a lack of experimental data on large-scale operations. Therefore, this study conducted pilot-scale tests on a prototype membrane under OARO conditions. The results showed that several challenges must be addressed to optimize its performance. Key limitations include the effects of concentration polarization, which reduce water flux at higher feed concentrations despite maintaining a consistent osmotic pressure difference. Additionally, membrane telescoping under high feed pressures can compromise structural integrity, leading to inefficiencies, increased fouling and reduced membrane lifespan. Another critical issue is the excessive dilution of the sweep solution, which decreases the osmotic pressure difference across the membrane and results in reduced water flux. Despite these challenges, the study demonstrates encouraging results, particularly the ability to achieve positive water fluxes even with highly concentrated solutions. Results are obtained for pressures from 20 to 28 bar and for different concentrations in the sweep solution. For a 1 M feed, water flow results are in the range of 1.90-4.60 LMH. For 2 M and 3 M in the feed, the water fluxes vary from 1 to 2 LMH and for the highest concentration of 4 M in the feed, the flux remains stable around 1 LMH. Operating at higher pressures and using concentrated sweep solutions consistently boosted transmembrane water flux, suggesting the potential for optimizing system performance by fine-tuning operational parameters. Overall, OARO technology shows promise for applications involving highly concentrated solutions, provided that the identified limitations are carefully managed through improved system design and operational strategies.

In the subsequent part of the investigation, OARO process was simulated to treat an effluent originated from the textile sector in a real industrial setting. The simulation was performed through the formulation of mass balances governing the process and constraints relations imposed from experimental results. The simulation resulted in a final concentrate stream at 113.34 g/L. The energy performance of OARO-based system was

also evaluated, considering three process configurations: a conventional multi-effect evaporation system and hybrid approaches integrating OARO before thermal treatment, and finally UHPRO before thermal treatment. The energy demand to sustain the treatment systems was compared, highlighting the potential energy efficiency advantages of membrane-assisted ZLD systems.

The results highlight the energy efficiency of hybrid systems which integrate membrane technologies, compared to the configuration based solely on thermal treatment. Both configurations significantly reduce the energy required for evaporation (13 kWh/m^3) by decreasing the volumetric flow rate sent to the evaporator, with thermal consumption reductions of about 60%. The configuration with UHPRO demonstrates lower overall specific energy consumption (SEC) compared to the configuration based on OARO, with values of 7.76 kWh/m^3 and 9.06 kWh/m^3, respectively. However, the energy analysis reveals opportunities for optimizing the OARO process. Indeed, the absence of energy recovery devices, such as pressure exchangers, limits its efficiency, since these could substantially reduce energy consumption by recovering excess pressure. In contrast, UHPRO lower SEC does not account for potential pressure losses and the complexity of a multi-stage system, which could increase its energy demand in real application.

Moreover, from an economic perspective OARO operation at lower pressures offers a distinct advantage, allowing for the use of standard, cost-effective and readily available components, reducing implementation and maintenance costs. Therefore, the potential for optimization in OARO makes it a competitive and promising option for further development in energy-efficient and cost-effective membrane-based systems.

These findings provide valuable insights into the feasibility and benefits of OARO technology, paving the way for further advancements and optimization toward industrial-scale applications. A possible future development of this study is to conduct experiments and process simulations using real solutions instead of solutions containing only NaCl, as used in the current experiments. This approach would allow to assess how the presence of a more complex chemical composition influences water fluxes and the overall performance of the OARO process. Tests on industrial wastewater or other types of real

solutions would provide data more representative for practical industrial-scale applications.

Appendix

1. **MATLAB code to solve the mathematical model used for OARO simulation on the real case study.**

```
% Script used to solve the system of equations for the simulation on OARO
% process
clear all
close all

% Definition of known variables
F= 150583;
Cf = 3.39;
Ccro = 43.436;
Jw1 = 2.5;
Jw2 = 2.5;
Jw3 = 2;


% Initial value of unknowns
gAm1 = 1;
gAm2 = 1;
gAm3 = 1;
gFro = F;
gCfro = Cf;
gCro = 11292;
gW = F;
gFin1 = 11292;
gCfin1 = Ccro;
gF1 = 11292;
gS1 = 1;
gSdil1 = 1;
gCsdil1 = Ccro;
gC1 = 11292;
gCc1 = Ccro;
gFin2 = 11292;
gCfin2 = Ccro;
gF2 = 11292;
gS2 = 1;
gSdil2 = 1;
gCsdil2 = Ccro;
gC2 = 11292;
gCc2 = Ccro;
gF3 = 11292;
gS3 = 1;
gC3 = 11292;
gCc3 = Ccro;
gSdil3 = 1;
gCsdil3 = Ccro;

initial_guess = [gAm1 , gAm2 , gAm3 , gFro , gCfro , gCro, gW , gFin1 ,
gCfin1 , gF1 , gS1 , gSdil1 , gCsdil1 , gC1 , gCc1 , gFin2 , gCfin2 , gF2 ,
gS2 , gSdil2 , gCsdil2 , gC2 , gCc2 , gF3 , gS3 , gC3 , gCc3 , gSdil3 ,
gCsdil3];
```

```
% Function
options = optimoptions('fsolve', 'Display', 'iter');
[x, fval, exitflag] = fsolve(@(x) equations(x, F, Cf, Ccro, Jw1, Jw2, Jw3),
initial_guess, options);

% Results of unknown variables

    Am1 = x(1)
    Am2 = x(2)
    Am3 = x(3)
    Fro = x(4)
    Cfro = x(5)
    Cro = x(6)
    W = x(7)
    Fin1 = x(8)
    Cfin1 = x(9)
    F1 = x(10)
    S1 = x(11)
    Sdil1 = x(12)
    Csdil1 = x(13)
    C1 = x(14)
    Cc1 = x(15)
    Fin2 = x(16)
    Cfin2 = x(17)
    F2 = x(18)
    S2 = x(19)
    Sdil2 = x(20)
    Csdil2 = x(21)
    C2 = x(22)
    Cc2 = x(23)
    F3 = x(24)
    S3 = x(25)
    C3 = x(26)
    Cc3 = x(27)
    Sdil3 = x(28)
    Csdil3 = x(29)
    eff = 0.75;
    P1 = (C1*5)/(36*eff);
    P2 = (C2*5)/(36*eff);
    P3 = (Sdil1*55)/(36*eff);
    P4 = (Sdil2*30)/(36*eff);
    P5 = (Sdil3*30)/(36*eff);
    Ptot = P1+P2+P3+P4+P5


% % Results
% disp('Soluzione trovata:');
% disp(x);
disp('Valore delle equazioni alla soluzione:');
disp(fval);
```

```
disp(['Flag di uscita: ', num2str(exitflag)]);


% Definition of the system of equations
function Fun = equations(x, F, Cf, Ccro, Jw1, Jw2, Jw3)

    % Name definition for each unknown
    Am1 = x(1);
    Am2 = x(2);
    Am3 = x(3);
    Fro = x(4);
    Cfro = x(5);
    Cro = x(6);
    W = x(7);
    Fin1 = x(8);
    Cfin1 = x(9);
    F1 = x(10);
    S1 = x(11);
    Sdil1 = x(12);
    Csdil1 = x(13);
    C1 = x(14);
    Cc1 = x(15);
    Fin2 = x(16);
    Cfin2 = x(17);
    F2 = x(18);
    S2 = x(19);
    Sdil2 = x(20);
    Csdil2 = x(21);
    C2 = x(22);
    Cc2 = x(23);
    F3 = x(24);
    S3 = x(25);
    C3 = x(26);
    Cc3 = x(27);
    Sdil3 = x(28);
    Csdil3 = x(29);

    Fun(1) = F+Sdil1-Fro;
    Fun(2) = F.*Cf+Sdil1.*Csdil1-Fro.*Cfro;
    Fun(3) = Fro-W-Cro;
    Fun(4) = Fro.*Cfro-Cro.*Ccro;
    Fun(5) = Cro+Sdil2-Fin1;
    Fun(6) = Cro.*Ccro+Sdil2.*Csdil2-Fin1.*Cfin1;
    Fun(7) = Fin1-F1-S1;
    Fun(8) = F1-Jw1.*Am1-C1;
    Fun(9) = F1.*Cfin1-C1.*Cc1;
    Fun(10) = S1+Jw1.*Am1-Sdil1;
    Fun(11) = S1.*Cfin1-Sdil1.*Csdil1;
    Fun(12) = C1+Sdil3-Fin2;
    Fun(13) = C1.*Cc1+Sdil3.*Csdil3-Fin2.*Cfin2;
    Fun(14) = Fin2-F2-S2;
    Fun(15) = F2-Jw2.*Am2-C2;
    Fun(16) = F2.*Cfin2-C2.*Cc2;
    Fun(17) = S2+Jw2.*Am2-Sdil2;
    Fun(18) = S2.*Cfin2-Sdil2.*Csdil2;
    Fun(19) = C2-F3-S3;
    Fun(20) = F3-Jw3.*Am3-C3;
```

```
    Fun(21) = F3.*Cc2-C3.*Cc3;
    Fun(22) = S3+Jw3.*Am3-Sdil3;
    Fun(23) = S3.*Cc2-Sdil3.*Csdil3;
    Fun(24) = Cc1-Cfin1-24.3;
    Fun(25) = Cc2-Cfin2-23.4;
    Fun(26) = Cc3-Cc2-22.2;
    Fun(27) = Cfin1-Csdil1-25.1;
    Fun(28) = Cfin2-Csdil2-24.3;
    Fun(29) = Cc2-Csdil3-23.4;


end
```

References

Abd El-Ghaffar, M. A., C Tieama, H. A. (2017). A Review of Membranes Classifications, Configurations, Surface Modifications, Characteristics and Its Applications in Water Purification. *Chemical and Biomolecular Engineering*, *2*(2), 57–82. https://doi.org/10.11648/j.cbe.20170202.11

Al-Amoudi, A. S., Ihm, S., Farooque, A. M., Al-Waznani, E. S. B., C Voutchkov, N. (2023). Dual brine concentration for the beneficial use of two concentrate streams from desalination plant - Concept proposal and pilot plant demonstration. *Desalination*, *5c4*, 116789. https://doi.org/10.1016/J.DESAL.2023.116789

Bai, W., Samineni, L., Chirontoni, P., Krupa, I., Kasak, P., Popelka, A., Saleh, N. B., C Kumar, M. (2023). Quantifying and reducing concentration polarization in reverse osmosis systems. *Desalination*, *554*, 116480. https://doi.org/10.1016/J.DESAL.2023.116480

Bartholomew, T. V., Mey, L., Arena, J. T., Siefert, N. S., C Mauter, M. S. (2017). Osmotically assisted reverse osmosis for high salinity brine treatment. *Desalination*, *421*, 3–11. https://doi.org/10.1016/j.desal.2017.04.012

Bartholomew, T. V., Siefert, N. S., C Mauter, M. S. (2018). Cost Optimization of Osmotically Assisted Reverse Osmosis. *Environmental Science and Technology*, *52*(20), 11813–11821. https://doi.org/10.1021/acs.est.8b02771 Berk, Z.

(2009). *Food Process Engineering and Technology*.

Bouma, A. T., C Lienhard, J. H. (2018). Split-feed counterflow reverse osmosis for brine concentration. *Desalination*, *445*, 280–291. https://doi.org/10.1016/J.DESAL.2018.07.011

Buonomenna, M. G. (2020). Design next generation membranes or rethink the "old" asymmetric membranes? In *Symmetry* (Vol. 12, Issue 2). MDPI AG. https://doi.org/10.3390/sym12020270

Cath, T. Y., Childress, A. E., C Elimelech, M. (2006). Forward osmosis: Principles, applications, and recent developments. *Journal of Membrane Science*, *281*(1– 2), 70–87. https://doi.org/10.1016/J.MEMSCI.2006.05.048

Chae, S. H., Moon, S., Hong, S. W., Lee, C., C Son, M. (2024). Performance investigation of osmotically assisted reverse osmosis using explainable

machine learning models: A comparative study. *Desalination*, *583*, 117647. https://doi.org/10.1016/J.DESAL.2024.117647

Chen, Q. B., Ren, H., Tian, Z., Sun, L., C Wang, J. (2019). Conversion and pre-concentration of SWRO reject brine into high solubility liquid salts (HSLS) by using electrodialysis metathesis. *Separation and Purification Technology*, *213*, 587–598. https://doi.org/10.1016/J.SEPPUR.2018.12.018

Chong, Y. K., Li, M., Wiley, D. E., Fletcher, D. F., C Liang, Y. Y. (2024). Review of modeling methodologies and state-of-the-art for osmotically assisted reverse osmosis membrane systems. *Desalination*, *587*, 117893. https://doi.org/10.1016/J.DESAL.2024.117893

Coday, B. D., Heil, D. M., Xu, P., C Cath, T. Y. (2013). Effects of transmembrane hydraulic pressure on performance of forward osmosis membranes. In *Environmental Science and Technology* (Vol. 47, Issue 5, pp. 2386–2393). https://doi.org/10.1021/es304519p

Date, M., Patyal, V., Jaspal, D., Malviya, A., C Khare, K. (2022). Zero liquid discharge technology for recovery, reuse, and reclamation of wastewater: A critical review. *Journal of Water Process Engineering*, *4S*, 103129. https://doi.org/10.1016/J.JWPE.2022.103129

Davenport, D. M., Deshmukh, A., Werber, J. R., C Elimelech, M. (2018). High- Pressure Reverse Osmosis for Energy-Efficient Hypersaline Brine Desalination: Current Status, Design Considerations, and Research Needs. *Environmental Science and Technology Letters*, *5*(8), 467–475. https://doi.org/10.1021/acs.estlett.8b00274

Davenport, D. M., Ritt, C. L., Verbeke, R., Dickmann, M., Egger, W., Vankelecom, I. F. J., C Elimelech, M. (2020). Thin film composite membrane compaction in high-pressure reverse osmosis. *Journal of Membrane Science*, *c10*, 118268. https://doi.org/10.1016/J.MEMSCI.2020.118268

Davenport, D. M., Wang, L., Shalusky, E., C Elimelech, M. (2021). Design principles and challenges of bench-scale high-pressure reverse osmosis up to 150 bar. *Desalination*, *517*, 115237. https://doi.org/10.1016/J.DESAL.2021.115237

Doran, P. M. (2013). *Bioprocess Engineering Principles* (2nd ed.). Academic Press.

Fonseca-Teodoro, P., Dunlop, J. E., C Gagen, E. J. (2022). *A review and comparison of approaches to treat coal mine affected water in Queensland: Student project report*. https://www.researchgate.net/publication/365358968

Fritzmann, C., Löwenberg, J., Wintgens, T., C Melin, T. (2007). State-of-the-art of reverse osmosis desalination. *Desalination*, *21c*(1–3), 1–76. https://doi.org/10.1016/j.desal.2006.12.009

Goh, P. S., Matsuura, T., Ismail, A. F., C Hilal, N. (2016). Recent trends in membranes and membrane processes for desalination. *Desalination*, *3S1*, 43–60. https://doi.org/10.1016/j.desal.2015.12.016

Gushing, R. S., C Lawler, D. F. (1998). Depth filtration: Fundamental investigation through three-dimensional trajectory analysis. *Environmental Science and Technology*, *32*(23), 3793–3801. https://doi.org/10.1021/es9707567

H. M. Beigi, B., Gadkari, S., C Sadhukhan, J. (2022). Osmotically assisted reverse osmosis, simulated to achieve high solute concentrations, at low energy consumption. *Scientific Reports*, *12*(1). https://doi.org/10.1038/s41598-022- 16974-x

Ismail, A. F., C Matsuura, T. (2016). *Membrane Technology for Water and Wastewater Treatment, Energy and Environment* (Vol. 1st). CRC Press.

Jafar Mazumder, M. A. (2020). A review of green scale inhibitors: Process, types, mechanism and properties. In *Coatings* (Vol. 10, Issue 10, pp. 1–29). MDPI AG. https://doi.org/10.3390/coatings10100928

Ju, J., Lee, S., Kim, Y., Cho, H., C Lee, S. (2023). Theoretical and Experimental Analysis of Osmotically Assisted Reverse Osmosis for Minimum Liquid Discharge. *Membranes*, *13*(10). https://doi.org/10.3390/membranes13100814

Kucera, J. (2010). *Reverse Osmosis: Design, Processes, and Applications for Engineers* (1st ed.). Wiley-Scrivener.

Li, N. N., Fane, A. G., Ho, W. S. W., C Matsuura, T. (2008). *ADVANCED MEMBRANE TECHNOLOGY AND APPLICATIONS*.

Liang, C. Z., Askari, M., Choong, L. T. (Simon), C Chung, T. S. (2021). Ultra-strong polymeric hollow fiber membranes for saline dewatering and desalination. *Nature Communications*, *12*(1). https://doi.org/10.1038/s41467-021-22684-1

Lin, S., Qi, H., Hou, P., C Liu, K. (2023). Resource recovery from textile wastewater: Dye, salt, and water regeneration using solar-driven interfacial evaporation.

Journal of Cleaner Production, *3S1*, 136148. https://doi.org/10.1016/J.JCLEPRO.2023.136148

Matin, A., Rahman, F., Shafi, H. Z., C Zubair, S. M. (2019). Scaling of reverse osmosis membranes used in water desalination: Phenomena, impact, and control; future directions. *Desalination*, *455*, 135–157. https://doi.org/10.1016/J.DESAL.2018.12.009

Mazumder, A., Sarkar, S., Sen, D., C Bhattacharjee, C. (2023). Membranes for industrial wastewater recovery and reuse. *Resource Recovery in Industrial Waste Waters*, 1–21. https://doi.org/10.1016/B978-0-323-95327-6.00029-4

McCutcheon, J. R., C Elimelech, M. (2006). Influence of concentrative and dilutive internal concentration polarization on flux behavior in forward osmosis. *Journal of Membrane Science*, *284*(1–2), 237–247. https://doi.org/10.1016/J.MEMSCI.2006.07.049

Medved, I., C Černý, R. (2013). Osmosis in porous media: A review of recent studies. *Microporous and Mesoporous Materials*, *170*, 299–317. https://doi.org/10.1016/J.MICROMESO.2012.12.009

Mickley, M. (2008). *Survey of High-Recovery and Zero Liquid Discharge Technologies for Water Utilities*. https://www.researchgate.net/publication/313555932

Mo, Z., Peters, C. D., Long, C., Hankins, N. P., C She, Q. (2022). How split-feed osmotically assisted reverse osmosis (SF-OARO) can outperform conventional reverse osmosis (CRO) processes under constant and varying electricity tariffs. *Desalination*, *530*, 115670. https://doi.org/10.1016/J.DESAL.2022.115670

Moreira, V. R., Lebron, Y. A. R., Couto, C. F., Maia, A., Moravia, W. G., C Amaral, M. C. S. (2022). Process development for textile wastewater treatment towards zero liquid discharge: Integrating membrane separation process and advanced oxidation techniques. *Process Safety and Environmental Protection*, *157*, 537–546. https://doi.org/10.1016/J.PSEP.2021.10.037

Muhammad Yaqub, C Lee, W. (2019). Zero-liquid discharge (ZLD) technology for resource recovery from wastewater: A review. *Science of The Total*

Environment, *c81*, 551–563. https://doi.org/10.1016/J.SCITOTENV.2019.05.062

Nakagawa, K., Togo, N., Takagi, R., Shintani, T., Yoshioka, T., Kamio, E., C Matsuyama, H. (2020). Multistage osmotically assisted reverse osmosis process for concentrating solutions using hollow fiber membrane modules. *Chemical Engineering Research and Design*, *1c2*, 117–124. https://doi.org/10.1016/j.cherd.2020.07.029

Nakao, T., Miura, Y., Furuichi, K., C Yasukawa, M. (2021). Cellulose triacetate (Cta) hollow-fiber (hf) membranes for sustainable seawater desalination: A review. In *Membranes* (Vol. 11, Issue 3). MDPI AG. https://doi.org/10.3390/membranes11030183

Panagopoulos, A. (2020). Process simulation and techno-economic assessment of a zero liquid discharge/multi-effect desalination/thermal vapor compression (ZLD/MED/TVC) system. *International Journal of Energy Research*, *44*(1), 473–495. https://doi.org/10.1002/er.4948

Panagopoulos, A., C Haralambous, K. J. (2020). Minimal Liquid Discharge (MLD) and Zero Liquid Discharge (ZLD) strategies for wastewater management and resource recovery – Analysis, challenges and prospects. *Journal of Environmental Chemical Engineering*, *8*(5), 104418. https://doi.org/10.1016/J.JECE.2020.104418

Peters, C. D., C Hankins, N. P. (2019). Osmotically assisted reverse osmosis (OARO): Five approaches to dewatering saline brines using pressure-driven membrane processes. *Desalination*, *458*, 1–13. https://doi.org/10.1016/J.DESAL.2019.01.025

Peters, C. D., Li, D., Mo, Z., Hankins, N. P., C She, Q. (2022). Exploring the Limitations of Osmotically Assisted Reverse Osmosis: Membrane Fouling and the Limiting Flux. *Environmental Science and Technology*, *5c*(10), 6678–6688. https://doi.org/10.1021/ACS.EST.2C00839

Pinnau, I., C Freeman, B. D. (1999). *Membrane Formation and Modification*. https://pubs.acs.org/sharingguidelines

Prihasto, N., Liu, Q. F., C Kim, S. H. (2009). Pre-treatment strategies for seawater desalination by reverse osmosis system. *Desalination*, *24S*(1), 308–316. https://doi.org/10.1016/J.DESAL.2008.09.010

Qasim, M., Badrelzaman, M., Darwish, N. N., Darwish, N. A., C Hilal, N. (2019). Reverse osmosis desalination: A state-of-the-art review. In *Desalination* (Vol. 459, pp. 59–104). Elsevier B.V. https://doi.org/10.1016/j.desal.2019.02.008

Rahman, S. N., Saleem, H., C Zaidi, S. J. (2023). Progress in membranes for pressure retarded osmosis application. *Desalination*, *54S*, 116347. https://doi.org/10.1016/J.DESAL.2022.116347

Salama, A., Alyan, A., El Amin, M., Sun, S., Zhang, T., C Zoubeik, M. (2021). The effect of the oleophobicity deterioration of a membrane surface on its rejection capacity: A computational fluid dynamics study. *Membranes*, *11*(4). https://doi.org/10.3390/membranes11040253

Shaffer, D. L., Arias Chavez, L. H., Ben-Sasson, M., Romero-Vargas Castrillón, S., Yip, N. Y., C Elimelech, M. (2013). Desalination and reuse of high-salinity shale gas produced water: Drivers, technologies, and future directions. In *Environmental Science and Technology* (Vol. 47, Issue 17, pp. 9569–9583). https://doi.org/10.1021/es401966e

She, Q., Zhang, L., Wang, R., Krantz, W. B., C Fane, A. G. (2017). Pressure-retarded osmosis with wastewater concentrate feed: Fouling process considerations. *Journal of Membrane Science*, *542*, 233–244. https://doi.org/10.1016/J.MEMSCI.2017.08.022

Shenvi, S. S., Isloor, A. M., C Ismail, A. F. (2015). A review on RO membrane technology: Developments and challenges. *Desalination*, *3c8*, 10–26. https://doi.org/10.1016/J.DESAL.2014.12.042

Singha, K., Maity, S., Pandit, P., Maiti, S., C Lakshmanan, S. O. (2021). Nanotechnologies for wastewater treatment. In *Sustainable Technologies for Textile Wastewater Treatments* (pp. 1–12). Elsevier. https://doi.org/10.1016/B978-0-323-85829-8.00009-2

Skuse, C., Gallego-Schmid, A., Azapagic, A., C Gorgojo, P. (2021). Can emerging membrane-based desalination technologies replace reverse osmosis? *Desalination*, *500*, 114844. https://doi.org/10.1016/J.DESAL.2020.114844

Tchobanoglous, G. ; B. F. L. ; S. H. D. (2003). *Wastewater Engineering: Treatment and Resource Recovery* (5th ed.). McGraw-Hill Education - Europe.

Tiraferri, A., Yip, N. Y., Phillip, W. A., Schiffman, J. D., C Elimelech, M. (2011). Relating performance of thin-film composite forward osmosis membranes to support layer formation and structure. *Journal of Membrane Science*, *3c7*(1– 2), 340–352. https://doi.org/10.1016/J.MEMSCI.2010.11.014

Togo, N., Nakagawa, K., Shintani, T., Yoshioka, T., Takahashi, T., Kamio, E., C Matsuyama, H. (2019). Osmotically Assisted Reverse Osmosis Utilizing Hollow Fiber Membrane Module for Concentration Process. *Industrial and Engineering Chemistry Research*, *58*(16), 6721–6729. https://doi.org/10.1021/acs.iecr.9b00630

Tong, T., C Elimelech, M. (2016). The Global Rise of Zero Liquid Discharge for Wastewater Management: Drivers, Technologies, and Future Directions. In *Environmental Science and Technology* (Vol. 50, Issue 13, pp. 6846–6855). American Chemical Society. https://doi.org/10.1021/acs.est.6b01000

Touati, K., Tadeo, F., Ho Chae, S., Ha Kim, J., C Alvarez Silva, O. (2017). *Pressure Retarded Osmosis: Renewable Energy Generation and Recovery*.

Turetta, M., Bertucco, A., Briani, F., Michelon, N., Vogel, J., Nguyen, X. T., C Barbera, E. (2024). Experimental investigation and mathematical modelling of a spiral wound membrane module for osmotically assisted reverse osmosis applications. *Journal of Water Process Engineering*, *c8*, 106355. https://doi.org/10.1016/J.JWPE.2024.106355

Vergili, I., Kaya, Y., Sen, U., Gönder, Z. B., C Aydiner, C. (2012). Techno-economic analysis of textile dye bath wastewater treatment by integrated membrane processes under the zero liquid discharge approach. *Resources, Conservation and Recycling*, *58*, 25–35. https://doi.org/10.1016/J.RESCONREC.2011.10.005

Vishnu, G., Palanisamy, S., C Joseph, K. (2008). Assessment of fieldscale zero liquid discharge treatment systems for recovery of water and salt from textile effluents. *Journal of Cleaner Production*, *1c*(10), 1081–1089. https://doi.org/10.1016/J.JCLEPRO.2007.06.005

Wang, H. ; Z. H. (2013). *Understand the Basics of Membrane Filtration*. www.aiche.org/cep

Wang, Y. N., Goh, K., Li, X., Setiawan, L., C Wang, R. (2018). Membranes and processes for forward osmosis-based desalination: Recent advances and future prospects. In *Desalination* (Vol. 434, pp. 81–99). Elsevier B.V. https://doi.org/10.1016/j.desal.2017.10.028

Wang, Z., Feng, D., Chen, Y., He, D., C Elimelech, M. (2021a). Comparison of Energy Consumption of Osmotically Assisted Reverse Osmosis and Low-Salt- Rejection Reverse Osmosis for Brine Management. *Environmental Science and Technology*, *55*(15), 10714–10723. https://doi.org/10.1021/acs.est.1c01638

Wang, Z., Feng, D., Chen, Y., He, D., C Elimelech, M. (2021b). Comparison of Energy Consumption of Osmotically Assisted Reverse Osmosis and Low-Salt- Rejection Reverse Osmosis for Brine Management. *Environmental Science and Technology*, *55*(15), 10714–10723. https://doi.org/10.1021/acs.est.1c01638

Warsinger, D. M., Swaminathan, J., Guillen-Burrieza, E., Arafat, H. A., C Lienhard V, J. H. (2015). Scaling and fouling in membrane distillation for desalination applications: A review. *Desalination*, *35c*, 294–313. https://doi.org/10.1016/J.DESAL.2014.06.031

Xue, Y. L., Zhang, R., Cao, B., C Li, P. (2021). Tubular membranes and modules. *Hollow Fiber Membranes: Fabrication and Applications*, 431–448. https://doi.org/10.1016/B978-0-12-821876-1.00011-1

Zobel, S., C Gries, T. (2010). The use of nonwovens as filtration materials. *Applications of Nonwovens in Technical Textiles*, 160–183. https://doi.org/10.1533/9781845699741.2.160

Zubair, M. M., Saleem, H., C Zaidi, S. J. (2023). Recent progress in reverse osmosis modeling: An overview. *Desalination*, *5c4*, 116705. https://doi.org/10.1016/J.DESAL.2023.116705